Carbon Dioxide as Feedstock in Microbial Cultivations

Von der Doktoratsschule für Chemie- und Verfahrenstechnik der TU Graz und der Fakultät für Mathematik und Naturwissenschaften der RWTH Aachen University zur Erlangung des akademischen Grades einer Doktorin der Technischen Wissenschaften bzw. Doktorin der Naturwissenschaften genehmigte Dissertation

vorgelegt von

Halima Aliyu ALHAFIZ (B.Eng., MSc.)

aus Kaduna, Nigeria

Berichter: Assoc. Prof. Regina Kratzer

Prof. Lars Lauterbach

Tag der mündlichen Prüfung: 30. 06. 2026

Diese Dissertation ist auf den Internetseiten der Universitätsbibliothek verfügbar.

Carbon Dioxide as Feedstock in Microbial Cultivations

Von der Fakultät für Mathematik und Naturwissenschaften der RWTH Aachen University zur Erlangung des akademischen Grades einer Doktorin der Naturwissenschaften genehmigte Dissertation

vorgelegt von

Halima Aliyu ALHAFIZ (B.Eng., MSc.)
aus Kaduna, Nigeria

Berichter: Assoc. Prof. Regina Kratzer
Prof. Lars Lauterbach

Tag der mündlichen Prüfung: 30. 06. 2026

Diese Dissertation ist auf den Internetseiten der Universitätsbibliothek verfügbar.

In memory of my beloved mother Aisha Mgbo Agha-Umar

Declaration of authorship

I, Halima Aliyu Alhafiz, declare that this thesis and the work presented in it are my own and has been generated by me as the result of my own original research.

I do solemnly swear that:

This work was done wholly or mainly while in candidature for the doctoral degree at these faculties and universities;

Where any part of this thesis has previously been submitted for a degree or any other

qualification at this university or any other institution, this has been clearly stated;

Where I have consulted the published work of others or myself, this is always clearly

attributed;

Where I have quoted from the work of others or myself, the source is always given. This thesis is entirely my own work, with the exception of such quotations;

I have acknowledged all major sources of assistance;

Where the thesis is based on work done by myself jointly with others, I have made clear

exactly what was done by others and what I have contributed myself;

Parts of this work have been published before as:

Alhafiz, H. A.*, Di Bisceglie, F., Meier, H. P. F., Weickardt, I., González, I. A. C., Navarro, J. G., Schoenmakers, P., Oyen, S. J., Lettau, E., Lombard, E., Cordero, P. R. F., Konarzycka-Bessler, M., Gorret, N., Schmidt, S., Schillberg, S., Mann, M., Guillouet, S. E., Kratzer, R., & Lauterbach, L.* (2025). *Cupriavidus necator* as a model organism for CO_2-based biotechnology. *Methods in enzymology*, *714*, 163–194. **https://doi.org/10.1016/bs.mie.2025.01.017**

Alhafiz, H. A., Longus, K., Verlinden, R. A. J., Lambauer, V., Kruschitz, A., & Kratzer, R.* (2025). Cultivation of *Cupriavidus necator strains* on hydrolyzed lignocellulosic feedstocks widely available in Europe. *Biotechnology reports (Amsterdam, Netherlands)*, *47*, e00899. **https://doi.org/10.1016/j.btre.2025.e00899**

Aachen, April 30, 2026 _____

(Halima Aliyu Alhafiz, B. Eng., MSc.)

Publications

Alhafiz, H. A.*, Di Bisceglie, F., Meier, H. P. F., Weickardt, I., González, I. A. C., Navarro, J. G., Schoenmakers, P., Oyen, S. J., Lettau, E., Lombard, E., Cordero, P. R. F., Konarzycka-Bessler, M., Gorret, N., Schmidt, S., Schillberg, S., Mann, M., Guillouet, S. E., Kratzer, R., & Lauterbach, L.* (2025). *Cupriavidus necator* as a model organism for CO_2-based biotechnology. *Methods in enzymology*, *714*, 163–194. https://doi.org/10.1016/bs.mie.2025.01.017

Alhafiz, H. A., Longus, K., Verlinden, R. A. J., Lambauer, V., Kruschitz, A., & Kratzer, R.* (2025). Cultivation of *Cupriavidus necator strains* on hydrolyzed lignocellulosic feedstocks widely available in Europe. *Biotechnology reports (Amsterdam, Netherlands)*, *47*, e00899. https://doi.org/10.1016/j.btre.2025.e00899

Alhafiz, H. A., Graber, M., Calabrese, D., Cordero, P. R. F., Lauterbach, L., Hochenauer, C., Reichhartinger, M. & Kratzer, R. Overcoming pH instability for a safe and sustainable polyhydroxybutyrate production by *Cupriavidus necator* DSM544. (Manuscript in preparation)

Alhafiz, H. A., Sasamoto, S., Huber, F., Cordero, P. R. F., Meyer, M., Sato, S., Bongartz, P. & Lauterbach, L. Membrane-integrated gas fermentation for H_2-driven synthesis of 2-methylpyrrolidine by *Cupriavidus necator*. (Manuscript in preparation)

Alhafiz, H.A., Cordero, P. R. F., Kratzer, R. & Lauterbach, L. Process modelling and simulation-guided evaluation of gas fermentation by *Cupriavidus necator* using superpro designer. (Manuscript in preparation)

Alhafiz, H. A., Linke, T., Hanke, B., Mann, M., Hoffmann, M., Cordero, P. R. F., Schmid, A., Maskow, T. & Lauterbach, L. Contribution of soluble hydrogenases and membrane-bound hydrogenases to the energy efficiency of *Cupriavidus necator*. (Manuscript in preparation)

* corresponding author

Scientific dissemination and activities

Oral presentations

1. Gas Fermentation and Kinetic Modeling of *Cupriavidus necator* for Sustainable Polyhydroxybutyrate Production. Flash talk and poster presentation at the DECHEMA Annual Meeting of Process Engineering and Materials Technology, November 10–11, 2025.
2. Carbon Dioxide as Feedstock in Microbial Cultivations. Oral presentation at the African-German Doctoral Summer School, Hamburg University of Applied Sciences, Hamburg, Germany, September 9–14, 2024.
3. Carbon Dioxide as Feedstock in Microbial Cultivations. Oral presentation, DocDay, Doctoral School of Chemical and Process Engineering, July 3, 2023.
4. Carbon Dioxide as Feedstock in Microbial Cultivations. Seminar presentation, Institute of Applied Microbiology, RWTH Aachen University, September 4, 2024.
5. Carbon Dioxide as Feedstock in Microbial Cultivations. Seminar presentation (Privatissimum), Institute of Biotechnology and Biochemical Engineering, TU Graz, November 11, 2022.
6. Carbon dioxide as feedstock for microbial cultivation: gas fermentation to match microbial requirements and technical feasibility. Seminar presentation, Institute of Applied Microbiology, RWTH Aachen University, January 21, 2026.
7. Utilization of Residues from the Olive Oil Industry as Value-Added Products. Oral presentation at the ESIEA International Student Camp: Process Development and Process Evaluation in the Biorefinery Industry, NLEG, Lisbon, Portugal, September 26–30, 2022.

Poster presentations

1. CO_2 as Feedstock in Microbial Cultivations: Gas Fermentation Matched to Microbial Requirements and Technical Feasibility. Poster presentation at the European Summit of Industrial Biotechnology, Graz, Austria, November 12–14, 2024.
2. High Cell Density Gas Fermentation for Carbon-Neutral Bioplastic Production by a Knallgas Bacterium. Poster presentation at the CO_2-Based Fuels and Chemicals Conference, Cologne, Germany, April 17–18, 2024.
3. Lignocellulosic Biomass as a Bioresource in Central Europe. Poster presentation at the European Summit of Industrial Biotechnology, Graz, Austria, November 14, 2022.
4. Lignocellulosic Biomass as a Bioresource in Central Europe. Long Night of Research, TU Graz, May 2022.

Other forms

1. Co-organizer of the Long Night of Research, TU Graz, May 2022.
2. Participant in the European Researchers' Night (ConCO_2rde), Fundação Champalimaud, Lisbon, Portugal, September 29, 2023. Presented CO_2-derived bioplastics to the public.
3. Co-organizer and co-moderator of the Final ConCO_2rde Workshop at the European Summit of Industrial Biotechnology (ESIB), November 11, 2024.

Supervision and scientific support

1. Saya Kato (Visiting scientist, KANEKA, Japan), April 2025 – April 2026
   Gas fermentation with *Cupriavidus necator*
2. Brunon K. Hanke (Bachelor's student), May 2025 – September 2025
   Characterisation of hydrogenase knockout strains of *Cupriavidus necator*
3. Ines Terwayet Bayouli (Visiting researcher, Ghent University), June 2023 – July 2023
   Hydrolysis and analysis of lignocellulosic biomasses
4. Philip Rogi (Bachelor's student), March 2023 – May 2023
   Hydrolysis of lignocellulosic biomasses
5. Andrea Strahlhofer (Master's student), December 2022 – January 2023
   Cultivation of *Cupriavidus necator* on lignocellulosic hydrolysates

Acknowledgement

My appreciation goes to Assoc. Prof. Marlene Kienberger, who first interviewed me and, recognizing that my research interests were not fully aligned with her group, recommended me to Assoc. Prof. Regina Kratzer. I am grateful that she later became a mentor to me.

I am profoundly thankful to my supervisor, Assoc. Prof. Regina Kratzer, for accepting me into her group and providing the funding that made this research possible. I am deeply grateful for her guidance, unwavering support, and kindness, both academically and beyond.

I would also like to sincerely thank Prof. Lars Lauterbach for accepting the role of my second supervisor. I am grateful for his support, funding, valuable guidance, and for creating opportunities for collaboration that enriched this work.

My appreciation extends to the members of my examination board for their time, insightful feedback, and evaluation of this thesis.

I am thankful to my students Philip Rogi, Andrea Strahlhofer, and Bruno Hanke for their dedication and assistance with experimental work. Your contributions were invaluable.

I would like to acknowledge my collaborators: Saya Kato from Kaneka Japan for her help with experiments; Tilman Linke from UFZ Leipzig for his support and assistance with calorimetric studies; to Biothrust for SEM analysis and fruitful discussions; Lenny Yap at IMBT, TU Graz for support with GC measurements; and Max Graber IAC at TU Graz for experimental support and insightful discussions.

My sincere thanks go to the Austrian centre of Industrial Biotechnology (ACIB), the entire BIOTE institute at TU Graz, especially Karin Longus for technical assistance, as well as the IAMB at RWTH Aachen, including Karl Hüser for technical support and Dr. Paul Cordero for his guidance, kindness, and fruitful discussions. I am also grateful to Prof. Lars Blank for his insightful feedback and valuable discussions. Furthermore, I acknowledge the entire ConCO_2rde project team (ESR 1-10) for their collaboration and unending support.

I am grateful to my colleagues Donato Calabrese, Meryem Bahceli, Karen Brunsbach, Claudia Tahiraj, Hongyi Fan, Pierre Schoenmakers, Hannes Mandon, Guiyeoul Lim, Subha Ghosh, and Klara Kastner for the stimulating discussions, encouragement, and the supportive working environment. You all made this journey smoother.

To the entire Alhafiz family and friends, including Ameenatu Rabiu, Maimuna Shehu and Shejla Imamovic, thank you for your constant love and support. To my sister, Zainab Aliyu Alhafiz, my confidant and pillar of strength, despite the distance, you have always been there for me. You are truly *nulli secundus* and I love you forever. To my father, Rtd. Maj. Aliyu Alhafiz, thank you for the support and prayers, جَزَاكَ اللهُ خَيْرًا. To my beloved mother, Haj. Aisha Mgbo Agha-Umar, though you are no longer here, I continue to feel your presence, your prayers, and your unwavering belief in me. May you continue to rest in peace.

And to the Lord of the heavens and the earth, whose grace and guidance have sustained me throughout this journey. I do not take any of your mercies for granted Ya Allah. اَلْحَمْدُ لِلّٰهِ!!!

Funding and contributions

The European Union's Horizon 2020 Research and Innovation programme under the Marie Skłodowska Curie grant agreement No. 955740 (ConCO2rde) and the European Union's Horizon 2020 Research and Innovation programme under grant agreements No. 953206 (Bionanopolys). The COMET center ACIB was funded under the COMET program by BMK, BMDW, SFG, Standortagentur Tirol, Lower Austria, and the Vienna Business Agency, managed by FFG (No. 872161).

The Werner Siemens Foundation (WSS) through the Forschungszentrum catalaix













Abstract

The increasing concentration of atmospheric carbon dioxide (CO_2) and the need for sustainable production systems necessitate the development of efficient carbon capture and utilization (CCU) technologies. Microbial catalysts represent a promising alternative to chemocatalysts for CO_2 reduction, as they enable highly selective conversion of CO_2 into value-added products such as polyhydroxybutyrate (PHB), single cell proteins, and isopropanol under mild conditions, while avoiding the need for high temperatures, pressures, and precious metal catalysts. However, industrial implementation is limited by challenges related to energy efficiency, gas–liquid mass transfer, process safety, and scalability. This thesis addresses these challenges using *Cupriavidus necator* as a model organism, with the aim of aligning microbial requirements with engineering feasibility for CO_2-based bioprocesses.

A key focus of this thesis was the role of hydrogenases in the energy metabolism of *C. necator*. Physiological characterization was performed under chemolithoautotrophic growth conditions (H_2: O_2: CO_2: N_2 = 3.8: 7.3: 13: 75.9%) using hydrogenase knockout strains expressing either soluble hydrogenase (SH^+) or membrane-bound hydrogenase (MBH^+), in two regulatory backgrounds: *hoxJ* (impaired hydrogenase regulation) and *hoxJ** (restored hydrogen-dependent regulation). SH^+ strains achieved approximately 2–3-fold higher biomass concentrations than MBH^+ strains. Calorimetric analysis showed that MBH^+ strains dissipated approximately 3.3-fold more heat than SH^+ in the *hoxJ* background and about 2.5-fold more in the *hoxJ** background.

In addition, safe and robust gas fermentation was established for *C. necator* DSM 544, a glucose-utilizing mutant that, unlike the wild-type H16, showed pronounced culture acidification during chemolithoautotrophic growth. Due to the cost implications of implementing ATEX-certified pH control systems, a calibration-based manual pH control strategy was developed, which proved sufficient for maintaining stable cultivation at laboratory scale without the need for complex systems. After transfer to a 1.2-L stirred-tank reactor and process intensification under a non-explosive gas composition of 5% CO_2, 40% H_2, 2% O_2, and N_2 as balance gas, stable chemolithoautotrophic cultivation was achieved, reaching up to 42 g L^{-1} cell dry weight with 72% PHB after ammonium depletion.

To overcome gas–liquid mass transfer limitations while enabling safe operation under otherwise explosive conditions, a membrane-integrated gas fermentation platform was established using hollow fiber modules in a 30 mL mini-fermenter. The system operated without a headspace and under diffusion-driven mass transfer, with H_2 supplied through a separate channel, allowing the use of an optimal but intrinsically explosive gas composition (70% H_2, 20% O_2, 10% CO_2) in a safe and controlled manner. Compared to conventional bubbling, the membrane system achieved a 2.7-fold higher hydrogen mass transfer coefficient (k_La), resulting in improved substrate availability. This enabled growth of recombinant *C. necator* expressing imine reductase (2.2 g L^{-1} CDW) while simultaneously supporting whole-cell biocatalysis, achieving 77.6% conversion of 2-methyl-1-pyrroline to 2-methylpyrrolidine, a valuable N-heterocyclic building block for pharmaceutical and fine chemical synthesis.

Furthermore, the feasibility of indirect CO_2 utilization was demonstrated through lignocellulosic biomass processing. Steam explosion pretreatment enhanced enzymatic hydrolysis (Cellic® CTec3 HS), releasing fermentable sugars from wheat straw, beech, spruce, pine, and Miscanthus. Wheat straw hydrolysate A2 (H_2SO_4-assisted steam explosion, ~180 °C) achieved the highest glucose yield (30.2 g L^{-1}), while A3 (water-only steam explosion) yielded

22.9 g L^{-1}. Deep-well screening of *C. necator* DSM 544 on diluted hydrolysates revealed robust growth (≥5-fold OD_{600} increase within 24 h across all substrates), with highest biomass correlating to glucose availability. Inhibitor effects were moderate; high levels in A2 reduced growth by ~50% relative to reference media. Wheat straw A3, with optimal sugar/inhibitor balance, supported shake-flask cultivation to 4.14 g L^{-1} CDW and 24.2% PHB under N-limitation without prior detoxification. These findings confirm *C. necator* DSM 544's tolerance to lignocellulosic inhibitors and its potential to integrate biorefinery streams into CO_2 valorization cascades.

Finally, to integrate the experimentally identified constraints on gas–liquid mass transfer and process performance into a predictive framework, a dynamic kinetic model for chemolithoautotrophic growth of *C. necator* DSM 544 was developed and implemented in SuperPro Designer® v14, integrating Monod-type kinetics (μ_{max} = 0.09 h^{-1}) with experimentally derived stoichiometry. Model validation against batch fermentation data accurately reproduced biomass growth (final CDW ~13–14 g L^{-1}), PHB accumulation (72% of CDW), and ammonium depletion over 142 hours. Sensitivity analysis showed that biological parameters (μ_{max}, α) caused only minor variations in CDW (±5.1%), whereas aeration rate exhibited a critical threshold behaviour below 0.25 vvm, where severe oxygen limitation led to negligible growth (from 13.8 to 0.047 g L^{-1}). Scale-up simulations from 1.27 L to 12.8 L preserved concentration profiles and productivity (~0.078 g L^{-1} h^{-1}), while total PHB production increased proportionally (0.014 to 0.139 kg per batch), demonstrating kinetic scalability but no improvement in process intensity.

Overall, this thesis demonstrates that safe and efficient CO_2 bioconversion can be achieved through integrated engineering strategies, including non-explosive operation, membrane-based gas delivery, and process modelling. By combining experimental validation with simulation-guided analysis, this thesis provides a framework for translating laboratory-scale gas fermentation into scalable systems, identifying gas–liquid mass transfer and process safety as key constraints. These findings contribute to the development of robust and economically viable bioprocesses for sustainable production of biopolymers and high-value chemicals from gaseous substrates.

Zusammenfassung

Die zunehmende CO_2-Konzentration in der Atmosphäre sowie der steigende Bedarf an nachhaltigen Produktionssystemen erfordern die Entwicklung effizienter Technologien zur Kohlenstoffabscheidung und -nutzung. Zur Reduktion von CO_2 bieten mikrobielle Katalysatoren eine vielversprechende Alternative zu chemischen Verfahren, da sie eine hochselektive Umwandlung in wertschöpfende Produkte wie Polyhydroxybutyrat (PHB), Einzellerproteine und Isopropanol unter milden Bedingungen ermöglichen, ohne den Einsatz hoher Temperaturen, Drücke oder Edelmetallkatalysatoren. Die industrielle Umsetzung wird jedoch durch Herausforderungen in Bezug auf Energieeffizienz, Gas-Flüssig-Stoffübergang, Prozesssicherheit und Skalierbarkeit eingeschränkt. Die vorliegende Dissertation adressiert diese Aspekte unter Verwendung von *Cupriavidus necator* als Modellorganismus, mit dem Ziel, mikrobielle Anforderungen und ingenieurtechnische Umsetzbarkeit für CO_2-basierte Bioprozesse in Einklang zu bringen.

Ein zentraler Schwerpunkt dieser Arbeit lag auf der Rolle von Hydrogenasen im Energiestoffwechsel von *Cupriavidus necator*. Die physiologische Charakterisierung erfolgte unter chemolithoautotrophen Wachstumsbedingungen (H_2: O_2: CO_2: N_2 = 3,8: 7,3: 13: 75,9 %). Hierfür wurden Hydrogenase-Knockout-Stämme eingesetzt, die entweder eine lösliche Hydrogenase (SH^+) oder eine membrangebundene Hydrogenase (MBH^+) exprimierten. Diese wurden jeweils in zwei regulatorischen Hintergründen untersucht: *hoxJ* (gestörte Hydrogenase-Regulation) und *hoxJ** (wiederhergestellte hydrogenabhängige Regulation). SH^+-Stämme erreichten etwa 2–3-fach höhere Biomassekonzentrationen als MBH^+-Stämme. Kalorimetrische Analysen zeigten, dass MBH^+-Stämme im *hoxJ*-Hintergrund etwa 3,3-fach mehr Wärme dissipierten als SH^+-Stämme und im *hoxJ**-Hintergrund etwa 2,5-fach mehr.

Darüber hinaus wurde eine sichere und robuste Gasfermentation für die glukoseverwertende Mutante *Cupriavidus necator DSM 544* etabliert, die im Gegensatz zum Wildtyp H16 während des chemolithoautotrophen Wachstums eine ausgeprägte Ansäuerung der Kultur zeigte. Aufgrund der Kosten für die Implementierung ATEX-zertifizierter pH-Regelungssysteme wurde eine kalibrierungsbasierte, manuelle pH-Regelstrategie entwickelt, die sich im Labormaßstab als ausreichend erwies, um eine stabile Kultivierung ohne komplexe Systeme zu gewährleisten. Nach der Übertragung in einen 1,2-L-Rührkesselreaktor und der Prozessintensivierung unter einer nicht-explosiven Gaszusammensetzung (5 % CO_2, 40 % H_2, 2 % O_2, N_2 als Restgas) wurde eine stabile chemolithoautotrophe Kultivierung erreicht. Nach Ammoniumverarmung wurden bis zu 42 g L^{-1} Zell-Trockengewicht mit 72 % PHB erzielt.

Zur Überwindung von Einschränkungen im Gas-Flüssig-Stoffübergang und zur Gewährleistung eines sicheren Betriebs wurde eine membranintegrierte Gasfermentationsplattform auf Basis von Hohlfasermodulen in einem 30-mL-Mini-Fermenter etabliert. Das System arbeitete ohne Gasraum und nutzte diffusionsgetriebenen Stofftransport, wobei H_2 über einen separaten Kanal zugeführt wurde. Dadurch konnte eine intrinsisch explosive Gaszusammensetzung (70 % H_2, 20 % O_2, 10 % CO_2) sicher und kontrolliert eingesetzt werden. Im Vergleich zur konventionellen Begasung erreichte das Membransystem einen 2,7-fach höheren Wasserstoff-Stoffübergangskoeffizienten (k_La) und verbesserte damit die Substratverfügbarkeit. Dies ermöglichte das Wachstum von rekombinantem *Cupriavidus necator* mit exprimierter Imin-Reduktase (2,2 g L^{-1} CDW) sowie die gleichzeitige Durchführung von Ganzzellbiokatalyse. Dabei wurde eine Umsetzung von 77,6 % von 2-Methyl-1-pyrrolin zu 2-Methylpyrrolidin erreicht, einem wertvollen N-heterozyklischen Baustein für die pharmazeutische und feinchemische Synthese.

Darüber hinaus wurde die Machbarkeit der indirekten CO_2-Nutzung durch die Verarbeitung lignozellulosischer Biomasse demonstriert. Eine Dampfexplosionsvorbehandlung verbesserte die enzymatische Hydrolyse (Cellic® CTec3 HS) und setzte fermentierbare Zucker aus Weizenstroh, Buche, Fichte, Kiefer und Miscanthus frei. Das Weizenstrohhydrolysat A2 (H_2SO_4-unterstützte Dampfexplosion, ~180 °C) erzielte die höchste Glukoseausbeute (30,2 g L^{-1}), während A3 (Dampfexplosion ohne Zusatzstoffe) 22,9 g L^{-1} lieferte. Deep-Well-Screenings von *C. necator* DSM 544 auf verdünnten Hydrolysaten zeigten robustes Wachstum (≥5-fache OD_{600}-Zunahme innerhalb von 24 h über alle Substrate), wobei die höchste Biomasse mit der Glukoseverfügbarkeit korrelierte. Inhibitorische Effekte waren moderat; hohe Konzentrationen in A2 reduzierten das Wachstum um etwa 50% im Vergleich zu Referenzmedien. Weizenstroh A3 mit einem optimalen Zucker/Inhibitor-Verhältnis ermöglichte eine Schüttelkolbenkultivierung bis zu 4,14 g L^{-1} CDW und 24,2% PHB unter Stickstofflimitierung ohne vorherige Entgiftung. Diese Ergebnisse bestätigen die Toleranz von *C. necator* DSM 544 gegenüber lignozellulosischen Inhibitoren sowie sein Potenzial zur Integration von Bioraffinerie-Strömen in CO_2-Verwertungskaskaden.

Zur Integration der experimentell identifizierten Einschränkungen hinsichtlich Gas-Flüssig-Stoffübergang und Prozessleistung in einen prädiktiven Rahmen wurde ein dynamisches kinetisches Modell für das chemolithoautotrophe Wachstum und die PHB-Produktion von *C. necator* DSM 544 entwickelt und in SuperPro Designer® implementiert, wobei Monod-Kinetiken (μ_{max} = 0,09 h^{-1}) mit experimentell ermittelter Stöchiometrie kombiniert wurden. Die Modellvalidierung anhand von Batch-Fermentationsdaten reproduzierte das Biomassewachstum (End-CDW ~13–14 g L^{-1}), die PHB-Akkumulation (72% des CDW) sowie den Ammoniumverbrauch über 142 Stunden präzise. Sensitivitätsanalysen zeigten, dass biologische Parameter (μ_{max}, α) nur geringe Variationen im CDW (±5,1%) verursachten, während die Belüftungsrate ein kritisches Schwellenverhalten unterhalb von 0,25 vvm aufwies, bei dem starke Sauerstofflimitierung zu vernachlässigbarem Wachstum führte (von 13,8 auf 0,047 g L^{-1}). Scale-up-Simulationen von 1,27 L auf 12,8 L bewahrten Konzentrationsprofile und Produktivität (~0,078 g L^{-1} h^{-1}), während die Gesamt-PHB-Produktion proportional anstieg (0,014 auf 0,139 kg pro Batch), was die kinetische Skalierbarkeit, jedoch keine Verbesserung der Prozessintensität zeigt.

Die Ergebnisse dieser Arbeit zeigen, dass eine sichere und effiziente CO_2-Biokonversion durch integrierte ingenieurtechnische Strategien erreicht werden kann, einschließlich nicht-explosiver Betriebsweisen, membranbasierter Gaszufuhr und Prozessmodellierung. Die Kombination experimenteller Validierung und simulationsgestützter Analyse liefert einen Rahmen für die Übertragung von Gasfermentation vom Labormaßstab auf skalierbare Systeme und identifiziert den Gas-Flüssig-Stoffübergang sowie die Prozesssicherheit als zentrale Einschränkungen. Insgesamt tragen diese Ergebnisse zur Entwicklung robuster und wirtschaftlich tragfähiger Bioprozesse für die nachhaltige Produktion von Biopolymeren und hochwertigen Chemikalien aus gasförmigen Substraten bei.

Table of contents

1 General introduction 1
1.1 Microbial valorization of CO_2 for a climate-neutral economy 1
1.2 Value-added products from *C. necator* CO_2 conversion 2
1.3 Energy metabolism in *C. necator* 5
1.4 Bioreactors and gas fermentation challenges 11
1.4.1 Definition of a bioreactor 11
1.4.2 Challenges in gas fermentation 11
1.4.3 Quantitative description of gas transfer 12
1.4.4 Role of stirred-tank reactors in addressing gas fermentation challenges 13
1.4.5 Safe operation of gas fermentation process 14
1.4.6 Additional process limitations in gas fermentation 15
1.5 Gas fermentation using membrane technology 17
1.6 Indirect CO_2 conversion using the concept of biorefinery 19
1.7 Downstream processing 21
1.8 Process modelling and scale-up considerations for gas fermentation 23
1.9 Aim and objectives of research 25
2 Materials and methods 28
2.1 Chemicals and reagents 28
2.2 Strains 28
2.2.1 Reference and production strains 28
2.2.2 Hydrogenase knockout strain set 29
2.3 Culture media 30
2.4 Investigation of hydrogenase-dependent energy metabolism 31
2.4.1 Growth experiments of hydrogenase knockout strains 32
2.4.2 Isothermal microcalorimetry 32
2.5 Set-up for gas fermentation 33
2.5.1 DURAN flask bioreactor 33
2.5.2 Stirred-tank bioreactor 36
2.6 Chemolithoautotrophic growth of *C. necator* DSM 544 on $CO_2/H_2/O_2$ 39
2.7 Set-up for membrane integrated gas fermentation 40
2.7.1 Reactor configuration and gas delivery 40
2.7.2 Volumetric mass transfer coefficient (k_La) determination 41
2.8 Growth of *C. necator* H16 expressing imine reductase (IRED) 42
2.8.1 Construction of *C. necator* H16 expressing IRED 42

2.8.2 Whole-cell biotransformation for pyrrolidine production 43
2.9 Downstream processing 44
2.10 Quantification of products 45
2.10.1 Quantification of poly(3-hydroxybutyrate) (PHB) by GC–FID 45
2.10.2 Qualitative characterization of PHB by ^{1}H NMR spectroscopy 46
2.10.3 Quantification of 2-methylpyrrolidine by GC–FID 47
2.11 Heterotrophic growth of *C. necator* DSM 544 on lignocellulosic biomasses 47
2.11.1 Biomass feedstocks 47
2.11.2 Preparation and pretreatment of lignocellulosic substrates 48
2.11.3 Enzymatic hydrolysis 49
2.11.4 Filtration of hydrolysed biomass 50
2.11.5 HPLC quantification of sugars and organic acids in hydrolysates 50
2.11.6 Deep-well screening cultivation on lignocellulosic hydrolysates 51
2.11.7 Inhibitor tolerance and substrate utilization assessment design 51
2.11.8 Shake-flask PHB production on selected hydrolysate 51
2.12 Process model development and implementation 52
2.12.1 Kinetic model formulation 53
2.12.2 Stoichiometric modelling 54
2.12.3 Model calibration and validation 55
2.12.4 Sensitivity analysis 56
2.12.5 Scale-up simulation 56
2.12.6 Assumptions and limitations 57
3 Results and discussion 58
3.1 Contribution of soluble and membrane-bound hydrogenases to energy metabolism in *C. necator* 58
3.1.1 Heterotrophic growth of different hydrogenase knockout strains 58
3.1.2 Autotrophic growth of different hydrogenase knockout strains in serum bottles 60
3.1.3 Heat flow and yield associated with chemolithoutotrophic growth of different hydrogenase knockout strains 62
3.1.4 Section summary and outlook 63
3.2 Establishment of stable gas fermentation of *C. necator* 65
3.2.1 Effect of buffer capacity and ammonium concentration on pH stability 66
3.2.2 Stabilization of autotrophic growth via manual pH control 68
3.2.3 Transferability across reactor configurations 70
3.2.4 Process intensification under intrinsically safe conditions 71

3.2.5 Culture robustness during transient CO_2 limitation 72
3.2.6 Structural verification of extracted PHB 73
3.2.7 Section summary 75
3.3 Membrane-integrated gas fermentation for 2-methylpyrrolidine biosynthesis 77
3.3.1 Chemolithoautotrophic growth performance in the membrane mini-fermenter 78
3.3.2 Hydrogen-driven biotransformation 80
3.3.3 Hydrogen mass transfer performance 83
3.3.4 Comparative analysis of membrane-based *C. necator* fermentation platforms. 84
3.3.5 Section summary 87
3.4 Utilization of lignocellulosic biomass hydrolysates for growth and PHB production 88
3.4.1 Biomass composition as basis for process evaluation 88
3.4.2 Effects of steam explosion pretreatment on biomass composition 89
3.4.3 Enzymatic hydrolysis performance and inhibitor formation 92
3.4.4 Growth of *C. necator* DSM 544 on lignocellulosic hydrolysates 94
3.4.5 PHB production from wheat straw hydrolysate A3 96
3.4.6 Section summary 98
3.5 Process modelling and simulation-guided evaluation of gas fermentation by *Cupriavidus necator* 99
3.5.1 Model validation against experimental data 100
3.5.2 Sensitivity analysis of model parameters and operating conditions 100
3.5.3 Scale-up assessment from laboratory to pilot scale 103
3.5.4 Section summary 104
4 General discussion 106
References 112
Supplementary information 127

List of figures

Figure 1.1: Pathways of carbon metabolism in *C. necator*. 6

Figure 1.2: Overview of energy metabolism in *C. necator* 7

Figure 1.3: Structural organization of the catalytic core of SH, MBH and RH in C. Necator .. 8

Figure 1.4: Stirred-tank bioreactor configuration 11

Figure 1.5: Gas fermentation set-ups across scales. 16

Figure 2.1: Schematic of the gas supply and reactor setup for 1L Duran flask 35

Figure 2.2: Schematic of the gas supply and reactor setup for 1.2 L Labfors reactor 38

Figure 2.3: Schematic of membrane-integrated mini-fermenter set-up 41

Figure 2.4: Workflow for PHB extraction using 1,3-dioxolane 45

Figure 2.5: Superpro Designer flowsheet for batch gas fermentation process 52

Figure 3.1: Heterotrophic growth of hydrogenase knockout strains in 20 ml pioreactors. 60

Figure 3.2: Autotrophic growth of *C. necator* hydrogenase knockout strains..... 62

Figure 3.3: Heat yield of *C. necator* hydrogenase knockout strains..... 63

Figure 3.4: Growth of *C. necator* DSM 544 in a DURAN flask. 68

Figure 3.5: Cultivation of *C. necator* DSM 544 under $H_2/CO_2/O_2$ conditions in a 1.2 L bioreactor 70

Figure 3.6: Growth of *C. necator* DSM 544 under $H_2/CO_2/O_2$ conditions in a stirred-tank bioreactor 71

Figure 3.7: Intensified Cultivation 6 of *C. necator* DSM 544 73

Figure 3.8: ^{1}H NMR spectra (80 mhz) of PHB extracted using 1,3-dioxolane 75

Figure 3.9: Dissolved gas profiles and growth curves from duplicate membrane-integrated *C. necator* cultivations..... 79

Figure 3.10: Time-course of 2-methylpyrrolidine production by *C. necator* 83

Figure 3.11: Growth of *C. necator* strain DSM 544 on different hydrolysates. 96

Figure 3.12: Effect of glucose and inhibitor concentration on the growth of *C. necator* 96

Figure 3.13: Growth and PHB production on wheat straw hydrolysate 97

Figure 3.14: Sugar and organic acid concentrations before and after fermentation 97

Figure 3.15: Validation and sensitivity analysis of *C. necator* gas fermentation model. 102

List of tables

Table 1.1: Properties of PHB compared to PP and PE 4

Table 1.2: Summarized comparison of the features of SH, MBH and RH 9

Table 2.1: Summary of reference and production strains 29

Table 2.2: Hydrogenase strain set used in this study 29

Table 2.3: Mineral media composition for the chemolithoautotrophic cultivation. 30

Table 2.4: Variations of the standard mineral medium used 31

Table 2.5: Steam explosion conditions for biomasses 49

Table 3.1: Volumetric mass transfer coefficient for hydrogen for mini-fermenter 84

Table 3.2: Key performance indicators for membrane-based gas fermentation 86

Table 3.3: Composition of biomasses before (in bold) and after pretreatment 91

Table 3.4: Sugar monomers, organic acids, furfural and HMF in the filtrates 93

Table 3.5: Comparison of process performance at laboratory and pilot Scale 104

List of abbreviations

ADP – Adenosine diphosphate
AH – Actinobacterial hydrogenase
ATEX – Atmosphères Explosibles (explosive atmospheres directive)
ATP – Adenosine triphosphate

CBB – Calvin–Benson–Bassham (cycle)
CCU – Carbon capture and utilization
CDW – Cell dry weight
CO – Carbon monoxide
CO_2 – Carbon dioxide

DO – Dissolved oxygen

ED pathway – Entner–Doudoroff pathway
EMP pathway – Embden–Meyerhof–Parnas pathway
ETC – Electron transport chain

GC–FID – Gas chromatography–flame ionization detection

H_2 – Hydrogen
HMF – Hydroxymethylfurfural
HOB – Hydrogen-oxidizing bacteria
HPLC – High-performance liquid chromatography
HTR – Hydrogen transfer rate

IARC – International Agency for Research on Cancer
IRED – Imine reductase

k_La – Volumetric mass transfer coefficient

LEL – Lower explosion limit

MBH – Membrane-bound hydrogenase

NAD^+ – Nicotinamide adenine dinucleotide (oxidized form)
NADH – Reduced nicotinamide adenine dinucleotide
NMR – Nuclear magnetic resonance
^1H NMR – Proton nuclear magnetic resonance

O_2 – Oxygen
OD600 – Optical density at 600 nm
OUR – Oxygen uptake rate

pH – Potential of hydrogen
PHA – Polyhydroxyalkanoate
PHB – Poly(3-hydroxybutyrate)
PHBHHx – Poly(3-hydroxybutyrate-co-3-hydroxyhexanoate)
PMF – Proton motive force

PP – Polypropylene
ppm – Parts per million

RAMOS – Respiration Activity Monitoring System
RH – Regulatory hydrogenase
rpm – Revolutions per minute
RuBisCO – Ribulose-1,5-bisphosphate carboxylase/oxygenase
RuBP – Ribulose-1,5-bisphosphate

SH – Soluble hydrogenase

Tg – Glass transition temperature
Tm – Melting temperature

v/v – Volume per volume
vvm – Volumes of gas per volume of liquid per minute

w/v – Weight per volume
WT – Wild type

1 General introduction

1.1 Microbial valorization of CO_2 for a climate-neutral economy

Anthropogenic CO_2 emissions are among the main drivers of climate change, accounting for approximately 76% of total global greenhouse gas emissions in 2025 (European Environment Agency, 2025). The concentration of CO_2 in the atmosphere has reached a record high of about 429.6 parts per million (ppm), levels not seen in over 2 million years (Down to Earth, 2025). In response, the European Green Deal sets a legally binding target of climate neutrality by 2050, implying deep reductions of greenhouse gas emissions and widespread adoption of carbon capture and utilization (CCU) technologies (European Commission, 2019). Biological CO_2 conversion using microorganisms offers a promising and flexible route to close the carbon cycle under mild conditions.

Hydrogen-oxidizing bacteria (HOBs), often referred to as Knallgas bacteria, oxidize H_2 to generate ATP and reducing power, with O_2 as the final electron acceptor for CO_2 fixation through the Calvin–Benson–Bassham (CBB) cycle (Lu & Yu, 2017). In contrast to photosynthetic organisms, CO_2 fixation in these microorganisms is independent of light, enabling faster growth and higher carbon conversion efficiency (Hreggvidsson et al., 1995; Nishihara et al., 1991). High growth rates have been reported for thermophilic *Hydrogenophilus thermoluleotus TH-1* (0.68 h^{-1}), *Hydrogenobacter thermophilus* (0.33 to 0.42 h^{-1}), *Hydrogenovibrio marinus* (0.6 to 0.7 h^{-1}), mesophilic *Cupriavidus necator* (0.42 h^{-1}) and *Xanthobacter autotrophicus* (0.2 h^{-1}) under chemolithoautotrophic conditions (Kawasumi et al., 1984; Nguyen et al., 2019; Nishihara et al., 1991; Tanaka et al., 1995; Vijayendran, 2023; Wilde & Schlegel, 1982). These rates place Knallgas bacteria among the fastest-growing autotrophs, giving them a clear advantage in scalability and volumetric productivity.

The commercial relevance of HOB-based gas fermentation is already evident. Several technology-driven enterprises such as Solar Foods (Finland), Silantes GmbH (Germany),

COLIPI (Germany), Kiverdi (USA), and Econutri (Austria) are applying gas fermentation to produce single-cell protein, feed and food or bio-based chemicals from CO_2.

An alternative microbial route involves acetogenic bacteria that operate anaerobically via the Wood–Ljungdahl pathway to convert CO_2 or CO with H_2 into reduced carbon compounds. Companies like LanzaTech (USA) have commercialized acetogenic fermentation for ethanol and other bulk chemicals (Liew et al., 2022). However, poor gas-liquid mass transfer also limits cell productivity, titers, and yields (Sun et al., 2019; Elisiário et al., 2022).

In this technological landscape, *C. necator* stands out as a leading platform for CO_2 valorization. It combines robust autotrophic growth on $H_2/CO_2/O_2$ gas mixtures with heterotrophic versatility, tolerance to complex feedstocks like lignocellulosic hydrolysates, and advanced genetic engineering tools. These attributes make *C. necator* an ideal model organism for developing efficient, safe, and adaptable CCU bioprocesses which is the focus of this thesis.

1.2 Value-added products from *C. necator* CO_2 conversion

Intracellular biopolymer poly(3-hydroxybutyrate) (PHB) serves as a carbon and energy storage compound during nutrient limitation, particularly nitrogen depletion. Native strains can accumulate PHB up to ~80–90% of cell dry weight while maintaining high CO_2 fixation efficiency (Lambauer & Kratzer, 2022). PHB is a biodegradable and biocompatible thermoplastic exhibiting mechanical properties similar to its petroleum counterparts, making it one of the most established bioplastic alternatives derived directly from CO_2 (Scheme 1a) (Bugnicourt et al., 2014; Koller et al., 2017a). From an application perspective, PHB exhibits material properties broadly comparable to commodity thermoplastics such as polypropylene (PP) and polyethylene (PE) (Table 1.1), while additionally offering complete biodegradability under environmental conditions (Li et al., 2025a; Turco et al., 2021). These characteristics, combined with superior O_2 and water vapor barrier properties, position PHB for packaging,

agricultural films, biomedical scaffolds, and drug delivery (Li et al., 2025a; Paloyan et al., 2025).

To improve PHB's brittleness, metabolic engineering produces copolymers like poly(3-hydroxybutyrate-co-3-hydroxyhexanoate) (PHBHHx) with enhanced flexibility (Miyahara et al., 2021), and poly(D-lactate-co-3-hydroxybutyrate) for tunable properties (Koh et al., 2024). In the environment, PHB undergoes relatively fast enzymatic biodegradation by microbial extracellular and intracellular depolymerases from bacteria and fungi, which hydrolyze the polyester backbone into water-soluble oligomers and monomers subsequently mineralized to CO_2 (aerobic) or CO_2/CH_4 (anaerobic). Degradation timelines vary by conditions: complete breakdown occurs in 2–6 weeks in moist soil (25°C, high microbial activity), 1–3 months in compost, but extends to 6–12 months in marine or low-humidity environments. This contrasts sharply with non-biodegradable petroleum plastics, enabling true circularity for CO_2-derived PHB (Julinová et al., 2023; Paloyan et al., 2025; Li et al., 2019).

Beyond its native PHB metabolism, *C. necator* has been engineered to produce a rapidly expanding portfolio of bulk and specialty chemicals directly from CO_2. Examples include single cell proteins, arginine, 1,2-propanediol, methyl ketones, α-humulene, isopropanol and octanol (Lauterbach and Lenz, 2019; Novak et al., 2025; Schoenmakers et al., 2025). In addition, *C. necator* can be used for H_2-driven reductive whole-cell biocatalysis, coupling its hydrogen-oxidizing metabolism to the stereoselective synthesis of pharmaceutical precursors. N-heterocycles represent critical scaffolds in ~70% of agrochemicals and >80% of recently approved drugs (2013–2023), up from 59% historically, driving demand for green synthetic routes. Imine reductases (IREDs) catalyze asymmetric reductive amination of imine precursors to chiral amines, which are key intermediates for these heterocycles offering high enantioselectivity under ambient conditions with broad substrate tolerance (Vitaku et al., 2014; Aleku, 2024; Gotor-Fernández and Gotor, 2020).

Conventional whole-cell IRED systems in *Escherichia coli* depend on glucose-fueled NADPH regeneration, constraining scalability and sustainability (Borlinghaus et al., 2019; Gand et al., 2016). *C. necator* provides a chemolithoautotrophic platform in which H_2 oxidation supplies reducing equivalents for NAD(P)H-dependent reactions, independent of organic carbon inputs. This enables carbon-neutral biotransformations using only renewable gases (H_2, CO_2, O_2). In addition, *C. necator* derives reducing power from H_2 oxidation via the respiratory chain, but NADPH-dependent reactions require additional redox balancing. Its genome contains four putative proton translocating transhydrogenase gene regions (PntA1, PntA2, PntA3, and PntA4), which help convert NADH into NADPH as needed for biosynthesis. Proof-of-concept studies have demonstrated heterologous IRED-mediated imine reduction and diamine oxidase–IRED cascades yielding N-heterocycles such as 2-methylpyrrolidine from 2-methyl-1-pyrroline (Scheme 1b), positioning *C. necator* as a versatile chassis for high-value chemical manufacturing from inorganic feedstocks (Cramm, 2009; Schoenmakers et al., 2026).

Table 1.1: Properties of PHB compared to PP and PE

Property	PHB	PP	PE
Density (g cm^{-3})	1.23	0.90	0.91–0.96
Glass transition, Tg (°C)	4–7	−10	< −30
Melting temperature, Tm (°C)	170–180	160–170	110–135
Tensile strength (MPa)	20–30 (brittle)	25–35	10–30
Elastic/Young's modulus (GPa)	3	1–1.5	0.2–1
Elongation at break (%)	3–5 (brittle)	>200	>100
Gas barrier to O_2/H_2O	very good	moderate	moderate
Biodegradability	biodegradable	not biodegradable	not biodegradable

(Source: Bugnicourt et al., 2014; Koller et al., 2017a; Li et al., 2025a; Turco et al., 2021)

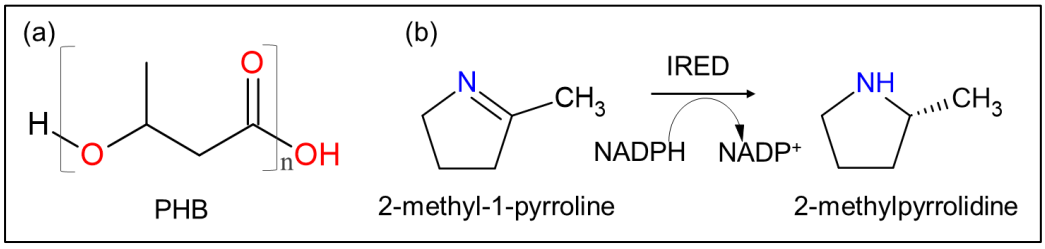

Scheme 1: Structures of (a) the PHB monomer repeat unit produced natively by *C. necator* and (b) (R)-2-methylpyrrolidine as an example of N-heterocycles

In this thesis, PHB and 2-methylpyrrolidine were selected as representative products of CO_2 conversion by *C. necator*. PHB exemplifies native storage polymer formation, whereas 2-methylpyrrolidine demonstrates the integration of H_2-driven redox metabolism with heterologous whole-cell biocatalysis for high-value chemical synthesis. As product yields and overall H_2 utilization efficiency ultimately depend on how electrons from H_2 oxidation are distributed between energy conservation and biosynthesis, the next section focuses on the energy metabolism that governs these conversion pathways.

1.3 Energy metabolism in *C. necator*

Unlike many heterotrophic bacteria, *C. necator* relies predominantly on the Entner–Doudoroff (ED) pathway (Figure 1.1) for carbohydrate metabolism. The oxidative pentose phosphate pathway contributes to redox balancing. Together, these pathways enable efficient sugar catabolism and supply pyruvate for biosynthesis and PHB production. This architecture allows seamless metabolic transitions between heterotrophic, mixotrophic, and autotrophic growth modes, since both sugar-based and H_2-driven metabolism converge at shared intermediates such as NAD(P)H, ATP, and acetyl-CoA (Lopar et al., 2014; Jahn et al., 2024; Ding et al., 2025).

For chemolithoautotrophic growth, *C. necator* derives reducing power and cellular energy from hydrogen oxidation, which drives CO_2 fixation via the Calvin–Benson–Bassham (CBB) cycle (Figure 1.1). H_2 serves as the electron donor, CO_2 as the sole carbon source, and O_2 as the terminal electron acceptor (Cramm, 2009; Lauterbach & Lenz, 2019; Bansal et al., 2026). Electrons released from hydrogen oxidation reduce NAD^+ and quinones, while proton translocation across the inner membrane generates ATP through oxidative phosphorylation. This tightly coupled metabolism enables efficient CO_2 assimilation and underpins the organism's high growth rate and suitability as a gas-fermentation chassis.

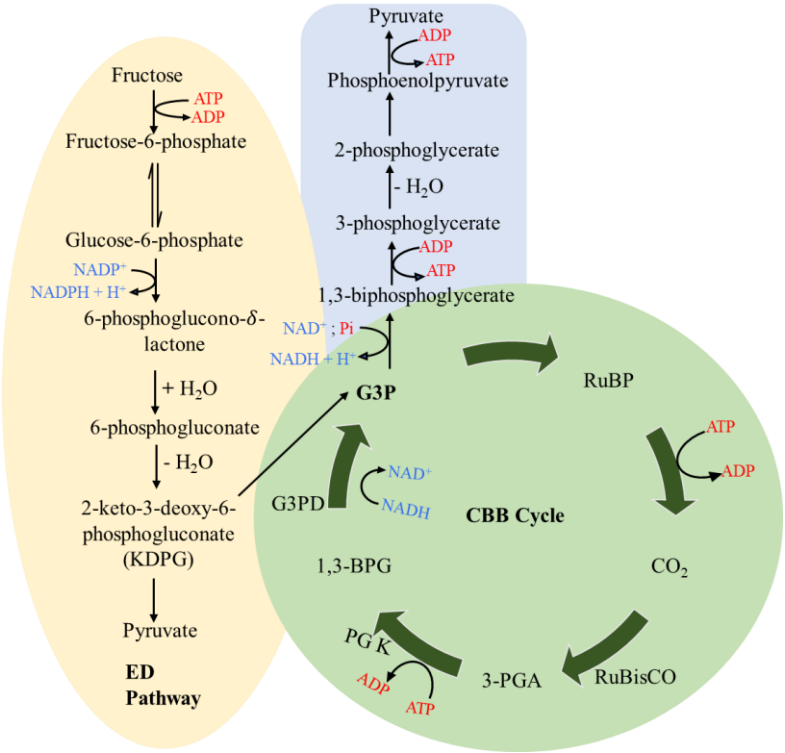

Figure 1.1: Pathways of carbon metabolism in *C. necator*. RuBisco: ribulose-1,5-biphosphate carboxylase/oxygenase; 3-PGA: 3-phosphogycerate; PGK: phosphoglycerate kinase; 1,3-BPG: 1,3-biphosphateglycerate; G3PD: glyceraldehyde-3-phosphate dehydrogenase; NADH: reduced nicotinamide adenine dinucleotide; NAD^+: nicotinamide adenine dinucleotide; ADP: adenosine diphosphate; ATP: adenosine triphosphate; G3P: glyceraldehyde-3-phosphate; RuBP: ribulose-1,5-biphosphate (adapted from Bansal et al., 2026, licensed under CC BY 4.0.)

The overall energy metabolism of *C. necator* during chemolithoautotrophic growth is illustrated in Figure 1.2. Hydrogen oxidation is mediated by a suite of [NiFe]-hydrogenases with distinct roles and cellular localizations. The soluble hydrogenase (SH) is located in the cytosol, where it reduces NAD^+ to NADH, supplying reducing power for biosynthesis and CBB cycle activity. Notably, the SH of *C. necator* is oxygen-tolerant, it detoxifies itself by converting O_2 primarily to water (and minor H_2O_2) using electrons from H_2 or NADH (Lauterbach and Lenz., 2013). The membrane-bound hydrogenase (MBH) donates electrons directly to the quinone pool of the respiratory chain, contributing to proton motive force generation and ATP synthesis. The regulatory hydrogenase (RH) functions primarily as a hydrogen sensor, modulating expression of hydrogenase genes, while the function of actinobacterial hydrogenase (AH) is not completely known (Cramm, 2009). Together, these

enzymes ensure flexible and efficient partitioning of electron flux between NADH production and ATP generation.

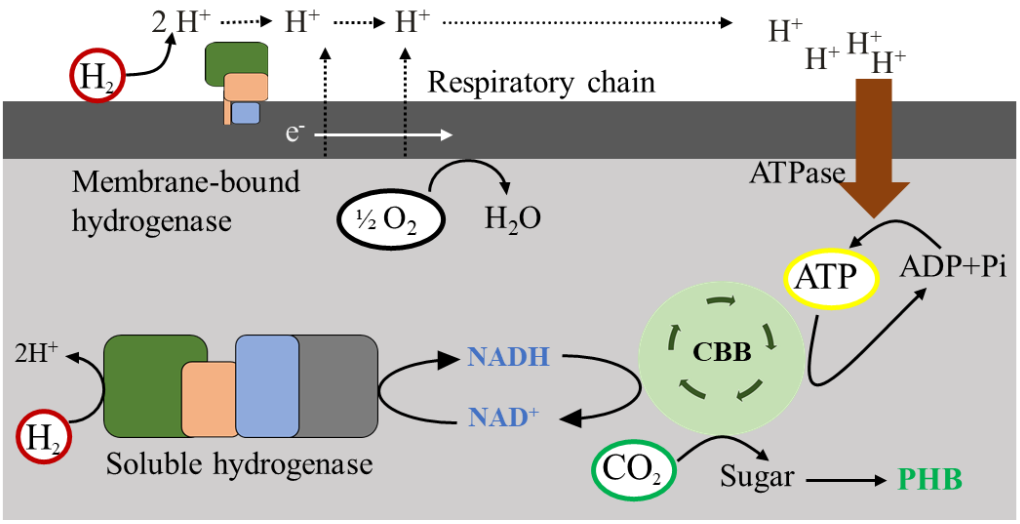

Figure 1.2: Overview of energy metabolism in *C. necator* (adapted from Alhafiz et al., 2025a, with permission from Elsevier)

The relative activities of SH and MBH determine the distribution of electrons derived from hydrogen oxidation. When SH activity predominates, electrons are transferred to NAD^+, generating reducing equivalents that support PHB biosynthesis, particularly under nitrogen-limited conditions. In contrast, when MBH activity dominates, electrons are fed into the respiratory chain, enhancing proton motive force generation and ATP production to support biomass formation. The structural organization of the catalytic cores of SH (hoxFUYH), MBH (hoxKGZ), and RH (hoxBC) are distinct. As shown in Figure 1.3, electron is transferred from left to right from the Ni-Fe active site to the corresponding electron transfer modules SH and MBH, ultimately leading to NAD^+ reduction in SH and entry into the respiratory chain for MBH. For RH, electron transfer starts from the Ni-Fe active site within the HoxBC module, with an additional phosphorylation-based signaling through the HoxJ-HoxA two-component system, which activates hydrogenase gene transcription (Cramm, 2009; Lauterbach & Lenz, 2019; Fan et al., 2022; Jahn et al., 2021; Teramoto et al., 2022).

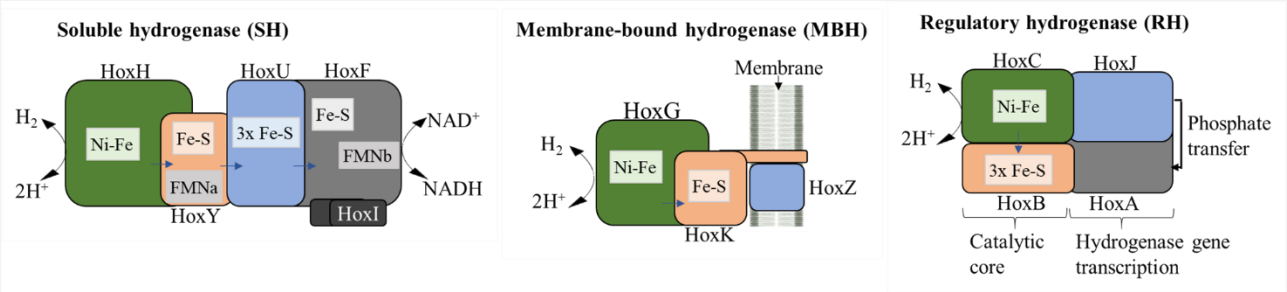

Figure 1.3: Structural organization of the catalytic core of SH, MBH and RH in *C. necator* (adapted from Lenz et al., 2018, with permission from Elsevier)

Hydrogenase maturation in *C. necator* is a highly coordinated process involving Hyp-encoded accessory proteins and Hox-regulated assembly factors. The large and small subunits of SH and MBH are synthesized separately, after which Hyp proteins catalyze insertion of the $NiFe(CN)_2CO$ cofactor into the large subunit and coordinate incorporation of iron–sulfur clusters into the small subunit. Nickel transporters near the maturation operons supply the required metal ions. While SH remains cytosolic to transfer electrons to NAD^+, MBH undergoes C-terminal processing and is translocated via the Tat pathway to the cytoplasmic membrane, where it participates in respiratory electron transfer and ATP generation. The regulatory hydrogenase (RH), which senses environmental hydrogen, follows a similar maturation pathway but functions primarily as a signal transducer (Fan et al., 2022; Jahn et al., 2024; Schiffels et al., 2013; Teramoto et al., 2022; Hartmann et al., 2020; Dragelj et al., 2023; Jugder et al., 2015). A comparative overview of SH, MBH, and RH, including operon organization, catalytic subunits, localization, electron acceptors, and physiological roles, is provided in Table 1.2.

Table 1.2: Summarized comparison of the features of SH, MBH and RH

Feature	SH	MBH	RH
Catalytic subunit	HoxH [NiFe]	HoxG [NiFe]	HoxC [NiFe]
Electron relay	HoxYH (Fe-S); HoxFU (FMN); HoxI (hexameric form)	HoxK (Fe-S); HoxZ (cyt b)	HoxB (Fe-S)
Localization	Cytosolic	Membrane (periplasmic)	Cytosolic
Acceptor	NAD^+ to NADH	Quinone pool	Unknown
Primary role	Redox power	Respiration (ATP generation)	H_2 sensing and transcriptional regulation

Hydrogenase gene expression is regulated by the HoxJ–HoxA two-component system. In the absence of H_2, HoxJ autophosphorylates and transfers the phosphoryl group to HoxA, resulting in an inactive HoxA. In the presence of H_2, this phosphotransfer is blocked, so HoxA remains active and stimulates σ^{54}-dependent transcription of the SH and MBH operons (Friedrich et al., 2005). Another study suggests that HoxJ integrates H_2 signal sensing and transduction and is also involved in global regulation, with its activity influenced by O_2 and possibly additional physiological factors such as the cellular carbon/energy state (Lenz et al., 2002; Friedrich et al., 2005). This compact regulatory architecture enables rapid metabolic response to H_2 availability. In the wild-type H16 strain, a serine replacement for a conserved glycine residue in the HoxJ G2 motif reduces autophosphorylation efficiency and results in constitutive, H_2-insensitive expression. Restoring the glycine residue (Ser422→Gly, HoxJ*) reinstates strong, H_2-dependent induction, improving regulatory responsiveness and optimizing resource allocation under H_2-rich conditions (Lenz & Friedrich, 1998; Jespersen et al., 2025).

Proteomic and transcriptomic analyses show that *C. necator* dynamically remodels its electron transport chain according to the dominant hydrogenase and growth condition. During SH-driven metabolism, when NADH is required for PHB formation, the organism upregulates

NADH dehydrogenase (Complex I, nuo), the cytochrome bc1 complex (qcrABC), and the cbb3-type terminal oxidase (ccoGNOP), supporting redox balance and polymer synthesis. Under MBH, ATP-demanding conditions, electrons are channelled into oxidative phosphorylation via ubiquinone-dependent respiratory pathways and terminal oxidases. Cramm (2009) reported that *C. necator* encodes five quinol oxidases and three cytochrome oxidases, and showed that bd-type oxidase activity increases under oxygen limitation, while cbb3 is a plausible low-oxygen oxidase. More recent transcriptomic and proteomic analyses refined this picture by showing that the low O_2-affinity aa3 complex is preferred during heterotrophic growth, whereas the high O_2-affinity cbb3 complex is preferred during formatotrophic growth (Cramm, 2009; Jahn et al., 2021; Jahn et al., 2024; Kitagawa et al., 2025; Gemünde et al., 2024).

The distinct redox properties of SH and MBH govern both the direction and energetic outcome of H_2 oxidation in *C. necator*. SH transfers electrons from H_2 ($E_0' \approx$ -414 mV) directly to NAD^+ ($E_0' \approx$ -320 mV), generating NADH for biosynthesis. MBH transfers electrons to the quinone pool, from which they can enter the respiratory chain and support proton motive force formation and ATP synthesis. When reducing power is needed under MBH-dominated metabolism, NADH must be regenerated from quinol by reverse electron transfer through Complex I, which consumes energy. Thus, SH-linked H_2 oxidation directly supplies reducing equivalents, whereas MBH-linked H_2 oxidation primarily supports respiration and may require additional energetic investment to provide NADH (Cramm, 2009; Fan et al., 2022).

Despite extensive biochemical and genetic characterization of *C. necator*'s hydrogenases, quantitative insights into how SH and MBH-driven electron fluxes translate into overall energy efficiency remain limited. Understanding how these hydrogenases shape the organism's energetic landscape is therefore essential for interpreting growth efficiency and product formation under $CO_2/H_2/O_2$ cultivation conditions.

1.4 Bioreactors and gas fermentation challenges

1.4.1 Definition of a bioreactor

A bioreactor is a controlled cultivation vessel designed to provide a defined physical and chemical environment for microbial growth and product formation. In typical systems, key features include the reactor vessel, agitation provided by impellers, and gas spargers that introduce gaseous substrates into the liquid phase. Baffles are installed to improve mixing by disrupting circular flow patterns, while additional control systems regulate temperature, pH, and pressure. Online sensors enable real-time monitoring of parameters such as dissolved oxygen, pH, and foam (Figure 1.4). Together, these components ensure a homogeneous culture environment and enable controlled bioprocess operation (Martens et al., 2014; Chisti & Moo-Young, 2003).

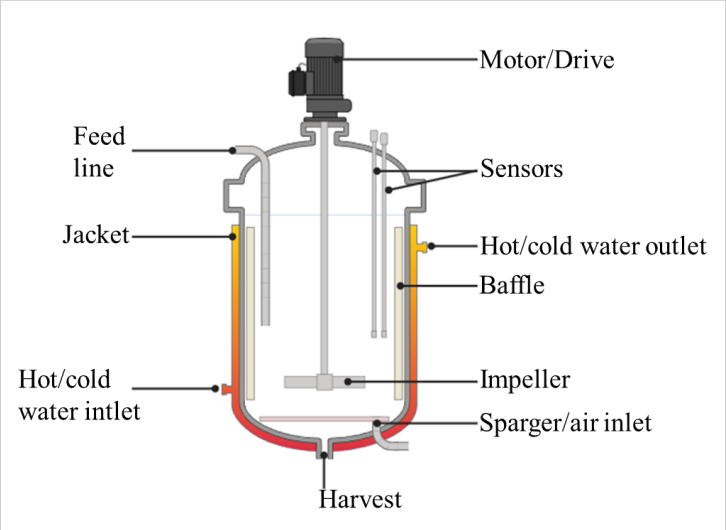

Figure 1.4: Stirred-tank bioreactor configuration (created in biorender.com)

1.4.2 Challenges in gas fermentation

Gas fermentation processes based on substrates such as H_2, CO_2, and O_2 enable the direct microbial conversion of inorganic carbon into biomass and value-added products. However,

compared to conventional liquid-phase fermentations, these systems present two major challenges: explosion risk and limited gas–liquid mass transfer.

The simultaneous presence of H_2 and O_2 introduces significant safety concerns. H_2 - O_2 mixtures exhibit extremely wide flammability limits, ranging from approximately 4–75% (v/v) H_2 in air, and possess very low minimum ignition energies (~0.02 mJ), making even minor process deviations potentially hazardous (Schröder & Holtappels, 2005; Sun, 2017). Within the European regulatory framework, such processes must comply with the ATEX directives 2014/34/EU and 1999/92/EC, which impose strict requirements on equipment design, instrumentation, and operation (Lambauer & Kratzer, 2022; Zhang et al., 2022).

In addition to safety constraints, gas fermentation is fundamentally limited by the low aqueous solubility of gaseous substrates. At 25 °C and atmospheric pressure, H_2 exhibits particularly low solubility (~0.78 mM), followed by O_2 (~1.26 mM), while CO_2 is comparatively more soluble (~34.1 mM). As a result, the transfer of H_2 from the gas to the liquid phase often becomes rate-limiting for microbial metabolism. Consequently, process performance depends on whether gas transfer can keep pace with microbial substrate uptake (Garcia-Ochoa & Gómez, 2009; Lambauer et al., 2023).

1.4.3 Quantitative description of gas transfer

The efficiency of gas–liquid mass transfer in bioreactors is commonly described by the volumetric mass transfer coefficient, k_La, which represents a key performance parameter in bioprocess engineering. Conceptually, k_La combines the liquid-side mass transfer coefficient (k_L), which reflects diffusion across the liquid boundary layer, with the interfacial area (a), representing the available gas–liquid contact surface per unit volume.

In practical terms, k_La defines the capacity of a bioreactor to supply gaseous substrates to the culture. For efficient operation, the gas transfer rate must exceed the microbial uptake rate; otherwise, substrate limitation will occur, leading to reduced growth and productivity (Inam et al., 2022; Zhu et al., 2022).

1.4.4 Role of stirred-tank reactors in addressing gas fermentation challenges

In gas fermentation, reactor design is critical because the conversion of gaseous substrates depends not only on microbial metabolism but also on efficient gas–liquid mass transfer. Accordingly, sufficient transfer rates must be maintained to meet cellular demand, typically quantified by k_La, which represents a key parameter for reactor performance and scale-up, as it defines the capacity of the system to supply gaseous substrates to the culture.

Figure 1.5 presents typical gas fermentation setups across different scales, ranging from a mini-fermenter (20–30 mL; Figure 1.5A) to 1.2 L (Figure 1.5B), 7.5 L (Figure 1.5C), and 10 L fermenters (Figure 1.5D). This progression illustrates the increasing complexity of reactor design, including gas delivery systems, process control, and safety measures required for handling reactive gas mixtures. In particular, maintaining safe operating conditions becomes increasingly demanding at larger scales, where precise control of gas composition and mass transfer is essential (Alhafiz et al., 2025a).

In stirred-tank and related gas fermentation systems, reactor design plays a critical role in enhancing gas–liquid mass transfer. Agitation provided by impellers promotes mixing and reduces boundary layer thickness, thereby increasing k_L. Gas spargers generate fine bubbles, maximizing interfacial area (a), while baffles improve flow patterns and bubble dispersion. These features collectively enhance k_La and support substrate availability for microbial growth.

However, achieving high mass transfer rates typically requires elevated agitation speeds, increased gas flow rates, or pressurization, which can significantly increase energy demand and mechanical complexity. In addition, conventional sparging systems involve direct mixing of hydrogen and oxygen in the gas phase, which poses inherent safety risks under certain operating conditions (Lambauer et al., 2023; Vlaeminck et al., 2024).

1.4.5 Safe operation of gas fermentation process

To mitigate explosion risks, gas fermentation processes are commonly operated under O_2-limited conditions, ensuring that the O_2 fraction in the gas phase remains below the lower explosion limit (LEL), although operation under H_2-limited conditions (< 3.8% v/v H_2) provides an alternative to prevent the formation of flammable mixtures. Conservative assessments place the LEL for H_2–O_2 mixtures at approximately 4.3% (v/v) O_2, requiring strict control of inlet gas composition and reactor headspace to prevent the formation of flammable mixtures (Schröder & Holtappels, 2005; Alhafiz et al., 2025a). It is important to clearly distinguish between the O_2 concentration in the gas phase and dissolved oxygen (DO) in the liquid phase, as these parameters are often mistakenly confused. Explosion limits are defined based on the gas-phase composition, not the dissolved oxygen concentration.

In the present system, low dissolved O_2 levels (<4%, typically around 2% air saturation) are maintained in the liquid phase. However, achieving these DO levels required relatively high O_2 fractions in the inlet gas stream, in some cases up to 28% (v/v). This discrepancy arises from limited gas–liquid mass transfer, particularly at low k_La values, such that high gas-phase O_2 concentrations are necessary to sustain sufficient O_2 supply for rapidly growing cells.

Consequently, despite low DO levels in the liquid phase, the reactor is operated within an explosive regime (ATEX zone 0), as the gas-phase composition exceeds the LEL. This highlights the fundamental decoupling between liquid-phase oxygen availability and gas-phase

explosion risk, and underscores the importance of considering both parameters independently when designing and operating gas fermentation systems.

Despite these constraints, high productivity can be achieved if gas transfer is sufficiently intensified. Elevated k_La values enable adequate substrate supply even at low O_2 concentrations, although this often comes at the cost of increased energy input and system complexity. Therefore, reactor design and operating strategy must carefully balance safety, efficiency, and biological performance (Lambauer et al., 2023).

1.4.6 Additional process limitations in gas fermentation

Beyond gas transfer and safety considerations, process stability represents an additional challenge in autotrophic cultivation of *C. necator*. Rapid medium acidification frequently occurs, leading to growth inhibition and reduced product yields. This effect is particularly pronounced in glucose-utilizing strains, where conventional phosphate buffer systems are often insufficient to maintain stable pH, even at high concentrations (Lambauer et al., 2025).

As a result, active pH control becomes necessary. However, automated pH regulation under explosive conditions requires ATEX-certified pumps and sensors, substantially increasing technical complexity and cost (Lambauer et al., 2023; Lambauer et al., 2025). To address this limitation, manual-based pH control strategies may offer a viable alternative, enabling stable cultivation without automated titration systems. By establishing predictive relationships between base addition and pH response, process stability can be maintained while avoiding the need for explosion-proof liquid-handling equipment.

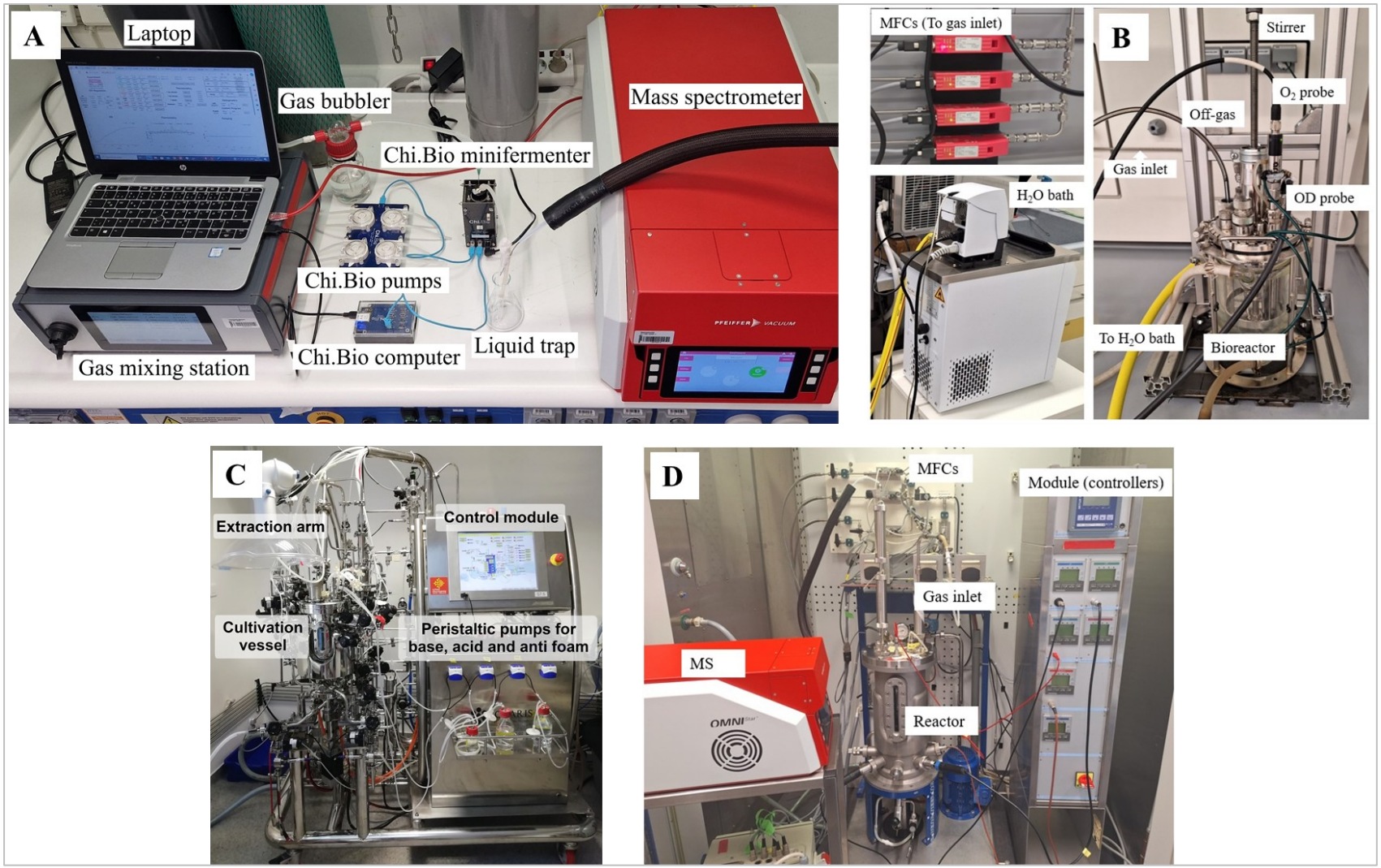

Figure 1.5: Gas fermentation set-ups across scales. (A) 30 mL mini-fermenter; (B) 1.2 L fermenter; (C) 7.5 L fermenter; (D) 10 L fermenter (adapted from Alhafiz et al., 2025a, with permission from Elsevier)

1.5 Gas fermentation using membrane technology

Membrane-based gas delivery systems represent a promising alternative to conventional sparging approaches, addressing both mass transfer limitations and safety concerns. In these systems, gaseous substrates are transferred into the liquid phase via diffusion across gas-permeable membranes, enabling bubble-free mass transfer.

This configuration eliminates direct mixing of H_2 and O_2 in the gas phase, significantly improving operational safety. In addition, membrane systems reduce foaming, mechanical shear stress, and energy demand for agitation, resulting in more stable and efficient process operation (Reij et al., 1998; Elisiário et al., 2022; Bongartz et al., 2021).

From an engineering perspective, gas transfer in membrane systems is governed by membrane surface area, permeability, and concentration gradients rather than by bubble formation and agitation intensity. This enables high mass transfer efficiency at comparatively low gas flow rates, improving substrate utilization and reducing energy consumption. Furthermore, precise control of dissolved gas concentrations enhances process stability and reproducibility under ATEX-relevant conditions (Elisiário et al., 2022; Lambauer et al., 2023).

Recent studies have demonstrated the potential of membrane-integrated reactors for CO_2-based bioprocesses, including improved H_2 utilization, enhanced CO_2 fixation rates, and stable long-term operation. However, important knowledge gaps remain, particularly regarding the performance and scalability of membrane systems for *C. necator* under explosive gas mixtures. Addressing these challenges is essential for establishing membrane-based gas fermentation as a robust platform for sustainable biomanufacturing (Li et al., 2025; Di Bisceglie et al., 2025).

Furthermore, miniaturized fermenter platforms enable systematic investigation of gas fermentation under well-defined and highly controlled conditions, providing a robust experimental basis for understanding mass transfer behaviour, microbial performance, and process stability. The transport principles and operating strategies established in these systems can be directly translated to conventional stirred-tank and larger-scale membrane-integrated reactors, thereby facilitating rational process development and scale-up. As such, mini-fermenter platforms serve as an effective intermediate step between fundamental laboratory studies and industrial implementation of H_2-driven gas fermentation (Schoenmakers et al., 2025; Hoyt et al., 2025).

Despite these advances, important knowledge gaps remain in the application of membrane-based gas delivery for hydrogen-driven microbial fermentation. In particular, systematic studies investigating the performance, stability, and scalability of membrane-integrated reactors for *C. necator* under explosive $H_2/CO_2/O_2$ gas mixtures remain scarce. Moreover, while membrane systems have primarily been explored for biomass and bulk product formation, their potential for enabling controlled, safe, and efficient synthesis of fine chemicals under chemolithoautotrophic conditions has not yet been comprehensively demonstrated. Addressing these gaps is essential for establishing membrane-integrated gas fermentation as a versatile and scalable platform for sustainable biomanufacturing.

Overall, membrane-based gas fermentation offers a transformative route for overcoming the long-standing engineering challenges associated with H_2-driven microbial cultivation. By combining enhanced safety, superior mass transfer performance, and precise substrate control, membrane-integrated reactor systems establish a robust technological foundation for scalable, efficient, and industrially viable CO_2 bioconversion.

1.6 Indirect CO_2 conversion using the concept of biorefinery

While direct gas fermentation enables microbial conversion of CO_2 into chemicals and materials, large-scale climate mitigation and circular bioeconomy strategies also require efficient utilization of renewable carbon from biomass. In this context, indirect CO_2 conversion through lignocellulosic biorefineries offers a complementary pathway by transforming plant-derived carbon, originally fixed from atmospheric CO_2 via photosynthesis, into fermentable substrates for microbial production of fuels, chemicals, and materials (Kircher, 2021; Singh et al., 2015).

Biorefineries are integrated processing systems that convert biomass into a spectrum of bio-based products using physical, chemical, and biological technologies, analogous to petroleum refineries. Second-generation biorefineries rely on non-food lignocellulosic feedstocks, including agricultural residues, forestry by-products, and dedicated energy crops, thereby avoiding competition with food supply chains and improving overall sustainability (Devi et al., 2022; Hassan et al., 2019). In Europe, annual biomass availability exceeds 1 billion tonnes of dry matter, derived mainly from agricultural residues (~9%), forest biomass (~27%), and energy crops (~9%), highlighting the substantial potential for fossil carbon displacement through biomass valorization (Gurría et al., 2022).

Lignocellulosic biomass is primarily composed of cellulose, hemicellulose, and lignin, forming a highly ordered and recalcitrant structure that resists enzymatic and microbial degradation. Cellulose fibers are embedded within a hemicellulosic matrix and encased by lignin, which provides mechanical strength and chemical resistance. This structural complexity severely limits direct microbial access to fermentable sugars, necessitating physicochemical pretreatment as a critical first step in biorefinery processing (Hassan et al., 2019; Jönsson & Martín, 2016). Effective pretreatment aims to disrupt the lignin–carbohydrate network,

increase surface area, reduce cellulose crystallinity, and enhance enzyme accessibility, thereby enabling efficient saccharification of polysaccharides.

Among available pretreatment technologies, steam explosion combined with enzymatic hydrolysis is widely regarded as one of the most economically viable and environmentally sustainable routes for lignocellulose deconstruction, due to its low chemical input, high sugar yields, industrial scalability, and favourable techno-economic performance (Hendriks & Zeeman, 2009; Alvira et al., 2010; Mosier et al., 2005; Yang & Wyman, 2008; Kim & Dale, 2005). During steam explosion, biomass is treated with high-pressure saturated steam followed by rapid depressurization, which causes structural fiber disruption, partial hemicellulose solubilization, and lignin redistribution, thereby significantly improving enzymatic digestibility while minimizing chemical input (Kataria et al., 2017; Singh et al., 2015; Amin et al., 2017). Subsequent enzymatic hydrolysis releases fermentable sugars, mainly glucose and xylose, generating hydrolysates suitable for microbial fermentation. However, excessive pretreatment severity can lead to formation of inhibitory compounds, including furfural, hydroxymethylfurfural (HMF), weak organic acids, and phenolics, which adversely affect microbial growth and productivity (Jönsson & Martín, 2016; Wang et al., 2014).

The integration of *C. necator* into lignocellulosic biorefineries offers a particularly attractive strategy due to its exceptional metabolic versatility. In addition to autotrophic growth on CO_2 and H_2, *C. necator* can grow heterotrophically on sugars and organic acids derived from lignocellulosic hydrolysates, enabling seamless coupling of biomass valorization with gas fermentation platforms (Lambauer & Kratzer, 2022; Sohn et al., 2021). Several studies demonstrate that native and adapted strains tolerate typical hydrolysate-derived inhibitors and efficiently convert mixed sugar streams into biomass and polyhydroxyalkanoates (PHAs), particularly PHB, without extensive detoxification requirements (Alhafiz et al., 2025b).

From a sustainability perspective, lignocellulosic biorefineries enable indirect recycling of atmospheric CO_2, since the carbon fixed during plant growth is transformed into biodegradable materials and chemicals that eventually re-enter the carbon cycle. This closed-loop carbon utilization supports significant reductions in life-cycle greenhouse gas emissions and decreases reliance on fossil-derived feedstocks (Kircher, 2021; Kähler et al., 2021). Within the framework of the European Green Deal, which targets climate neutrality by 2050, integrated biomass-based processing routes represent a cornerstone of future sustainable manufacturing strategies (Gurría et al., 2022).

Despite substantial progress in lignocellulosic biorefineries, important knowledge gaps remain in understanding how pretreatment strategies, hydrolysate composition, and inhibitory by-products influence microbial growth performance, biomass accumulation, and biopolymer production. Systematic studies addressing the cultivation of *C. necator* on complex lignocellulosic hydrolysates under conditions relevant for high cell density fermentation and PHB synthesis remain limited. Furthermore, quantitative assessments of how substrate composition and inhibitor tolerance impact process robustness, productivity, and yield are still scarce. Bridging these gaps is essential for developing scalable and economically viable biomass-based fermentation routes that complement direct CO_2 conversion pathways within circular bioeconomy frameworks.

1.7 Downstream processing

Downstream processing typically constitutes a major fraction of the total production cost of PHB, with reports indicating that it can account for up to ~40% of overall bioprocessing expenses in PHA systems. Consequently, replacing conventional halogenated solvent-based recovery routes with greener alternatives is increasingly important for improving both process sustainability and economic viability. Conventional PHB purification generally involves an initial ethanol-based degreasing of the dried biomass, followed by dissolution of the

intracellular polymer in chlorinated solvents, most commonly chloroform, and subsequent recovery via antisolvent precipitation, washing, and drying steps. Although chloroform is highly effective in solubilizing high-molecular-weight PHB and enables the recovery of polymer with high purity, its use is associated with significant safety, environmental, and regulatory concerns. Moreover, the combined consumption of ethanol and chloroform substantially increases operating costs due to solvent procurement, handling, recovery, and disposal, particularly at industrial scale, where solvent volumes can reach several cubic meters. Chloroform is classified by the International Agency for Research on Cancer (IARC) as "possibly carcinogenic to humans" (Group 2B), based on sufficient evidence of carcinogenicity in experimental animals. In addition, chronic exposure is associated with hepatotoxicity and nephrotoxicity, as chloroform metabolism generates reactive intermediates that damage liver and kidney tissues. As a result, stringent occupational and environmental regulations governing exposure limits, emissions, and waste disposal further increase the compliance costs associated with chloroform-based downstream processing schemes (Amabile et al., 2024; Levett et al., 2016; IARC, 1999; Public Health England, 2024; Fang et al., 2008; de Oliveira Santos et al., 2025).

To address the toxicity and cost limitations associated with conventional chloroform–ethanol extraction systems, 1,3-dioxolane has been proposed as a promising alternative solvent for PHB recovery from both dried and wet biomass. 1,3-Dioxolane is a water-miscible cyclic acetal capable of efficiently dissolving PHB at elevated temperatures, enabling polymer extraction followed by recovery through antisolvent precipitation or phase separation with water. Optimized extraction protocols have demonstrated PHB purities exceeding 99% and recovery yields of approximately 94% from dried cells, while preserving the molecular weight distribution as well as the thermal and mechanical properties of the polymer, comparable to those obtained using conventional chlorinated solvents. Unlike chloroform, 1,3-dioxolane is

non-halogenated, exhibits lower toxicity, and is considered more environmentally benign, with reported applicability as a substitute for hazardous solvents such as dichloromethane and dichloroethane in various industrial processes. Furthermore, its complete miscibility with water facilitates the integration of water-based precipitation and solvent-recycling schemes, which can substantially reduce net solvent consumption and operating costs compared to once-through chloroform–ethanol extraction. Collectively, these features highlight the potential of 1,3-dioxolane-based downstream processing as a more sustainable and economically favourable approach for PHB recovery, particularly in the context of CO_2-based bioplastic production (Wongmoon & Napathorn., 2022; Amabile et al., 2024; Alhafiz et al., 2025a)

1.8 Process modelling and scale-up considerations for gas fermentation

Gas fermentation offers a promising route for sustainable carbon capture and utilization; however, its industrial implementation is challenged by complex interactions between microbial physiology, gas–liquid mass transfer, reactor hydrodynamics, energy efficiency, and process safety. These interdependencies become increasingly critical during scale-up, where variations in operating conditions, reactor geometry, pressure, and gas delivery strategy can profoundly influence microbial performance, productivity, and process stability (Daniell et al., 2012; Liew et al., 2016; Lambauer et al., 2023). Consequently, rational process design and scale-up of gas fermentation systems require predictive tools capable of integrating biological kinetics with engineering constraints.

Process modelling and simulation provide a powerful framework for evaluating technical feasibility, identifying operational bottlenecks, and guiding experimental development. In contrast to empirical trial-and-error approaches, simulation enables systematic exploration of operating windows, reactor configurations, and scale-dependent effects while minimizing experimental effort, material consumption, energy demand, and safety risks (Towler & Sinnott, 2012; Shuler & Kargi, 2017). This capability is particularly valuable for hydrogen-driven gas

fermentation, where experiments are costly, time-intensive, and subject to strict safety regulations, making extensive laboratory-based optimization both resource-intensive and operationally challenging (Liew et al., 2016; Lambauer et al., 2023).

Most existing simulations for (PHB) production rely on simplified stoichiometric reaction models, which describe microbial growth and polymer synthesis using fixed yields and elemental balances. A representative example is the SuperPro Designer® heterotrophic PHA process model developed by Intelligen Inc., which applies stoichiometric reaction schemes for large-scale techno-economic assessment and process synthesis. While such models provide valuable insight into material and energy balances, equipment sizing, and cost estimation, they fail to capture the dynamic nature of microbial growth, nutrient limitation, and metabolic phase transitions, which critically determine productivity and process robustness under changing operating conditions (Chen, 2010; Koller et al., 2017b).

In recent years, model-based studies have addressed PHB production from CO_2 using steady-state and stoichiometric process frameworks, enabling conceptual optimization of material flows and energy efficiency. Notably, Mozumder et al. (2015) developed a process model for autotrophic PHB production from CO_2, providing valuable insight into theoretical conversion efficiencies and optimal operating windows. However, such approaches neglect the dynamic fermentation behaviour associated with microbial growth kinetics, nitrogen limitation, and intracellular polymer accumulation, thereby limiting their predictive capability for transient cultivation dynamics and scale-dependent performance.

In contrast, physiology-based kinetic modelling provides a mechanistic framework for describing microbial growth, substrate uptake, and polymer biosynthesis as time-dependent processes. Dynamic kinetic models enable simulation of fermentation trajectories, allowing prediction of transient responses to fluctuations in substrate availability, gas transfer, and

environmental conditions (Shuler & Kargi, 2017; Mozumder et al., 2014). Despite their predictive potential, the integration of microbial kinetic models into industrial process simulation environments remains limited, particularly for gas fermentation systems, where mass transfer, safety constraints, and energy balances exert dominant influence (Daniell et al., 2012; Liew et al., 2016). As a result, a substantial gap persists between microbial-scale kinetic understanding and industrial-scale process design.

Bridging this gap is essential for enabling robust, scalable, and resource-efficient gas fermentation processes. The integration of microbial kinetics with industrial process simulation platforms offers a promising route for systematically evaluating how changes in operating conditions and scale affect biological performance, energy efficiency, and technical feasibility. By enabling rapid in silico screening of process configurations, simulation-based approaches significantly reduce reliance on extensive experiments, thereby conserving time, energy, and material resources while enhancing process safety and development efficiency (Towler & Sinnott, 2012; Biegler et al., 2010).

Overall, advanced process modelling and scale-up methodologies represent critical enabling tools for the industrial deployment of gas fermentation technologies, providing a rational basis for matching microbial requirements with engineering constraints and guiding the development of safe, efficient, and economically viable CO_2-based bioprocess.

1.9 Aim and objectives of research

The primary aim of this thesis was to understand the technological implementation of direct and indirect CO_2-based microbial bioprocesses using *C. necator*, with particular emphasis on safe operation, product formation, and process scalability. By integrating experimental cultivation studies, energy metabolism analysis, membrane-based reactor technology, downstream processing, and process modelling, this work sought to systematically bridge

microbial physiology with engineering feasibility in order to support the development of sustainable and industrially viable CO_2 bioconversion platforms.

To achieve this general aim, the following specific objectives were pursued:

1. To elucidate the role of hydrogenase-driven energy metabolism in determining growth efficiency and product formation
    a. Quantify the contributions of soluble and membrane-bound hydrogenases (SH and MBH) to growth.
    b. Apply calorimetric technique to assess the individual contribution of SH and MBH to the energy efficiency of *C. necator*.
2. To establish safe and robust gas fermentation strategies for autotrophic cultivation of *C. necator*
    a. Adapt and optimize existing ATEX-compliant gas fermentation platform for *C. necator* DSM 544
    b. Develop cultivation strategies to mitigate strain-specific process challenges, particularly pH drift and culture instability.
    c. Demonstrate high-density biomass growth and efficient PHB production under intrinsically safe cultivation regimes.
    d. Develop a sustainable downstream processing strategy for PHB recovery
3. To develop and apply membrane-based gas fermentation platform for intensified and controlled bioprocessing
    a. Integrate and operate hollow fiber membrane modules within mini-fermenter platforms for bubble-free and intrinsically safe gas delivery.
    b. Demonstrate the feasibility of coupling autotrophic metabolism with whole-cell biocatalysis for high-value chemical production, exemplified by pyrrolidine synthesis.

4. To evaluate the feasibility of lignocellulosic biomass-derived hydrolysates as renewable substrates for heterotrophic growth and PHB production by *C. necator*
    a. Investigate microbial growth performance and PHB accumulation on complex hydrolysate substrates.
    b. Assess inhibitor tolerance and substrate utilization efficiency under conditions relevant for biopolymer production.
5. To integrate experimental fermentation data into dynamic process modelling and simulation frameworks
    a. Develop kinetic models describing autotrophic growth and PHB formation based on experimental fermentation data.
    b. Implement these models in industrial process simulation tools to evaluate scale-dependent performance, as well as sensitivity analysis.

Collectively, these objectives form a coherent framework for the systematic development of safe, efficient, and scalable CO_2-based microbial production systems, contributing fundamental insights and technological solutions toward sustainable biomanufacturing and circular carbon utilization.

2 Materials and methods

This chapter describes the materials, culture media, fermentation systems, and experimental procedures used in this thesis. Particular emphasis is placed on the different cultivation set-ups employed for autotrophic and heterotrophic growth of *C. necator* strains, including bottle-based, stirred-tank, and membrane-integrated fermentation systems. The chapter further details gas supply strategies, operating conditions for safe and non-explosive gas fermentation, pH control strategy, and analytical methods applied for biomass and product characterization.

2.1 Chemicals and reagents

All chemicals used for media preparation, gas fermentation experiments, and analytical procedures were of analytical grade and obtained from standard commercial suppliers (Sigma-Aldrich, Carl Roth), unless otherwise stated. Ammonium concentrations were determined using an enzymatic assay kit (K-AMIAR, Megazyme International).

2.2 Strains

2.2.1 Reference and production strains

For autotrophic growth and PHB production from CO_2, *C. necator* DSM 544 (H1 G^+3, Leibniz Institute DSMZ, German Collection of Microorganisms and Cell Cultures, Braunschweig, Germany). DSM 544 is a glucose-utilizing mutant derived from *C. necator* DSM 530 and carries a constitutively expressed glucose-6-phosphate dehydrogenase, characteristic of classical G^+ mutants originally generated in the Schlegel laboratory (Schlegel & Gottschalk, 1965; Morlino, 2023).

In addition, *C. necator* H16 (DSMZ strain) was used for gas fermentation experiments targeting reductive biotransformation (Section 3.3). The H16 strain harboured a plasmid encoding a heterologous imine reductase (IRED) from *Myxococcus landrumus*, enabling stereoselective reductive amination reactions under chemolithoautotrophic conditions. The construction of this

strain was performed in a previous work (Schoenmakers et al., 2026), and only its cultivation and application in gas fermentation were addressed in this thesis. Table 2.1 summarizes these reference strains.

Table 2.1: Summary of reference and production strains

Strain	Relevant characteristics	Source/Reference
C. necator DSM544	H1 $G^{+}3$	DSMZ, Germany
Recombinant *C. necator* H16	IRED1, *M. landrumus* Plasmid pPS22	Constructed by P. Schoenmakers

2.2.2 Hydrogenase knockout strain set

To elucidate the contribution of individual hydrogenases and hydrogenase regulation to growth and energy metabolism, a defined set of hydrogenase knockout strains derived from *C. necator* H16 was investigated. These strains differed in both their regulatory background and hydrogenase expression. Two regulatory backgrounds were considered as summarized in Table 2.2:

hoxJ background: carrying the native *hoxJ* gene variant, which has impaired regulatory hydrogenase signalling and therefore does not control hydrogenase expression.

*hoxJ** background: carrying the restored *hoxJ** gene variant with the Ser→Gly reversion, which restores normal regulatory hydrogenase function and H_2-dependent induction of hydrogenase expression.

Table 2.2: Hydrogenase strain set used in this study

Strain	Relevant Characteristics	Source/Reference
C. necator H16	*hoxJ*, SH^{+} MBH^{+}	DSM 428
C. necator HF520	*hoxJ*, Δ*hoxG*, SH^{+}, MBH^{-}	O. Lenz (TUB)
C. necator HF388	*hoxJ*, Δ*hoxH*, SH^{-} MBH^{+}	O. Lenz (TUB)
C. necator HF433	*hoxJ**, SH^{+} MBH^{+}	O. Lenz (TUB)
C. necator HF511	*hoxJ**, Δ*hoxG*, SH^{+}, MBH^{-}	O. Lenz (TUB)
C. necator HF512	*hoxJ**, Δ*hoxH*, SH^{-} MBH^{+}	O. Lenz (TUB)

Unless otherwise stated, all strains were maintained under appropriate antibiotic selection and stored as glycerol stocks at −80 °C.

2.3 Culture media

The mineral media used in this study for chemolithoautotrophic cultivation of *C. necator* are summarized in Table 2.3, which compares the compositions of two media used, mineral medium (MM) and the autotrophic medium (AUT). Final concentrations of all components are shown. For pre-cultures AUT medium was supplemented with 0.4 % (w/v) fructose (FN medium), as described previously (Alhafiz et al., 2025a).

Table 2.3: Mineral media composition for the chemolithoautotrophic cultivation of *C. necator.* Final concentrations are shown. AUT (autotrophic media); MM (mineral medium)

Main components	AUT	(mM)	MM	(mM)
Phosphate buffer	Na_2HPO_4	25.00	Na_2HPO_4	25.00
	KH_2PO_4	11.00	KH_2PO_4	11.00
Nitrogen source	NH_4Cl	37.40	$(NH_4)_2SO_4$	11.40
Other nutrients	$MgSO_4$	0.81	$MgSO_4$	0.81
	$CaCl_2$	68.00	$CaCl_2$	0.14
	$NiCl_2$	0.00100		
	$FeCl_3$*	0.018		
			NH_4Fe (III) citrate	0.172
Tungsten solution			Na_2WO_4	0.00018
Trace element solution (TES or SL6)	H_3BO_3	0.00485	H_3BO_3	0.00970
	$CoCl_2$	0.00084	$CoCl_2$	0.00170
	$ZnSO_4$	0.00035	$ZnSO_4$	0.00070
	$MnCl_2$	0.00253	$MnCl_2$	0.00030
	$NiCl_2$	0.00008	$NiCl_2$	0.00168
	$CuCl_2$	0.00006	$CuSO_4$	0.00007
	Na_2MoO_4	0.00012	Na_2MoO_4	0.00027

*Prepared in 0.1 N HCL and sterile filtered.

MM supplemented with 50 mg L^{-1} kanamycin sulphate was used for cultivating *C. necator* DSM 544 (Sections 3.1 and 3.4). Modifications to the standard MM formulation (Table 2.3) are summarized in Table 2.4. AUT was used for bioenergetic experiments and for cultivations involving *C. necator* H16 expressing IRED. While MM served as the standard autotrophic

medium at BIOTE, TU Graz, AUT was employed as the standard autotrophic medium at iAMB, RWTH Aachen University. Importantly, both media supported stable chemolithoautotrophic growth of *C. necator* under the investigated conditions.

Table 2.4: Variations of the standard mineral medium used

	Components (mM)	Standard MM	MM1	MM2	MM3
Phosphate buffer	Na_2HPO_4	25.00	25.00	83.33	152.78
	KH_2PO_4	11.00	11.00	36.70	67.50
Nitrogen source	$(NH_4)_2SO_4$	11.40	52.40	52.40	52.40
Magnesium source	$MgSO_4$	0.81	1.13	1.13	1.94

The Standard MM corresponds to the formulation of Alhafiz et al. (2025a). MM1–3 represent modified versions with adjusted phosphate buffer, ammonium, and magnesium concentrations. MM1 was used in Cultivation 1, MM2 in Cultivation 2 and 5, the Standard MM in Cultivations 3 and 4, and MM3 in Cultivations 6.

To ensure chemical stability and to prevent precipitation or decolouration of medium components, major constituents were prepared and sterilised separately prior to mixing. In particular, phosphate buffer solutions, nitrogen sources, magnesium salts, calcium salts, iron solutions, tungsten solution, and trace element solutions were sterilised individually by autoclaving or sterile filtration as appropriate. Iron-containing solutions were prepared in dilute hydrochloric acid and sterile filtered, as indicated in Table 2.3. All components were combined aseptically after cooling to room temperature.

2.4 Investigation of hydrogenase-dependent energy metabolism

To elucidate the contribution of different hydrogen oxidation pathways to energy conversion efficiency in *C. necator*, a systematic experimental framework was established using hydrogenase knockout strains combined with growth and calorimetric analysis. The experimental strategy was designed to decouple the effects of soluble hydrogenase (SH), membrane-bound hydrogenase (MBH), and regulatory hydrogenase (RH) activity on microbial growth performance and energy conservation during heterotrophic and chemolithoautotrophic cultivation.

2.4.1 Growth experiments of hydrogenase knockout strains

Growth experiments were conducted under both heterotrophic and autotrophic conditions to assess the physiological performance of the hydrogenase knockout strains (Section 2.2.2).

Heterotrophic cultivation was performed in Pioreactor v1.1 units (20 mL vials) containing 15 mL AUT medium. Cultures were inoculated to an initial OD_{600} of 0.1. Pioreactors provided integrated heating to 30°C, stirring at 500 rpm, and automated OD_{600} monitoring for high-throughput parallel cultivations with real-time growth data. These experiments served to confirm baseline growth capacity independent of hydrogen oxidation and to evaluate potential secondary effects of hydrogenase deletions on central metabolism.

Autotrophic cultivations were carried out in 250 mL serum bottles sealed with gas-tight butyl rubber stoppers suitable for hydrogen handling, containing 50 mL AUT medium. Headspace was first purged, then filled with either of two gas compositions using a gas mixing station (PCU-10; Vögtlin):

H_2: O_2: CO_2: N_2 = 3.8: 7.3: 13: 75.9 (v/v)
H_2: O_2: CO_2 = 84: 3: 13 (v/v)
Precultures grown autotrophically with H_2: O_2: CO_2: N_2 = 70: 3: 5: 22 (v/v) at 30 °C and 120 rpm were used to inoculate main cultures to an initial OD_{600} of 0.1. Bottles were incubated on shakers at 30 °C and 120 rpm. Daily sampling for growth determination (OD_{600}) was followed by headspace gas exchange to maintain defined gas composition.

2.4.2 Isothermal microcalorimetry

To quantify the total metabolic heat released during growth, isothermal microcalorimetry experiments were performed using a TAM IV calorimeter (TA Instruments) at the Helmholtz Centre for Environmental Research UFZ, Leipzig in collaboration with Tilman Linke. Cultures of different hydrogenase knockout strains were incubated under defined autotrophic conditions

(H_2: O_2: CO_2: N_2 = 3.8: 7.3: 13: 75.9 (v/v)). Heat flow (µW) was recorded continuously over time, providing a direct, real-time measure of metabolic activity. Precultures grown autotrophically with H_2: O_2: CO_2 = 84: 3: 13 (v/v) at 30 °C and 120 rpm were used to inoculate main cultures to an initial OD_{600} of 0.1. The cumulative heat production was obtained by integrating it to the respective CDW achieved from the different strains.

2.5 Set-up for gas fermentation

2.5.1 DURAN flask bioreactor

Chemolithoautotrophic cultivations on $H_2/CO_2/O_2$ were performed in a double-walled 1000 mL DURAN® glass flask bioreactor, designed to enable controlled temperature operation while maintaining intrinsic explosion safety. The double-walled design allowed temperature regulation via an external oil bath, which was set to 30 °C and provided uniform heat transfer to the culture medium. This configuration enabled temperature control comparable to that of a stirred-tank bioreactor, while retaining the simplicity and flexibility of a flask-based system.

The DURAN flask was equipped with a gas-tight screw cap assembly allowing sterile gas inlet and outlet connections. Substrate gases ($H_2/CO_2/O_2$) were supplied via individual mass flow controllers and mixed upstream before entering the reactor (Figure 2.1). The gas inlet terminated in a PTFE frit to promote fine gas dispersion and enhance gas–liquid mass transfer. Off-gas was routed through sterile filters and safely vented. The entire gas-handling system was designed to prevent backflow and leakage, with check valves and H_2-tight tubing used throughout.

Agitation was provided by a magnetic stir bar driven by an external stirring plate. Importantly, the reactor was placed inside a fume hood (ventilation rate = 580 $m^3\ h^{-1}$, Vögtlin Instruments GmbH, Switzerland) so that any gas leaks could be diluted and safely removed by the airflow. Gas cylinders were stored outside the hood in safety cabinets; CO_2 and H_2 were kept together,

while O_2 was stored separately to reduce explosion risk. Prior to cultivation, the flask and all fittings were sterilized by autoclaving. The assembled system was then connected to the gas supply, and leak-tightness was verified by purging with N_2 gas. Following this, the culture was inoculated and hydrogen-containing gas mixtures were introduced. Sampling was carried out using a syringe through a septum, with hydrogen supply temporarily halted and the headspace purged with N_2 to ensure safe handling.

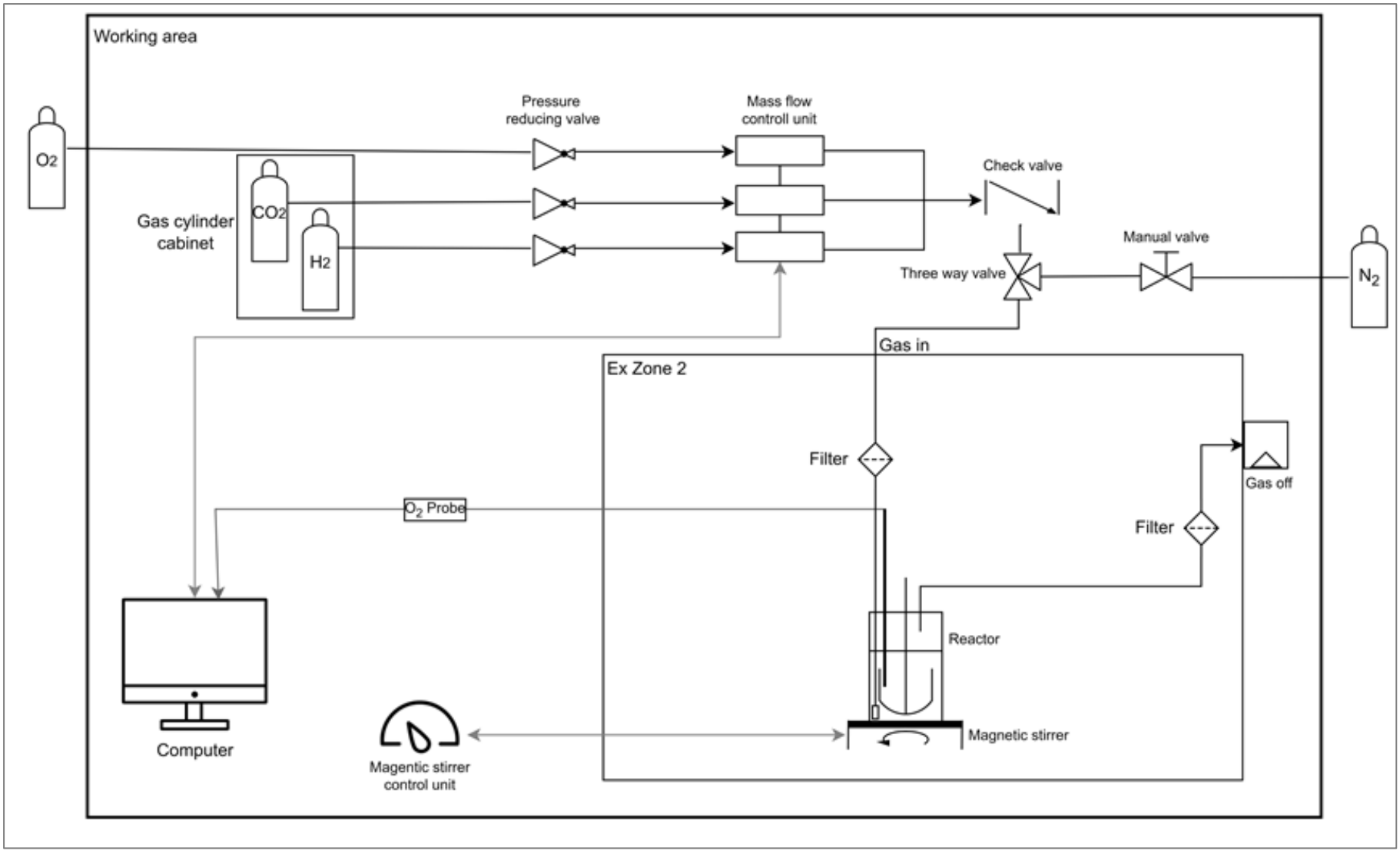

Figure 2.1: Schematic of the gas supply and reactor setup for 1L Duran flask (reproduced from Lambauer and Kratzer, 2022, licensed under CC BY 4.0.)

2.5.2 Stirred-tank bioreactor

For controlled stirred-tank gas fermentations, a Labfors bioreactor with a double-walled 1.2 L reaction vessel was modified for a safe gas fermentation. To comply with ATEX-related safety requirements, all standard electrical components were removed from the immediate reactor environment, and the agitation and temperature-control hardware were relocated outside the ventilated hood (ventilation rate = 580 m^3 h^{-1}, Vögtlin Instruments GmbH, Switzerland). Specifically, the original motor and thermostat were replaced by an external three-phase drive motor and an external water bath with circulation pump, with elongated shaft and tubing routing so that potential ignition sources remained outside the hazardous area.

The gas supply system used mass flow controllers (MFCs) to regulate individual gas streams (H_2/CO_2/O_2) and on-site gas mixing. A H_2 gas detector installed inside the fume hood was connected to an emergency shutdown chain: H_2 detection triggered closure of a magnetic valve, stopping gas feed, and stopping the bioreactor motor, combined with alarm signals. The bioreactor was equipped with dissolved-gas analytics suitable for ATEX systems. Dissolved oxygen was measured using an ex-zone certified electrochemical/optical probe (VisiFerm mA 225 H3). Dissolved CO_2 was monitored using an optical fiber-based CO_2 dipping probe considered intrinsically safe; probe electronics were positioned away from the reactor to reduce ignition risk. Reactor lid and sensors were connected to an equipotential socket to ensure equipotential bonding/grounding of the full setup.

Operationally, the bioreactor was autoclaved, and the dissolved gas probes installed aseptically. The assembled system was connected to substrate gas and off-gas lines, and leak-tightness was verified using N_2 purge and leak detector spray. During chemolithoautotrophic operation, temperature and agitation were held constant, while dissolved gases were controlled via automation (LabVIEW) to maintain defined setpoints. For safe sampling, H_2 was temporarily

set to zero, the system was purged with H_2-free gas for ~10 min, and samples were taken via syringe through a septum port; after sampling, tightness was rechecked.

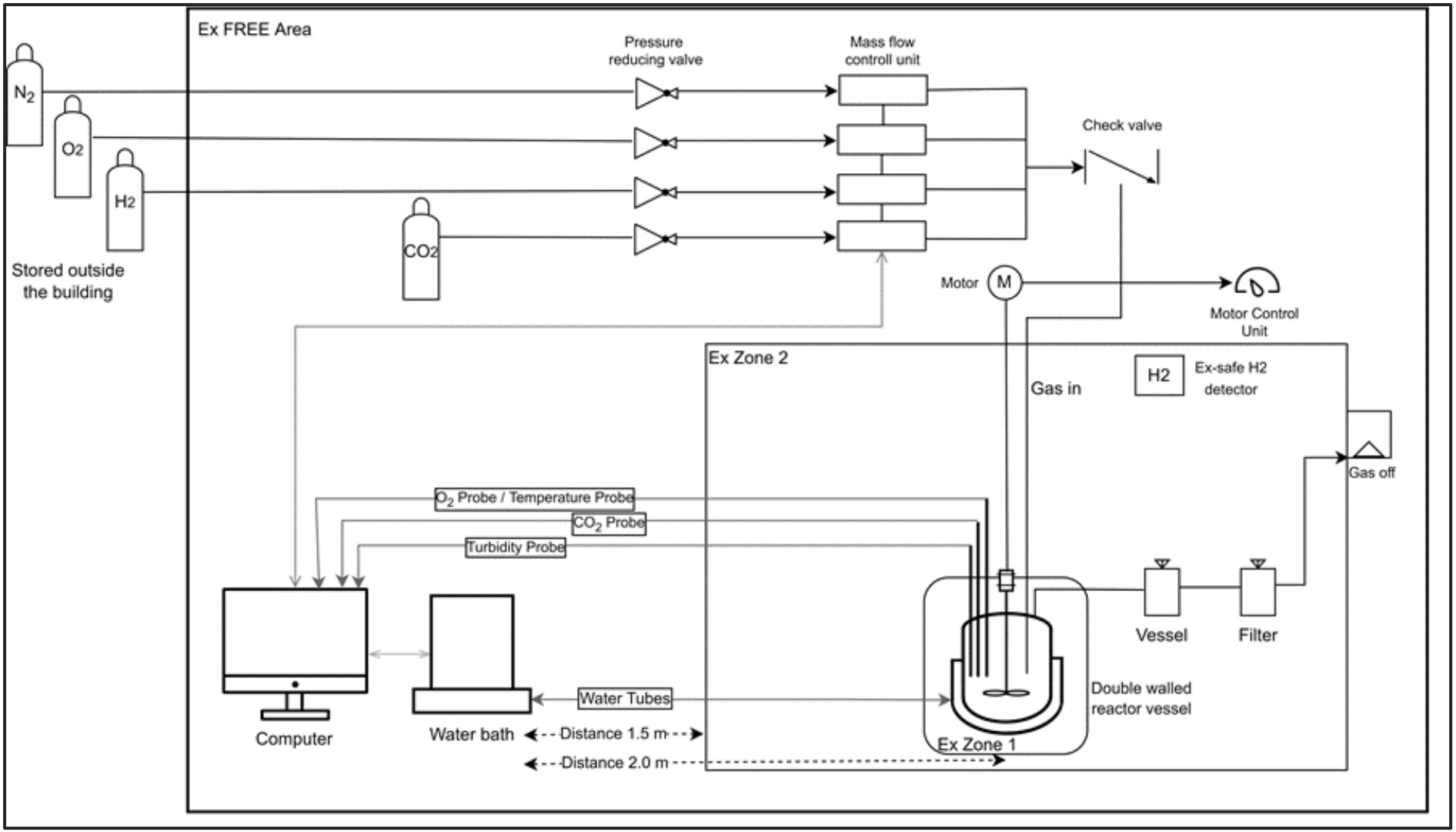

Figure 2.2: Schematic of the gas supply and reactor setup for 1.2 L Labfors reactor (reproduced from Lambauer et al., 2023, licensed under CC BY 4.0.)

2.6 Chemolithoautotrophic growth of *C. necator* DSM 544 on $CO_2/H_2/O_2$

Chemolithoautotrophic cultivations of *C. necator* DSM 544 were performed using $CO_2/H_2/O_2$ gas mixtures in two different reactor configurations, as described in Section 2.4. Cultivations 1–4 were carried out in 1-L DURAN® GLS 80 wide-neck threaded glass bottles, while Cultivations 5 and 6 were performed in a 1.2-L double-walled Labfors bioreactor (Infors HT, Bottmingen, Switzerland).

For the 1-L DURAN bottle cultivations (Cultivations 1–4), cultures were agitated at 240 rpm with an initial gas composition of 5% CO_2, 93% H_2, and 2% O_2 (v/v). The total gas flow rate was maintained constant at 400 mL min^{-1}. H_2 was used to complete the gas mixture after setting the CO_2 and O_2 fractions. Dissolved oxygen concentration was controlled at 2% throughout the cultivation.

Cultivations 5 and 6 were conducted in the Labfors bioreactor at an agitation speed of 887 rpm. The supply gas consisted of 5% CO_2, 40% H_2, 2% O_2, and N_2 as a balancing gas. The total gas flow rate was maintained at 1 L min^{-1}. In this configuration, CO_2 and O_2 were supplied to maintain concentrations of 5% and 2%, respectively, while H_2 accounted for 470 mL min^{-1} of the total flow. To enhance gas–liquid mass transfer, N_2 was added at 530 mL min^{-1}, yielding a total flow of 1000 mL min^{-1} and increased gas-induced turbulence. Dissolved O_2 was controlled at 2% throughout the cultivation.

All cultivations were performed using mineral medium (MM) supplemented with 50 mg L^{-1} kanamycin sulphate at a temperature of 30 °C, as described in Section 2.3. Medium modifications applied in individual cultivations are summarized in Table 2.3. Pre-cultures were prepared in 50 mL standard MM supplemented with 10 g L^{-1} glucose and 50 mg L^{-1} kanamycin sulphate in 300-mL Erlenmeyer flasks, incubated at 30 °C and 120 rpm. Cultures were inoculated into autotrophic media after reaching exponential growth.

Cell growth was monitored by measuring optical density at 600 nm (OD_{600}). Cell dry weight (CDW) was determined by harvesting defined culture volumes, followed by lyophilization until constant weight. Ammonium depletion was quantified enzymatically using the K-AMIAR assay kit (Megazyme International, Wicklow, Ireland).

2.7 Set-up for membrane integrated gas fermentation

2.7.1 Reactor configuration and gas delivery

Membrane-integrated gas fermentation experiments were conducted using a 30 mL Chi.Bio mini-fermenter platform equipped with a hollow fiber membrane gas delivery module (BioThrust GmbH, Germany), enabling bubble-free and intrinsically safe gas transfer (Figure 2.3). All experiments were performed inside a fume hood to ensure compliance with laboratory safety requirements for hydrogen handling.

The gas delivery module consisted of a poly(4-methyl-1-pentene) (PMP) hollow fiber membrane with a total active membrane surface area of 84 mm^2 per side. PMP was selected due to its high permeability for hydrogen and oxygen, chemical inertness, and mechanical stability under fermentation conditions. The membrane featured two physically separated gas channels, allowing independent supply of H_2 and a premixed stream of O_2 and CO_2. H_2 was delivered through one channel, while O_2 and CO_2 were supplied through the second channel, thereby preventing direct contact between H_2 and O_2 in the gas phase. Gas transfer into the liquid phase occurred via diffusion across the membrane, eliminating explosion risks associated with conventional sparging while maintaining efficient substrate availability.

Gas flow rates were controlled using Bronkhorst mass flow controllers, maintaining a total gas flow of 3 mL min^{-1}, with agitation maintained at 973 rpm and a defined gas composition of 70% H_2, 20% O_2, and 10% CO_2, optimized for autotrophic cultivation of *C. necator*.

Dissolved H_2, O_2 and CO_2 concentrations were continuously monitored using microsensors installed in an external recirculation loop (Unisense for H_2 and PreSens for O_2 and CO_2). This enabled real-time assessment of gas availability and uptake. Off-gas composition was analyzed online using a Pfeiffer Omnistar quadrupole mass spectrometer, allowing direct monitoring of gas consumption during cultivation.

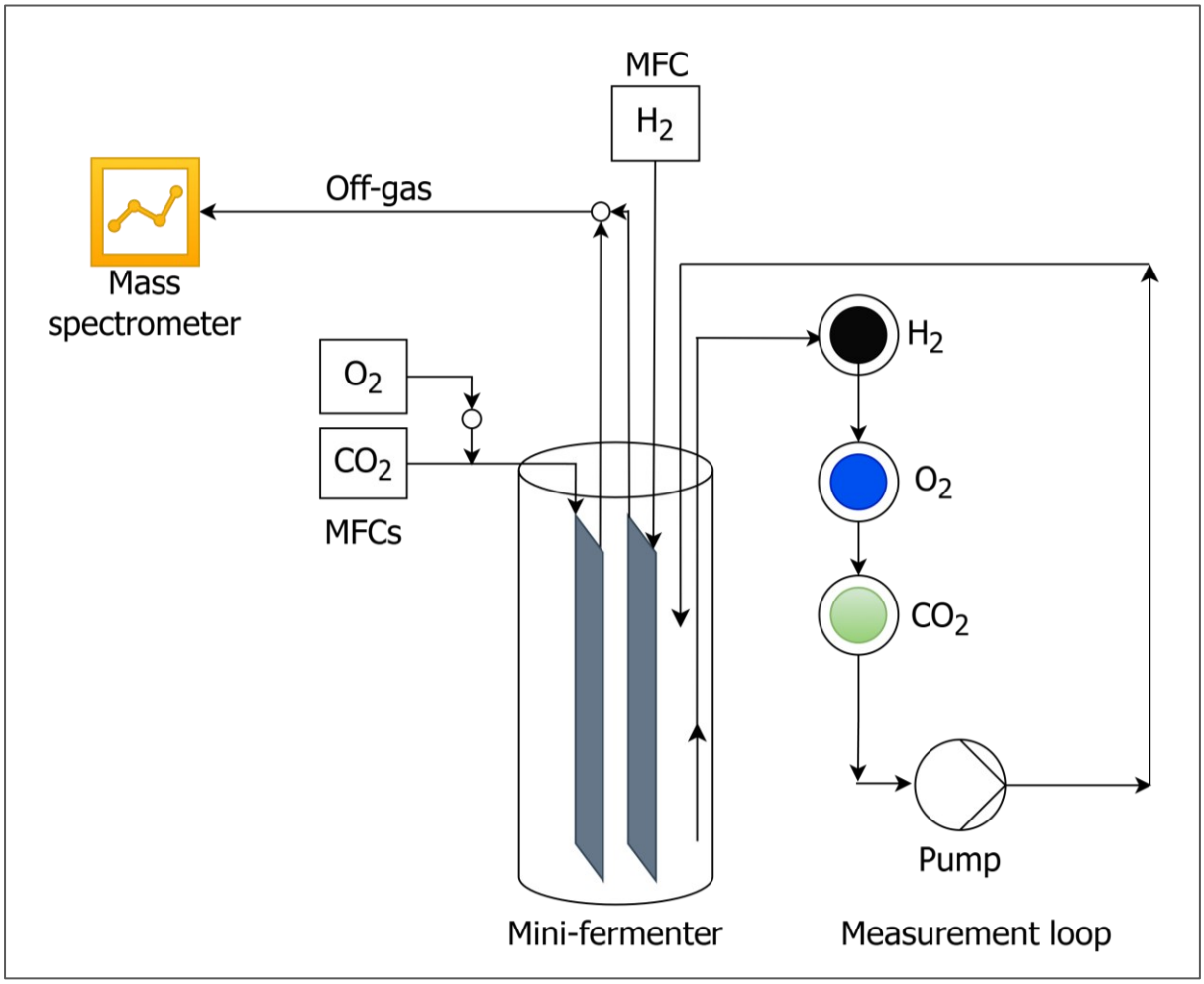

Figure 2.3: Schematic of membrane-integrated mini-fermenter set-up (created in drawio.com)

2.7.2 Volumetric mass transfer coefficient (k_La) determination

The volumetric mass transfer coefficients (k_La) for H_2 in the membrane-integrated mini-fermenter was determined using the dynamic gassing-out method. Experiments were performed in cell-free AUT medium to ensure that changes in dissolved gas concentrations reflected purely physical mass transfer rather than biological consumption. Prior to each

experiment, the medium was purged with N_2 to remove dissolved gases and establish baseline conditions.

Following purging, H_2 was supplied at a defined gas composition through the membrane gas delivery system at a total flow rate of 3 mL min^{-1}. Dissolved gas concentration was recorded while agitation was maintained at 973 rpm. The k_La values were calculated according to Equation 2.4:

$$\frac{dC}{dt} = k_L a(C^* - C) \quad \text{..... 2.4}$$

where C is the dissolved gas concentration at time t and C^* is the equilibrium saturation concentration, calculated from Henry's law based on operating temperature, total pressure, and inlet gas composition. The slope of the linear region of the semi-logarithmic plot of ln ($C^* - C$) versus time was used to determine k_La.

To assess the influence of membrane-based gas delivery on mass transfer performance, k_La measurements were conducted both with and without the membrane module under identical agitation and gas flow conditions. This comparison enabled quantitative evaluation of the contribution of membrane-mediated diffusion to overall gas–liquid mass transfer in the mini-fermenter system.

2.8 Growth of *C. necator* H16 expressing imine reductase (IRED)

2.8.1 Construction of *C. necator* H16 expressing IRED

The recombinant *C. necator* H16 strain expressing IRED was constructed in a previous study (Schoenmakers et al., 2026) and used in this work. *C. necator* H16 was cultivated in FN medium until the culture reached an OD_{600} of approximately 0.6. Cells were harvested by centrifugation at 4,000 rpm for 10 min at 4 °C and washed twice with ice-cold 10% (v/v) glycerol to remove residual salts. The cell pellet was then resuspended in 1 mL of ice-cold 10% glycerol to prepare electrocompetent cells.

For transformation, 100 µL of the electrocompetent cell suspension was mixed with 1 µL of plasmid DNA from *Myxococcus landrumus*, carrying the IRED gene under the control of an arabinose-inducible promoter. Electroporation was performed using a single pulse at 2,500 V with a pulse length of 5 ms. Immediately after electroporation, 700 µL of complex recovery medium was added, and the cells were incubated at 37 °C with shaking at 1,000 rpm for 1 h to allow phenotypic expression of the antibiotic resistance marker. Transformants were selected by plating the recovered cells onto FN agar plates supplemented with kanamycin (400 mg L^{-1}). Plates were incubated at 30 °C until colonies appeared. Successful transformants were used for autotrophic cultivation and whole-cell biotransformation experiments.

2.8.2 Whole-cell biotransformation for pyrrolidine production

Whole-cell biotransformation experiments were performed using recombinant *C. necator* H16 expressing IRED, cultivated under chemolithoautotrophic conditions. The preculture was grown in a 100 mL serum bottle containing AUT medium and supplied with a gas mixture consisting of 70% H_2, 3% O_2, 5% CO_2, and 22% N_2 (v/v) at 30 °C. This preculture was used to inoculate the main culture to an initial OD_{600} of 0.1.

The main cultivation was conducted in the Chi.Bio membrane-integrated mini-fermenter (Section 2.7) with 30 mL of AUT medium operated at 30 °C and supplied with 70% H_2, 20% O_2, 10% CO_2. Cultures were grown until an OD_{600} of approximately 0.7 was reached, corresponding to mid-exponential growth. At this point, expression of the IRED enzyme was induced by addition of 0.2% (w/v) arabinose to the culture. Simultaneously with induction, the whole-cell biotransformation was initiated by addition of 2-methyl-1-pyrroline to a final concentration of 80 mM. This compound served as the substrate for IRED-catalyzed reduction to 2-methylpyrrolidine, using intracellular reducing equivalents generated from H_2 oxidation. The biotransformation was carried out under continued autotrophic conditions, with gas supply, agitation, and temperature maintained as described for the cultivation phase. Samples

were taken at defined time intervals throughout the experiment to determine cell dry weight (CDW) and to quantify formation of 2-methylpyrrolidine. Samples for product analysis were taken and prepared for product analysis.

2.9 Downstream processing

Downstream processing was performed exclusively for the recovery of intracellular poly(3-hydroxybutyrate) (PHB) produced by *C. necator*. Following cultivation, biomass samples were harvested and processed using a solvent-based extraction protocol adapted from literature, employing 1,3-dioxolane as a non-halogenated alternative to conventional chlorinated solvents.

Culture samples were first centrifuged at high speed (20,000 × g, 5 min) to separate the biomass from the culture supernatant. The resulting cell pellets were washed with deionized water to remove residual medium components and subsequently lyophilized to constant weight. Lyophilization ensured reproducible biomass handling and facilitated efficient solvent penetration during polymer extraction.

PHB extraction was carried out by suspending the dried biomass in a 5% (w/v) solution of 1,3-dioxolane, followed by incubation at 80 °C for 6 h under gentle agitation (50 rpm). Under these conditions, PHB was selectively solubilized while non-polymeric cellular components remained insoluble. After extraction, the suspension was cooled on ice to terminate dissolution.

Polymer recovery was achieved by precipitation through the addition of a threefold volume of deionized water, inducing phase separation and polymer aggregation. The precipitated PHB was collected by filtration, washed twice with deionized water to remove residual solvent and impurities, and dried at 70 °C until a constant mass was obtained. The resulting material appeared as a white, fibrous solid characteristic of purified PHB (Figure 2.4)

This downstream processing approach enables efficient recovery of high-purity PHB while avoiding the use of halogenated solvents such as chloroform. The use of 1,3-dioxolane provides a more environmentally benign and operationally safer alternative, suitable for laboratory-scale recovery of PHB from autotrophically cultivated *C. necator* biomass.

Analytical methods used for quantification and structural verification of PHB are described in Section 2.10.

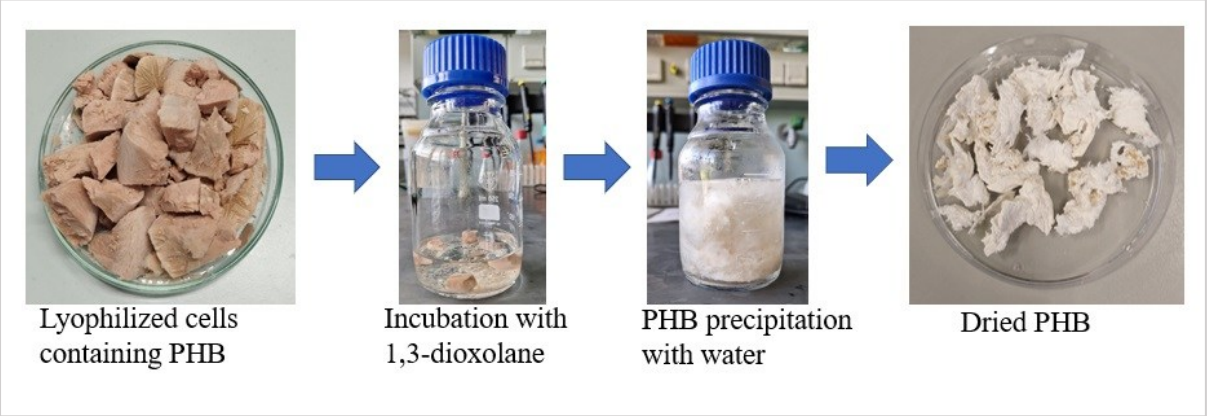

Figure 2.4: Workflow for PHB extraction using 1,3-dioxolane (reproduced from Alhafiz et al., with permission from Elsevier)

2.10 Quantification of products

2.10.1 Quantification of poly(3-hydroxybutyrate) (PHB) by GC–FID

Quantitative determination of poly(3-hydroxybutyrate) (PHB) content was performed by gas chromatography with flame ionization detection (GC–FID) following acidic methanolysis of the extracted polymer. 5–10 mg of dried PHB were weighed into sealed glass vials. Chloroform (1 mL) was added to dissolve the polymer, followed by 1 mL of methanol containing 15% (v/v) sulfuric acid. The vials were tightly sealed and incubated at 100 °C for 2.5 h to convert PHB into its corresponding methyl ester, methyl-3-hydroxybutyrate.

After methanolysis, samples were cooled on ice and 1 mL of deionized water was added to induce phase separation. Subsequently, 1 mL of chloroform containing 0.2% (v/v) internal

standard was added, and the mixture was vortexed for 1 min. After phase separation, the organic (lower) phase was carefully transferred to GC vials using a Pasteur pipette.

GC–FID analysis was performed using a ZB-5 capillary column, with the detector temperature set to 275 °C. External calibration curves were prepared using commercial PHB standards (2–10 mg) subjected to the same methanolysis and extraction procedure. PHB content was calculated based on the peak area of methyl-3-hydroxybutyrate relative to the internal standard. This method enables reliable and reproducible quantification of PHB across a wide concentration range (Juengert et al., 2018; Lambauer & Kratzer, 2022; Wongmoon & Napathorn, 2022).

2.10.2 Qualitative characterization of PHB by ^{1}H NMR spectroscopy

Qualitative structural confirmation of PHB was carried out using proton nuclear magnetic resonance (^{1}H NMR) spectroscopy. Dried PHB samples (15 mg) extracted from Cupriavidus necator cultivations were dissolved in 1 mL of deuterated chloroform ($CDCl_3$) by gentle agitation. A commercially available PHB standard was prepared in the same manner for comparison. All samples were transferred to NMR tubes and analyzed using a Magritek Spinsolve 80 ULTRA benchtop NMR spectrometer operating at a proton resonance frequency of 80 MHz.

^{1}H NMR spectra were recorded at ambient temperature and evaluated for characteristic chemical shifts of the PHB repeating unit. Diagnostic resonances corresponding to the methine (–CH–), methylene (–CH_2–), and methyl (–CH_3) protons of the polyester backbone were clearly observed. The spectra of biogenic PHB showed excellent agreement with the commercial reference, confirming the chemical identity and structural integrity of the extracted polymer.

2.10.3 Quantification of 2-methylpyrrolidine by GC–FID

Quantification of 2-methylpyrrolidine produced during whole-cell biotransformation experiments was performed by gas chromatography with flame ionization detection (GC–FID) following chemical derivatization and liquid–liquid extraction. Culture samples were collected at defined time points and immediately quenched by addition of 10% (v/v) 10 M NaOH to terminate enzymatic activity. Quenched samples were centrifuged at 20,000 × g for 2 min to remove biomass and particulate matter.

An equal volume of clarified supernatant was mixed with an equal volume of derivatization solution containing 1 M acetic anhydride in ethyl acetate. The mixture was vortexed for 2 min to allow derivatization of the amine product and subsequently centrifuged to achieve phase separation. Due to the lower density of ethyl acetate, the organic phase formed the upper layer and was carefully transferred to GC vials for analysis.

GC–FID analysis was carried out using an Agilent GC system equipped with an HP-1ms UI column (30 m × 250 µm × 0.25 µm). Hydrogen was used as the carrier gas at a linear velocity of 30 cm s^{-1}. Injector and detector temperatures were maintained at 250 °C and 330 °C, respectively. Quantification was based on external calibration curves prepared from commercially available 2-methylpyrrolidine standards subjected to the same quenching, derivatization, and extraction procedure to ensure analytical consistency and accuracy.

2.11 Heterotrophic growth of *C. necator* DSM 544 on lignocellulosic biomasses

2.11.1 Biomass feedstocks

Five lignocellulosic raw materials were used: wheat straw, beech wood chips, pine wood chips, spruce wood chips, and *Miscanthus* × *giganteus*. In addition, northern bleached softwood kraft (NBSK) pulp served as a reference cellulose substrate. Biomass particle sizes ranged from

approximately 20–40 mm in length depending on source material, and all substrates were stored at 6 °C prior to pretreatment.

2.11.2 Preparation and pretreatment of lignocellulosic substrates

Physicochemical pretreatment of lignocellulosic feedstocks was performed to reduce biomass recalcitrance and enhance enzymatic accessibility of cellulose and hemicellulose. Steam explosion pretreatment was carried out by collaborators at the Bioprocess Pilot Facility (BPF), Delft, The Netherlands, using a 40 L pilot steam gun reactor (25 L working volume). Prior to pretreatment, biomass feedstocks were prewetted with either water or sulfuric acid solution depending on the targeted pretreatment severity (Table 2.5).

Biomasses and liquids were mixed in plastic drums to achieve a final acid concentration of 0.5% (w/w) H_2SO_2 when applied, with overall moisture contents adjusted to 30–60%. Prewetted biomasses were stored at 6 °C in sealed bags or buckets before steam explosion. Steam explosion was performed in batch mode. The reactor was preheated by running two empty sequential experiments at the process temperature and draining condensate to relieve pressure in the 4 barg steam lines.

The prewetted biomass (typically ~20 L per run) was loaded into the vessel, and residual air was displaced with steam until a temperature of 115 °C was reached. The system was degassed to improve pretreatment efficiency, after which the biomass was treated for 10 min at the saturated steam pressure corresponding to the target pretreatment temperature. At the end of the residence time, the explosion valve was opened and the biomass slurry was discharged into a cyclone collector using steam pressure. The steam-exploded material was cooled, weighed, packaged in closed buckets and stored at 6–7 °C until enzymatic hydrolysis (Section 2.6.3). The reactor and cyclone were cleaned between runs using 10 L water (Yang and Tucker, 2013; Alhafiz et al., 2025b).

Pretreatment conditions were varied across feedstocks to compare higher-temperature treatment without acid to acid-catalysed pretreatment at lower temperatures, as summarized in Table 2.5. Representative photographs of raw biomasses are provided in Figure C1 (supplementary information), and photographs of biomasses after steam explosion are provided in Figure C2 (supplementary information).

Table 2.5: Steam explosion conditions for biomasses

Biomass	Pretreatment Conditions	Sample #
A Wheat straw	No additive, 160°C	A1
	0.5% H_2SO_4, 160°C	A2
	No additive, 180°C	A3
B Beech	0.5% H_2SO_4, 160°C	B1
	0.5% H_2SO_4, 180°C	B2
	No additive, 190°C	B3
C Spruce	0.5% H_2SO_4, 160°C	C1
	0.5% H_2SO_4, 180°C	C2
	No additive, 190°C	C3
D Pine	0.5% H_2SO_4, 160°C	D1
	0.5% H_2SO_4, 180°C	D2
	No additive, 190°C	D3
E Miscanthus	0.5% H_2SO_4, 160°C	E1
	0.5% H_2SO_4, 180°C	E2
	No additive, 180°C	E3
	No additive, 190°C	E4

2.11.3 Enzymatic hydrolysis

Enzymatic hydrolysis was performed on steam-exploded lignocellulosic solids. For each pretreated sample, the dry matter content was determined using a moisture analyzer (MA 50, Sartorius) at 105 °C. Hydrolysis was conducted according to Novy et al. (2015) with minor modifications, primarily the use of a commercial cellulase/hemicellulase cocktail (Cellic® CTec3 HS, Novozymes; stored at 6 °C).

Hydrolysis reactions were prepared in 500 mL Erlenmeyer flasks with ground stoppers at 15% (w/w) solids loading (37.5 g dry mass) in 20 mM sodium acetate buffer (pH 4.8) to a total working volume of 250 mL. Enzyme loading followed the supplier recommendation (~3 g

Cellic® CTec3 HS per 100 g cellulose); reactions were initiated by aseptic addition of 0.44 g enzyme preparation (~ 0.4 mL). For the pulp reference, threefold enzyme dosage was applied. Flasks were incubated at 50 °C and 200 rpm for 72 h (Certomat BS-1). Reactions were terminated by heating in a 100 °C water bath for 10 min to inactivate enzymes.

2.11.4 Filtration of hydrolysed biomass

Following heat inactivation, residual solids were separated from the soluble hydrolysate fraction by vacuum filtration. The filtration setup comprised a polypropylene Büchner funnel (390 mL) fitted with two glass-fiber filter circles (MN 85/70 BF; nominal retention 0.6 µm), connected to a 2 L DURAN™ gas-wash bottle (Drechsel type) positioned on a balance, and further connected to a vacuum pump (Vacuubrand MZ 2C NT; ultimate pressure 7.0 mbar). Vacuum was regulated to ~100 mbar using a manual regulator and gauge (Figure S3 supplementary). Filtered hydrolysates were collected and stored at 4 °C until use in analytical characterization and cultivation experiments.

2.11.5 HPLC quantification of sugars and organic acids in hydrolysates

Filtered hydrolysates were quantified for major monosaccharides (glucose, xylose, arabinose, galactose, mannose, and cellobiose), organic acids (formic and acetic acid), and sugar-degradation products (furfural and 5-hydroxymethylfurfural, HMF) using a Merck-Hitachi LaChrome HPLC system equipped with an autosampler (L-7250), refractive index detector (L-7490), and UV detector (L-7400). The analytes (including organic acids, furfural, and HMF) were separated on an Aminex HPX-87H column with an Aminex H guard column (Bio-Rad) operated at 65 °C, using 5 mM H_2SO_2 as the mobile phase at 0.6 mL min^{-1}. Arabinose and mannose were analyzed using the same HPLC system equipped with an Aminex HPX-87P column and P guard column (Bio-Rad); the main column was operated at 80 °C with deionized water as eluent at 0.4 mL min^{-1}.

2.11.6 Deep-well screening cultivation on lignocellulosic hydrolysates

Initial screening cultivations on hydrolysates were carried out in 2 mL polypropylene 96-deep-well plates covered with sterile polyester sealing foil (STR-SEAL-PLT, 50 µm; SealPlate, Carl Roth) to reduce evaporation and cross-contamination. Cultivation mixtures (final volume 1.0 mL per well) were prepared by combining 200 µL of 5× concentrated mineral medium (MM), 500 µL hydrolysate, and a defined volume of preculture to achieve an initial OD_{600} of approximately 1.0; sterile distilled water was added to reach the final volume. All cultivation media were supplemented with kanamycin sulphate (50 mg L^{-1}). Reference wells contained defined sugar mixtures (glucose and xylose) at 2.5 or 7.5 g L^{-1} to benchmark growth on hydrolysate substrates. Plates were shaken at 1300 rpm on a Hei-MIX-Titramax 100 (Heidolph) in a thermostatically controlled room at 30 °C for 3 days.

2.11.7 Inhibitor tolerance and substrate utilization assessment design

To assess inhibition effects independently from differences in carbon availability, hydrolysate-based media were additionally prepared under standardized carbon conditions. Specifically, hydrolysates were tested (i) as 50% (v/v) hydrolysate in the culture broth and (ii) under dilution to a target glucose concentration of ~2 g L^{-1} in the final medium, enabling comparison of growth performance across hydrolysates with different initial sugar and inhibitor profiles. This experimental design supported evaluation of inhibitor tolerance and relative substrate utilization under conditions relevant for subsequent cultivations.

2.11.8 Shake-flask PHB production on selected hydrolysate

PHB production was evaluated in shake-flask cultivations using the most promising hydrolysate with respect to overall growth performance and apparent inhibitor robustness. A cultivation for PHB production was carried out in 100 mL shake flasks using 50% (v/v) wheat straw hydrolysate supplemented with mineral medium MM1. The culture medium was adjusted

to pH 6.8 prior to inoculation. Cultures were inoculated to an initial OD_{600} of 1.0 and incubated at 120 rpm. Samples were collected over the cultivation for determination of biomass formation and PHB accumulation using analytical procedures.

2.12 Process model development and implementation

A process model for autotrophic PHB production by *C. necator* DSM 544 was developed using SuperPro Designer v14 (Intelligen Inc., USA). The process was developed using experimental conditions of DURAN flask fermentation (cultivation 4). The simulation was based on a batch gas fermentation system using CO_2 as the carbon source, H_2 as the electron donor, O_2 as the terminal electron acceptor, and ammonium sulphate ($(NH_4)_2SO_4$) as the nitrogen source. The process configuration is illustrated in Figure 2.5. The fermenter (P-1 / FR-101) was modelled as a stirred tank reactor receiving water, defined medium, inoculum, and a premixed gas stream defined as a stock mixture containing 5% CO_2, 93% H_2, and 2% O_2 (v/v). The premixed gas stream served as both carbon and energy source for autotrophic growth. A vent stream was included to account for unconsumed gases and gaseous by-products, while the liquid broth stream represented the final fermentation output containing biomass, PHB, and residual components. This configuration enables simultaneous modelling of biological reactions and gas-phase interactions within a single unit operation.

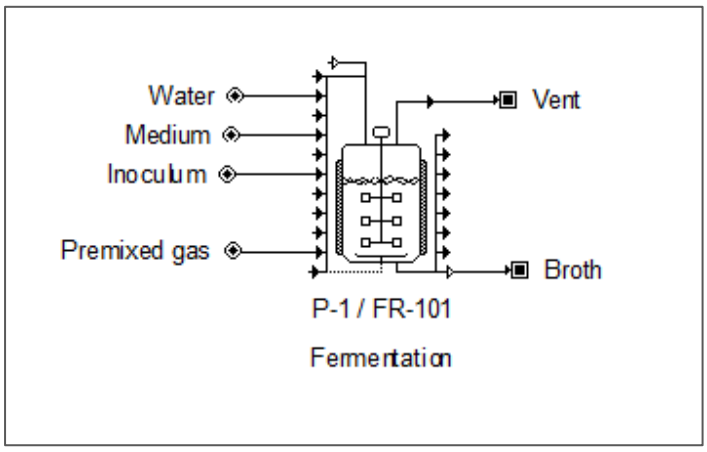

Figure 2.5: Superpro Designer flowsheet for batch gas fermentation process for PHB production by *C. necator*

2.12.1 Kinetic model formulation

The biochemical behaviour of *C. necator* DSM 544 during autotrophic fermentation was described using a combination of kinetic rate expressions and experimentally derived stoichiometric relationships. The model distinguishes between biomass growth, PHB accumulation and neutralization for pH balance. The general form of the growth rate expression is shown in Equation 2.5.

$$r_X = [\alpha\mu_{max}.(\text{S1 term}).(\text{S2 term}) + \beta]\,X \quad \ldots\ldots 2.5$$

where r_X is the growth rate (g L^{-1} h^{-1}), μ_{max} (h^{-1}) is the maximum specific growth rate, α is the dimensionless empirical fitting coefficient, β is the maintenance coefficient (h^{-1}), X (g L^{-1}) is the biomass concentration, and S represents the different kinetic models for growth, PHB accumulation and neutralization.

For growth, the S1-term was defined using a Monod-type expression with respect to dissolved oxygen as shown in Equation 2.6.

$$S1 = \frac{S_{O_2}}{K_s + S_{O_2}} \quad \ldots\ldots 2.6$$

where S_{O_2} is the dissolved oxygen concentration and K_s is the Monod's constant for O_2 which was set to 0.3 mg L^{-1}. In addition, μ_{max} was set to 0.09 h^{-1} representative of the result of the Duran flask fermentation (see Section 3.1) and α set to 1. This formulation reflects oxygen-limited autotrophic growth, with no additional inhibition terms applied to biomass formation.

For PHB accumulation, S1 term was still defined but for slow growth (μ_{max} = 0.045 h^{-1}) and S2 term represents the inhibition equation for inhibition with respect to the nitrogen source (ammonium sulphate) as shown in Equations 2.7a and 2.7b respectively.

$$S1 = \frac{S_{O_2}}{K_s + S_{O_2}} \quad \ldots\ldots 2.7a$$

$$S2 = 1 - \frac{S_N}{K_{mic}} \quad \ldots\ldots 2.7b$$

where S_{O_2} is the dissolved oxygen concentration, and K_s is the Monod constant for oxygen, which was set to 0.2 mg L^{-1}. S_N represents the ammonium sulphate concentration, while K_{mic} is the ammonium sulphate inhibition constant, set to 350 mg L^{-1}. The maximum specific growth rate $\mu_{max}$was set to 0.045 h^{-1}, and the dimensionless empirical fitting coefficient α was assigned a value of 1. To further account for ammonium sulphate inhibition for PHB accumulation, an additional S3 term was defined just like in S2 but with a K_{mic} set to 750 mg L^{-1}. The S2-term was defined as an inhibition function based on ammonium concentration, representing nitrogen limitation as the primary trigger for PHB accumulation. The S3-term represents PHB inhibition, limiting further polymer accumulation at high intracellular PHB levels. Consequently, PHB formation was governed entirely by ammonium limitation, PHB inhibition, and biomass concentration.

Furthermore, the neutralization reaction was described using a first-order kinetic model (S term = [S]), where [S] denotes the substrate concentration. In this model, S1 corresponds to H_2SO_4, whereas S2 represents NaOH.

2.12.2 Stoichiometric modelling

Stoichiometric equations for biomass growth, acid neutralization, and PHB production were derived based on elemental balances of carbon, hydrogen, oxygen, and nitrogen using experimental data from DURAN flask fermentation (section 3: cultivation 4). The detailed derivation of the stoichiometric coefficients, including elemental balances and oxygen uptake rate (OUR)-based calculations, is provided in Appendix D (supplementary information).

Biomass formation was expressed on a C-mol basis using CO_2 as the carbon source, H_2 as the electron donor, O_2 as the terminal electron acceptor, and ammonium sulphate ($(NH_4)_2SO_4$) as the nitrogen source. The balanced stoichiometric equation for biomass growth, derived from elemental balances and implemented in the model, is given in Equation 2.8.

The oxygen requirement for biomass formation was calibrated using OUR data during the PHB-free growth phase (0–34 h), resulting in a value of 2.87 mol O_2 per C-mol biomass. This value reflects the respiratory demand of *C. necator* under autotrophic growth conditions and was incorporated into the growth stoichiometry to ensure consistency with experimental observations.

$$O_2 + 7.76H_2 + 2.87O_2 + 0.12(NH_4)_2SO_4 \rightarrow CH_{1.68}O_{0.46}N_{0.24} + 7.28H_2O + 0.12H_2SO_4 \quad \text{..... 2.8}$$

During growth, ammonium sulphate dissociation leads to the formation of sulfuric acid, resulting in acidification of the medium. To maintain optimal pH conditions for *C. necator*, neutralization with sodium hydroxide (NaOH) was included in the model. The neutralization reaction was represented as shown in Equation 2.9.

$$H_2SO_4 + 2NaOH \rightarrow Na_2SO_4 + 2H_2O \quad \text{.....2.9}$$

The stoichiometric equation for PHB production was derived using the repeating unit $C_4H_6O_2$, ensuring conservation of carbon, hydrogen, and oxygen atoms. Both assimilation and energy (respiratory) requirements were considered in the formulation.

The oxygen demand for PHB synthesis was determined using OUR data during the PHB accumulation phase (51–142 h), resulting in an estimated requirement of 2.3 mol O_2 per C-mol PHB. The resulting stoichiometric equation used in the model is given in Equation 2.10 and was implemented in SuperPro Designer to ensure accurate representation of substrate consumption and product formation.

$$4CO_2 + 27.4H_2 + 9.2O_2 \rightarrow C_4H_6O_2 + 24.H_2O \quad \text{..... 2.10}$$

2.12.3 Model calibration and validation

The model was calibrated using experimental batch fermentation data for *C. necator* DSM 544 (1 L Duran flask experiment). Model performance was evaluated by comparing simulated and

experimental profiles of biomass concentration (CDW), PHB accumulation, and ammonium consumption over 142 hours of cultivation.

Validation focused on reproducing key process characteristics, including lag phase behaviour, exponential growth kinetics, timing of ammonium depletion, onset of PHB accumulation, and final biomass and PHB concentrations. Agreement between simulated and experimental profiles confirmed the suitability of the kinetic and stoichiometric parameters.

2.12.4 Sensitivity analysis

Sensitivity analysis was conducted to evaluate the robustness of the model to variations in key biological parameters and operating conditions. The maximum specific growth rate (μ_{max}) and the dimensionless empirical fitting coefficient (α) were varied within ±20% of their baseline values using a 3×3 factorial design.

The influence of gas supply was evaluated by varying the volumetric aeration rate (VVM) over the range 0.24–0.36 vvm. This analysis was used to identify threshold behaviour associated with oxygen limitation and to assess the dependence of process performance on gas availability.

2.12.5 Scale-up simulation

Scale-up from laboratory to pilot scale was performed by increasing the inlet medium volume while maintaining identical medium composition, kinetic parameters, and operating conditions. The medium composition was defined on a per-liter basis; therefore, scale-up was achieved by increasing the total volume rather than altering concentrations.

Due to the mass-balance-driven nature of SuperPro Designer, the resulting working volumes were approximately 1.27 L for the laboratory-scale model and 12.8 L for the pilot-scale scenario. Process performance at both scales was compared in terms of biomass concentration,

PHB concentration, batch duration, volumetric productivity, total product output, and substrate and utility requirements.

2.12.6 Assumptions and limitations

The model assumes homogeneous mixing and does not explicitly account for hydrodynamic effects such as k_La, mixing gradients, or bubble dynamics. Oxygen limitation is represented through Monod-type kinetics. Despite these limitations, the model provides a consistent and experimentally validated framework for evaluating process performance and scalability at the level of kinetic and stoichiometric process design.

3 Results and discussion

3.1 Contribution of soluble and membrane-bound hydrogenases to energy metabolism in *C. necator*

In this section, a systematic comparison of hydrogenase knockout strains differing in SH and MBH expression under both heterotrophic and autotrophic conditions is presented. To quantify the energetic contribution of each hydrogenase system, growth behaviour and heat production profiles obtained by isothermal microcalorimetry are presented. These data provide mechanistic insight into hydrogen oxidation pathways and enable calculation of energy efficiency during cultivation.

The work presented in this section forms the basis of a manuscript currently in preparation.

Alhafiz, H. A., Linke, T., Hanke, B., Mann, M., Hoffmann, M., Cordero, P. R. F., Schmid, A., Maskow, T. & Lauterbach, L. Contribution of soluble hydrogenases and membrane-bound hydrogenases to the energy efficiency of *Cupriavidus necator*. (Manuscript in preparation)

Author contributions

Halima Aliyu Alhafiz: Experimental design, Methodology, Assembly and set-up of bioreactor systems, Autotrophic cultivations, Data analysis and writing-original draft
Tilman Linke: Methodology, Calorimetry experiments, Data analysis and writing-original draft
Brunon Hanke: Heterotrophic and Autotrophic cultivations
Marcel Mann: Resources, Methodology, Supervision, Writing-review and editing
Maximilian Hoffmann: Support with RAMOS experiments
Paul R. F. Cordero: Conceptualization, Writing-review and editing
Andreas Schmid: Resources, Methodology, Supervision, Writing-review and editing
Thomas Mascow: Resources, Methodology, Supervision, Writing-review and editing
Lars Lauterbach: Conceptualization, Methodology, Funding, Supervision, Writing-review and editing

3.1.1 Heterotrophic growth of different hydrogenase knockout strains

Figure 3.1 presents the heterotrophic growth profiles of *C. necator* strains differing in hydrogenase composition (SH^+, MBH^+, or SH^++MBH^+) under two regulatory backgrounds.

Continuous lines represent the hoxJ background, in which the regulatory hydrogenase (RH) is non-functional, resulting in constitutive expression of the hydrogenase operons. Dashed lines correspond to the hoxJ* background, which contains a functional RH and therefore regulates hydrogenase expression in response to H_2 availability.

Under the tested heterotrophic conditions, the differences between the SH^++MBH^+, SH^+, and MBH^+ strains within the same regulatory background were relatively small. Although minor variations in final biomass concentration are observable, these differences are not pronounced, particularly when compared to the stronger physiological effects typically observed under autotrophic conditions (Section 3.1.2). This suggests that, during heterotrophic growth on organic substrates, the presence or absence of individual hydrogenases has only a limited impact on overall biomass formation. In this metabolic regime, energy generation and reducing equivalents are primarily derived from substrate oxidation, thereby reducing the relative contribution of hydrogenase-dependent electron flow.

In contrast, a clearer distinction is observed between the two regulatory backgrounds. Across all hydrogenase configurations, the *hoxJ** strains (dashed lines) consistently reached higher biomass concentrations than the corresponding *hoxJ* strains (continuous lines). Since *hoxJ* leads to constitutive hydrogenase expression due to a non-functional RH, continuous synthesis of large, cofactor-rich enzyme complexes likely imposes an additional metabolic burden on the cell. This interpretation is supported by proteomic data showing that the SH and MBH subunits are strongly induced during lithoautotrophic growth in *C. necator*, with roughly 20-fold and 13-fold higher abundance, respectively, than in succinate-grown cells. Hydrogenases require substantial resources for transcription, translation, cofactor insertion, and maturation; under heterotrophic conditions with limited or no H_2, constitutive production of these enzymes may therefore represent an unnecessary energetic cost (Kohlmann et al., 2011; Horch et al., 2010). In the *hoxJ** background, hydrogenase expression remains regulated in response to H_2

availability, reducing expression under heterotrophic conditions and thereby avoiding unnecessary protein synthesis. This regulatory advantage is reflected in improved growth performance, with estimated specific growth rates of around 0.17–0.23 $h^{-1}$for the *hoxJ* strains and 0.20–0.25 h^{-1} for the *hoxJ** strains across all hydrogenase configurations. A similar trend was reported by Jahn et al. (2024), who observed increased growth rates (from 0.10 h^{-1} to 0.12–0.14 h^{-1}) when hydrogenase-associated metabolic burden was alleviated under comparable non-lithoautotrophic conditions.

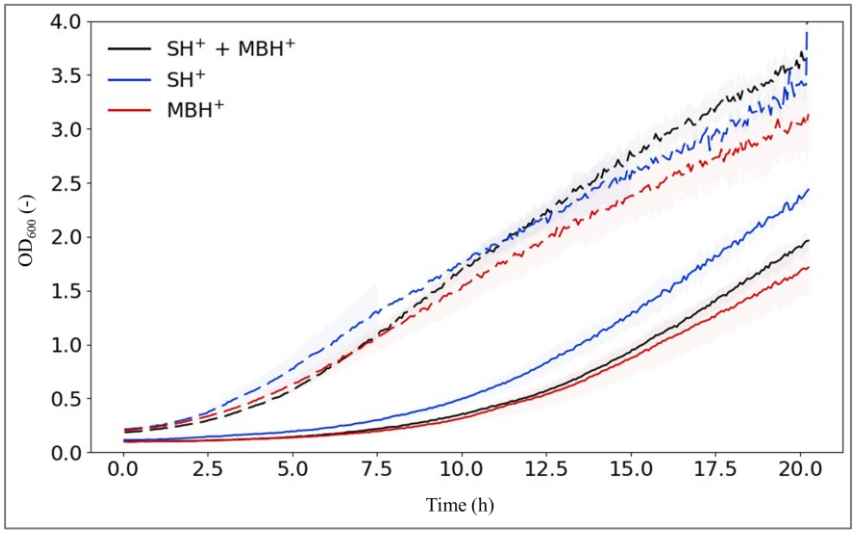

Figure 3.1: Heterotrophic growth of hydrogenase knockout strains in 20 mL pioreactors. Continuous lines represent the hoxJ background, while dashed lines represent the hoxJ* background. Shaded areas indicate standard deviation of biological replicates (n=2).

3.1.2 Autotrophic growth of different hydrogenase knockout strains in serum bottles

Autotrophic growth of the hydrogenase knockout strains was assessed in sealed serum bottle cultivations under two distinct non-explosive gas compositions due to safety concerns (Figure 3.2). Under hydrogen-limited conditions (H_2: O_2: CO_2: N_2 = 3.8: 7.3: 13: 75.9%; Figure 3.2 A), all strains exhibited low biomass accumulation. Although 3.8% H_2 is generally sufficient to sustain autotrophic growth in continuously gassed systems, this batch-type headspace replacement every 24 h likely caused transient H_2 depletion between gas exchange intervals. Consequently, overall growth was limited by electron donor availability. Under these conditions, only minor differences were observed among the SH^+, SH^++MBH^+ (wild-type), and

MBH^+ strains, and the influence of the regulatory background was minimal. These findings indicate that, under strong substrate limitation, hydrogenase composition and regulatory state exerted little influence compared to the overriding effect of hydrogen availability.

In contrast, hydrogen-excess conditions (H_2: O_2: CO_2 = 84: 3: 13%; Figure 3.2 B) revealed pronounced strain-dependent differences. The SH^+ strain achieved the highest biomass concentration, followed closely by the SH^++MBH^+ strain, whereas the MBH^+ strain showed substantially reduced growth. Interestingly, the SH^+ strain performed comparably to, or slightly better than, the SH^++MBH^+ strain. These physiological outcomes reflect the distinct metabolic roles of the two hydrogenases. The SH catalyzes the direct reduction of NAD^+ to NADH, supplying reducing power necessary for CO_2 fixation via the CBB cycle. In contrast, MBH donates electrons to the quinone pool to support proton motive force generation, thereby contributing primarily to ATP synthesis rather than direct reductive metabolism.

These results are consistent with regulatory insights from Lenz and Friedrich (1998) and systems-level analyses by Jahn et al. (2024). Lenz and Friedrich (1998) described the HoxBC–HoxJ–HoxA signal transduction system controlling hydrogenase gene expression in *C. necator*, wherein HoxBC functions as the primary H_2 sensor and HoxJ modulates transcriptional activation in response to H_2 availability. Complementarily, Jahn et al. (2024) demonstrated through genome-wide fitness profiling that both SH and MBH support lithoautotrophic growth, although disruption of hydrogenase components substantially impairs competitive fitness under H_2-dependent conditions.

The present serum bottle results provide direct physiological validation of these mechanistic findings and is consistent with the findings of Schink & Schlegel (1978). Under H_2-rich conditions, SH-containing strains displayed superior growth, underscoring the dominant role of NADH-generating hydrogen oxidation in sustaining high autotrophic flux. In contrast, under

H_2 limitation, strain-specific and regulatory effects were largely masked by mass transfer constraints, highlighting that gas-phase availability is the principal determinant of growth in closed-batch systems. The measurable influence of the regulatory background only under H_2-excess conditions further supports the model proposed by Lenz and Friedrich, in which H_2-responsive regulation fine-tunes hydrogenase expression according to substrate abundance. When H_2 is plentiful, deregulated or constitutive expression of SH and MBH does not impair fitness; however, when H_2 becomes limiting, regulatory advantages are superseded by physical substrate constraints.

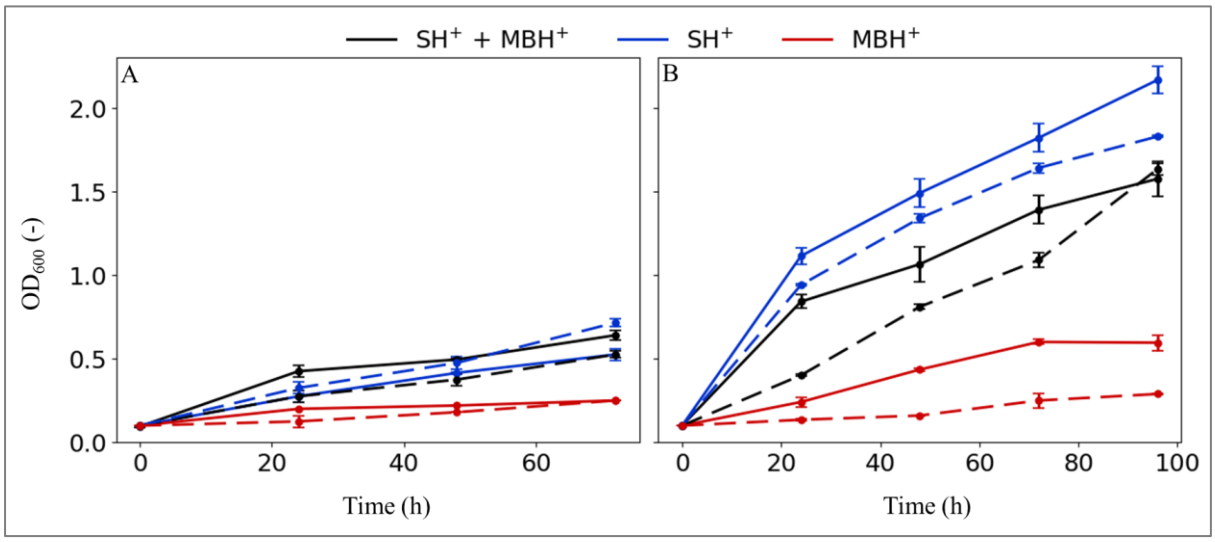

Figure 3.2: Autotrophic growth of *C. necator* hydrogenase knockout strains in sealed serum bottle cultivations under: (A) Low hydrogen conditions (H_2: O_2: CO_2: N_2 = 3.8: 7.3: 13: 75.9%); (B) Hydrogen-excess conditions (H_2: O_2: CO_2 = 84: 3: 13%). Continuous lines represent the *hoxJ* background, and dashed lines represent the *hoxJ** background. Data points represent mean values of biological replicates (n=2).

3.1.3 Heat flow and yield associated with chemolithoautotrophic growth of different hydrogenase knockout strains

To quantify heat release across the hydrogenase knockout strains and assess their energy efficiency under chemolithoautotrophic conditions, isothermal microcalorimetry was performed using a TAM IV microcalorimeter. Cultures were incubated under a gas composition of 3.8% H_2, 7.3% O_2, 13% CO_2, and 75.9% N_2. The heat flow profiles showed clear strain-dependent differences in metabolic activity, with SH-containing strains generally

exhibiting stronger early heat evolution than MBH-only strains, indicating faster H_2-driven metabolism (Figure E1, supplementary information). Peak heat flow alone is not sufficient for comparing energetic performance, because it reflects only the maximum instantaneous rate and not the total metabolic output relative to biomass formation. Therefore, total heat release was integrated over time and normalized to biomass concentration to calculate heat yield (kJ/g biomass), providing a more meaningful measure of energetic efficiency. As shown in Figure 3.3, MBH-only strains consistently displayed the highest heat yields, indicating the greatest energy dissipation, with MBH dissipating approximately 3.3-fold more heat than SH in the *hoxJ* background and about 2.5-fold more in the *hoxJ** background. In addition, the *hoxJ** regulatory background reduced heat dissipation compared with *hoxJ*, demonstrating that functional hydrogenase regulation improves energy efficiency under autotrophic conditions.

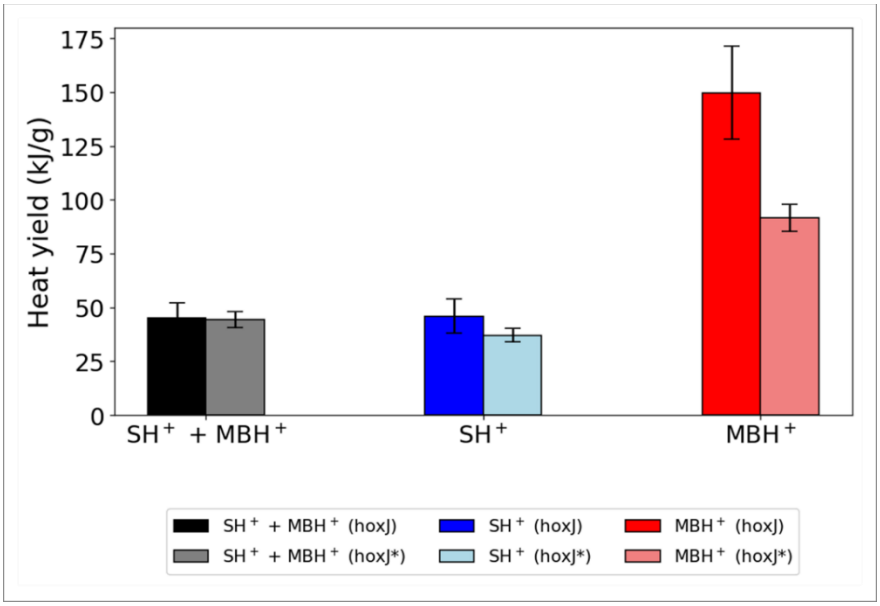

Figure 3.3: Heat yield of *C. necator* hydrogenase knockout strains cultivated with 3.8%, H_2, 7.3% O_2, 13% CO_2, 75.9% N_2 in a TAM IV isothermal microcalorimeter. Data represents triple experiments.

3.1.4 Section summary and outlook

This section demonstrates that the contribution of hydrogenases to energy metabolism in *C. necator* is highly dependent on the growth regime and regulatory control. Under heterotrophic conditions, hydrogenase composition had minimal impact on growth, while regulatory control

via *hoxJ** improved biomass formation by reducing the metabolic burden associated with unnecessary enzyme expression. In contrast, under autotrophic conditions, hydrogenase function became important: strains containing the SH exhibited superior growth when compared to MBH. Calorimetric analysis further revealed that these physiological differences are reflected in energy dissipation patterns, with MBH-only strains dissipating significantly more energy as heat. Additionally, functional regulation (*hoxJ**) consistently reduced heat dissipation, highlighting the role of hydrogenase regulation in optimising energy use.

As an outlook, coupling these findings with hydrogen transfer rate (HTR) data from a Respiration Activity Monitoring System (RAMOS) experiment will enable a quantitative assessment of energy efficiency based on the fraction of consumed H_2 that is conserved in biomass versus dissipated, providing a more complete understanding of substrate-to-biomass energy conversion.

3.2 Establishment of stable gas fermentation of *C. necator*

In this section, the autotrophic growth behaviour of *C. necator* DSM 544 under $H_2/CO_2/O_2$ gas fermentation conditions is investigated. The objective is to identify the factors governing culture stability and productivity, with particular emphasis on pH behaviour, nutrient composition, and reactor configuration. Initial experiments focus on elucidating the origin of culture acidification observed during autotrophic growth of DSM 544, followed by the development and validation of a practical pH stabilization strategy. The section concludes with an evaluation of process intensification under intrinsically safe operating conditions.

Part of the methodology used in this section is published as a methods paper.

Alhafiz, H. A.*, Di Bisceglie, F., Meier, H. P. F., Weickardt, I., González, I. A. C., Navarro, J. G., Schoenmakers, P., Oyen, S. J., Lettau, E., Lombard, E., Cordero, P. R. F., Konarzycka-Bessler, M., Gorret, N., Schmidt, S., Schillberg, S., Mann, M., Guillouet, S. E., Kratzer, R., & Lauterbach, L.* (2025). *Cupriavidus necator* as a model organism for CO_2-based biotechnology. *Methods in enzymology*, *714*, 163–194.

https://doi.org/10.1016/bs.mie.2025.01.017

Author contributions

Halima Aliyu Alhafiz: Conceptualization, Methodology, Writing-original draft and reviewing/editing

Federico Di Bisceglie: Methodology, Writing-original draft

Franziska P. F. Meier: Methodology, Writing-original draft

Isabel Weickardt: Methodology, Writing-original draft

Itzel A. C. González: Methodology, Writing-original draft

Javier G. Navarro: Methodology, Writing-original draft

Pierre Schoenmakers: Methodology, Writing-original draft

Sven J. Oyen: Methodology, Writing-original draft

Elisabeth Lettau: Methodology, Writing-original draft

Eric Lombard: Methodology

Paul R. F. Cordero: Methodology, Writing-reviewing/editing

Monika Konarzycka-Bessler: Methodology, Supervision, Writing-reviewing/editing

Nathalie Gorret: Methodology, Supervision, Funding, Writing-reviewing/editing

Sandy Schmidt: Methodology, Supervision, Funding, Writing-reviewing/editing

Stefan Schillberg: Methodology, Supervision, Writing-reviewing/editing

Marcel Mann: Writing-reviewing/editing

Stephane E. Guillouet: Methodology, Supervision, Funding, Writing-reviewing/editing

Regina Kratzer: Methodology, Supervision, Funding, Writing-reviewing/editing

Lars Lauterbach: Conceptualization, Methodology, Supervision, Funding, Writing-reviewing/editing

In addition, the results presented in this section forms the basis of a manuscript currently in preparation.

Alhafiz, H. A., Graber, M., Calabrese, D., Cordero, P. R. F., Lauterbach, L., Hochenauer, C., Reichhartinger, M. & Kratzer, R. Overcoming pH instability for a safe and sustainable polyhydroxybutyrate production by *Cupriavidus necator* DSM544. (Manuscript in preparation)

Author contributions

Halima Aliyu Alhafiz: Conceptualization, Experimental design, Methodology, Set-up of bioreactor systems, Autotrophic cultivations and Data analysis, PHB extraction, Analytics, Writing-original draft

Maximilian Graber: Support with Autotrophic cultivations, Writing-original draft

Donato Calabrese: NMR characterization of PHB

Paul R. F. Cordero: Formal analysis, Writing-reviewing/editing

Lars Lauterbach: Funding, Resources, Supervision, Writing-reviewing/editing

Christoph Hochenauer: Resources, Supervision, Writing-reviewing/editing

Markus Reichhartinger: Methodology, Software, Supervision, Writing-reviewing/editing

Regina Krazer: Conceptualization, Funding, Resources, Supervision, Formal analysis, Writing-reviewing/editing

3.2.1 Effect of buffer capacity and ammonium concentration on pH stability

C. necator DSM 544 was cultivated autotrophically in a 1 L Duran flask bioreactor supplied with a $H_2/CO_2/O_2$ gas mixture (93: 5: 2 %) at 240 rpm using different modifications of mineral medium to assess the influence of buffering capacity and nitrogen availability on pH stability and microbial growth. Phosphate buffer concentration, ammonium sulphate concentration, and

magnesium sulphate levels were systematically varied (Table 2.3) to evaluate their individual and combined effects on culture performance. The resulting growth behaviour and pH profiles are summarized in Figure 3.4.

Cultivation 1 was performed using MM1, which contained a high ammonium concentration corresponding to 2.5 g L^{-1} NH_4^+-N. Despite this increased robustness, cultivation in MM1 resulted in a rapid decline in culture pH (Figure 3.4A), accompanied by limited biomass formation (Figure 3.4B). This observation indicates that, under the applied conditions, proton release associated with ammonium assimilation exceeded the neutralization capacity of the phosphate buffer present in MM1.

To compensate for the observed acidification, the phosphate buffer concentration was increased in MM2 (Cultivation 2). Acidification still occurred during growth (Figure 3.4B), demonstrating that phosphate buffering alone was insufficient to maintain pH stability during autotrophic cultivation of DSM 544. In Cultivation 3, the standard mineral medium with reduced ammonium concentration (Alhafiz et al., 2025a) was tested to assess whether excessive nitrogen supply was the primary driver of acidification. However, pH decline was again observed, indicating that the instability could not be attributed solely to ammonium load (Figure 3.4A).

Taken together, these results demonstrate that neither increased buffering capacity nor reduced ammonium availability was sufficient to prevent acidification during autotrophic growth of DSM 544. Instead, the persistent pH decline suggests an intrinsic metabolic imbalance. This interpretation is supported by recent studies reporting that *C. necator* strains engineered for glucose assimilation exhibit altered redox and proton flux distributions, which can manifest as extracellular acidification during autotrophic growth (Koh et al., 2024; Lin & Ng, 2025). In contrast, Lambauer et al. (2023) reported stable pH profiles during gas fermentation with the

wild-type strain *C. necator* H16, highlighting the strain-specific nature of the observed instability.

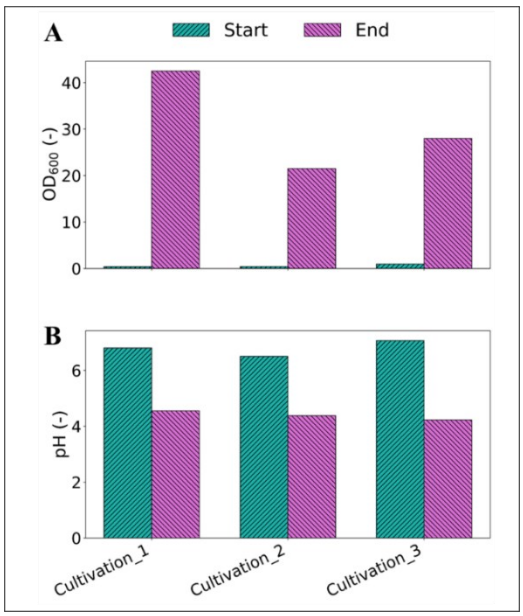

Figure 3.4: Growth of *C. necator* DSM 544 in a DURAN flask for Cultivations 1-3 under different phosphate buffering strategies and ammonium concentrations. Shown are start and final optical density (OD_{600}) after approximately 72 h (A); and initial and final culture pH (B).

3.2.2 Stabilization of autotrophic growth via manual pH control

To mitigate the pronounced culture acidification observed during autotrophic growth of *C. necator* DSM 544, a manual pH control strategy was implemented in Cultivation 4. This approach was based on a prior calibration experiment that demonstrated an approximately linear relationship between NaOH addition, and the resulting pH increase within the pH range 6.0–6.7 (R^2 = 0.9961; Figure A4, Supplementary Information). For a culture volume of 1 L, the addition of 1 mL of 5 mM NaOH increased the pH by approximately 0.405 units, enabling predictive and reproducible pH adjustment.

Application of this calibration-based strategy allowed the culture pH to be maintained within the target range of 6.4–6.9 throughout the cultivation, as shown in Figure 3.5A. In contrast to earlier cultivations without pH control, pH remained stable during exponential growth, enabling sustained biomass formation. As a result, *C. necator* DSM 544 reached a cell dry

weight of 13.5 g L^{-1} under these conditions, demonstrating that pH instability was the primary limiting factor in previous experiments.

The stabilized pH environment also enabled a clear transition from growth to storage metabolism. As ammonium was progressively depleted from the medium (Figure 3.5B), biomass formation slowed and PHB accumulation commenced, reaching a maximum content of approximately 71% of cell dry weight. This metabolic shift is consistent with the well-established physiology of *C. necator*, where nitrogen limitation triggers redirection of carbon and reducing equivalents toward intracellular PHB synthesis. Importantly, the onset and progression of PHB accumulation occurred once pH stability was ensured, confirming that nitrogen availability, rather than pH, governed the timing of polymer synthesis.

The metabolic state of the culture during these phases is further reflected by the oxygen uptake rate (OUR) profile shown in Figure 3.5C. During exponential growth, OUR increased steadily, corresponding to rising respiratory activity associated with hydrogen oxidation and CO_2 fixation. Under stable pH conditions, OUR remained elevated throughout the growth phase, indicating sustained metabolic activity and the absence of growth inhibition. As ammonium became limiting and PHB accumulation dominated, OUR gradually declined, consistent with reduced growth-associated respiration and a shift toward storage metabolism.

Short, transient drops in OUR coincided with brief interruptions in gas supply during sampling. In each case, OUR rapidly recovered once gas flow was restored, demonstrating that the culture maintained metabolic activity and was not irreversibly affected by these disturbances. This response highlights the physiological robustness of *C. necator* DSM 544 under autotrophic conditions when pH is maintained within an optimal range.

Taken together, the combined analysis of pH control (Figure 3.5A), ammonium depletion and PHB accumulation (Figure 3.5B), and respiratory activity (Figure 3.5C) demonstrates that

manual pH control is an effective and robust strategy for stabilizing autotrophic growth of *C. necator* DSM 544. By preventing acidification, this approach enables sustained metabolic activity, high biomass formation, and efficient PHB accumulation under gas fermentation conditions.

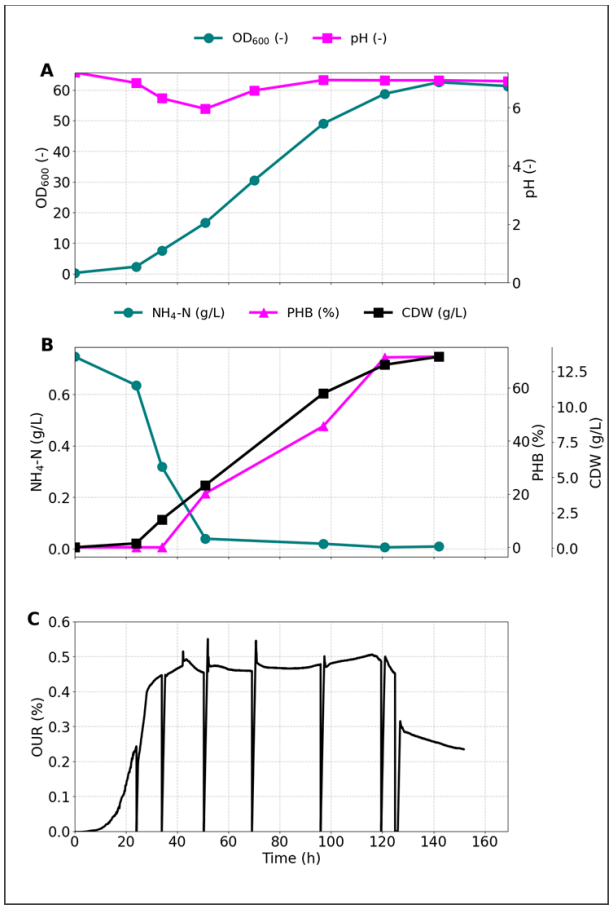

Figure 3.5: Cultivation of *C. necator* DSM 544 in DURAN flask with manual pH control under $H_2/CO_2/O_2$ conditions. (A) OD_{600} and culture pH over time; (B) NH_4–N consumption, cell dry weight (CDW), and PHB accumulation; (C) Oxygen uptake rate (OUR)

3.2.3 Transferability across reactor configurations

To evaluate the robustness of the pH stabilization strategy beyond flask-based systems, Cultivation 5 was conducted in a 1.2 L Labfors stirred-tank bioreactor operated at 887 rpm. Manual pH adjustment was applied without any automated control. Despite differences in reactor geometry, agitation, and gas–liquid mass transfer characteristics, stable pH control within the target range of 6.4–6.9 was achieved (Figure 3.6).

The cultivation resulted in a maximum cell dry weight of approximately 12 g L^{-1}, comparable to that obtained in the Duran flask system. Both systems exhibited steady increases in OD_{600} and CDW, minor transient pH deviations, and similar final biomass concentrations. These results indicate that, under the investigated conditions, the simpler Duran flask setup can reliably reproduce key growth and stability trends observed in a stirred-tank bioreactor, supporting its use as a representative small-scale platform for evaluating gas fermentation strategies prior to further process development.

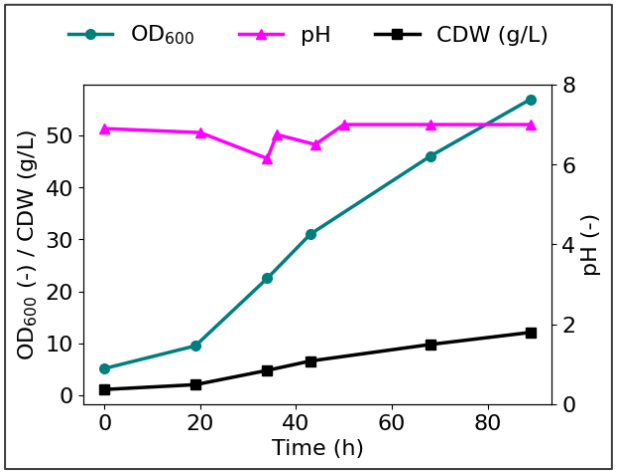

Figure 3.6: Growth of *C. necator* DSM 544 with manual pH control under $H_2/CO_2/O_2$ conditions in 1.2-L stirred-tank bioreactor

3.2.4 Process intensification under intrinsically safe conditions

Based on the insights gained from Cultivations 1–5, Cultivation 6 was designed to intensify the autotrophic process while maintaining non-explosive operation. The experiment was conducted in the 1.2 L Labfors bioreactor at 887 rpm using a modified gas composition (5% CO_2, 40% H_2, 2% O_2, 53% N_2), with N_2 serving as a filling gas.

The principal distinction between the Duran flask and Labfors bioreactor systems lies in their gas–liquid mass transfer capacity, with reported k_La values of approximately 20 h^{-1} and 110 h^{-1}, respectively (Lambauer et al., 2023; Lambauer & Kratzer, 2022). The higher k_La enabled

improved substrate availability at comparable dissolved oxygen levels, facilitating higher growth rates and cell densities. For Cultivation 6, MM3 was employed, combining elevated ammonium concentration with proportionally increased phosphate buffer and magnesium sulphate levels. While the increased ammonium supply delayed the onset of PHB accumulation, it enabled higher biomass formation prior to nitrogen depletion, thereby increasing the cellular capacity for subsequent PHB storage.

Under these conditions, a maximum cell dry weight of approximately 42 g L^{-1} was achieved, with PHB accounting for up to 70% of the biomass following ammonium depletion (Figure 3.7A). These results represent a substantial improvement over earlier cultivations and were achieved without pressurization or elevated oxygen concentrations. In comparison, Tanaka et al. (1995) reported nearly twice the cell dry weight using a basket-type agitator at an exceptionally high k_La of 2970 h^{-1} and oxygen concentrations below 7%, which would not be considered intrinsically safe by current standards given the revised oxygen lower explosion limit of approximately 4.3% (Schröder & Holtappels, 2005). Similarly, Vlaeminck et al. (2024) achieved comparable biomass and PHB levels under pressurized conditions (up to 3 bar) and extensive process control. In contrast, the present work demonstrates that high-density autotrophic PHB production is feasible under milder, non-pressurized, and inherently safer operating conditions (Lambauer et al., 2023).

3.2.5 Culture robustness during transient CO_2 limitation

The oxygen uptake rate (OUR) profile recorded during Cultivation 6 (Figure 3.7B) revealed a temporary decline in metabolic activity corresponding to a period of CO_2 limitation caused by exhaustion of the CO_2 gas supply. The sharp decrease in OUR reflects the immediate dependence of *C. necator* DSM 544 on CO_2 availability for autotrophic metabolism. Upon reintroduction of CO_2, the OUR rapidly increased, indicating prompt recovery of metabolic activity and continued growth without apparent loss of viability.

This response demonstrates a high degree of physiological robustness under transient substrate limitation, an important trait for large-scale gas fermentation processes where fluctuations in gas supply can occur. The ability to rapidly resume autotrophic metabolism following CO_2 starvation further underscores the suitability of *C. necator* DSM 544 for dynamic gas fermentation environments.

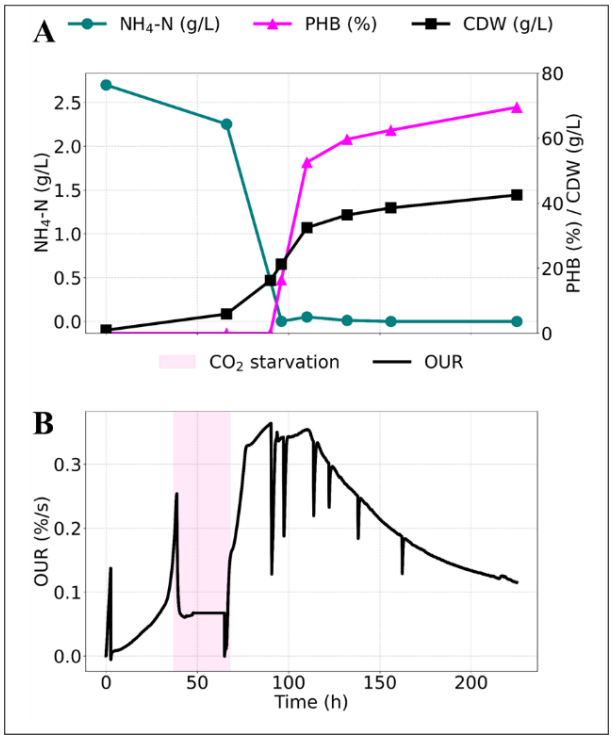

Figure 3.7: Intensified Cultivation 6 of *C. necator* DSM 544 performed in a 1.2-L stirred-tank bioreactor (A); Oxygen uptake rate (OUR) profile of *C. necator* DSM 544 (B).

3.2.6 Structural verification of extracted PHB

Structural verification of the extracted polymer was carried out using ^{1}H NMR spectroscopy to assess chemical identity and purity. The ^{1}H NMR spectra of PHB recovered from *C. necator* DSM 544 cultivated under autotrophic conditions are shown in Figure 3.8. All samples exhibited the characteristic resonance signals of PHB, including the methine proton at δ 5.27 ppm, the methylene protons at δ 2.50 ppm, and the methyl protons at δ 1.26 ppm. These signals correspond to the repeating 3-hydroxybutyrate units of the polyester backbone and are

consistent with a commercial reference spectrum for PHB and with PHB previously reported for gas-grown *C. necator* (Lambauer & Kratzer, 2022).

Comparison of the extracted samples with a commercial PHB reference revealed excellent spectral agreement, with no detectable impurity peaks arising from residual biomass components, lipids, or solvent-derived contaminants. This confirms that the 1,3-dioxolane extraction protocol enabled effective separation of intracellular PHB from cellular material while preserving polymer integrity (Aramvash et al., 2015a). Notably, the spectra obtained from PHB extracted after different cultivation strategies (cultivations 4 and 6, section 3.1) were indistinguishable, indicating that neither cultivation conditions nor pH control strategy adversely affected polymer structure or purity.

Beyond analytical validation, the use of 1,3-dioxolane represents a significant improvement over conventional halogenated solvent systems such as chloroform. As a non-halogenated, water-miscible solvent with lower toxicity and improved environmental compatibility, 1,3-dioxolane enables integration of aqueous precipitation and solvent recycling strategies, thereby reducing solvent consumption and downstream processing costs (Aramvash et al., 2015b). The clean NMR spectra obtained in this study demonstrate that this greener solvent system is not only environmentally advantageous but also suitable for producing high-purity, analytical-grade PHB.

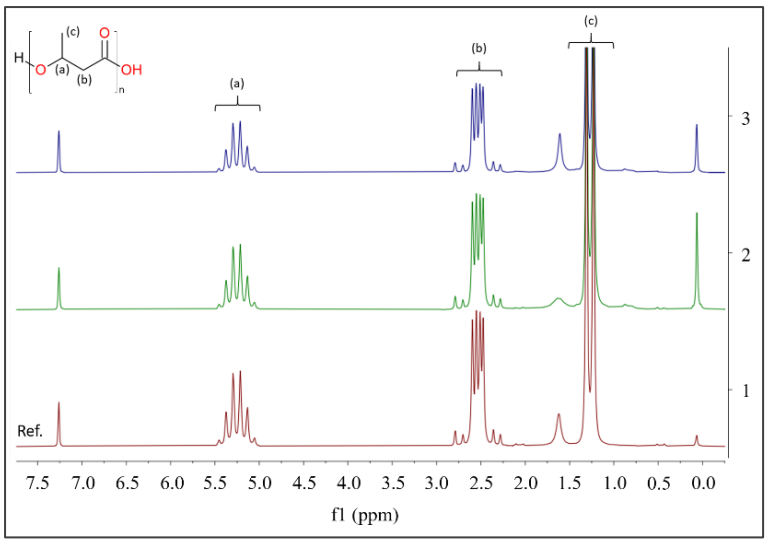

Figure 3.8: ^{1}H NMR spectra (80 MHz) of PHB extracted using 1,3-dioxolane from *C. necator* DSM 544. Commercial reference PHB (bottom); cultivation 4 (middle); cultivation 6 (top)

3.2.7 Section summary

The autotrophic growth of *C. necator* DSM 544 under $H_2/CO_2/O_2$ fermentation conditions was systematically established and optimized. Initial experiments demonstrated that uncontrolled culture acidification represented the primary limitation to stable growth, which could not be resolved solely through increased buffer capacity or modified ammonium supply. These findings indicate that pH instability is intrinsically linked to strain-specific metabolic characteristics of *C. necator* DSM 544, a glucose-utilizing mutant, rather than medium composition alone, and likely reflects altered intracellular flux and proton-balancing behaviour relative to wild-type *C. necator* strains.

Implementation of a calibration-based manual pH control strategy successfully mitigated acidification, enabling stable autotrophic growth, biomass formation, and efficient PHB accumulation without reliance on ATEX-certified automated control systems. The approach proved robust across different reactor configurations, with comparable performance observed in both flask-based and stirred-tank systems. Process intensification through improved gas–liquid mass transfer and optimized nutrient composition further enabled high cell density

cultivation, achieving up to 42 g L^{-1} cell dry weight with PHB contents of approximately 70% under intrinsically safe operating conditions.

Furthermore, high-purity PHB can be recovered from autotrophically grown *C. necator* DSM 544 using a non-halogenated 1,3-dioxolane-based extraction protocol. The ^{1}H NMR analysis verifies that the polymer is chemically identical to commercial PHB and free of detectable impurities, demonstrating that sustainable downstream processing strategies can be successfully coupled with safe gas fermentation. Together, these results directly address the objective of establishing a safe, stable, and scalable cultivation framework for H_2-driven CO_2 fermentation using *C. necator* under ATEX-relevant constraints.

3.3 Membrane-integrated gas fermentation for 2-methylpyrrolidine biosynthesis

In this section, a membrane-integrated gas fermentation platform was developed and evaluated for controlled hydrogen-driven bioprocessing. The objective was to establish a mini-fermenter system capable of delivering gaseous substrates in a safe and efficient manner while enabling precise monitoring of microbial metabolism and catalytic activity. A hollow fiber membrane module was integrated into a mini-fermenter to provide bubble-free gas delivery and physically separated supply of H_2 and O_2/CO_2, thereby preventing formation of explosive gas mixtures while maintaining optimal gas compositions for chemolithoautotrophic growth of *C. necator*. Using this platform, the feasibility of coupling chemolithoautotrophic metabolism with whole-cell redox biocatalysis was investigated through the hydrogen-driven reduction of 2-methyl-1-pyrroline to 2-methylpyrrolidine catalyzed by a heterologously expressed imine reductase.

The work presented in this section forms the basis of a manuscript currently in preparation.

Alhafiz, H. A., Sasamoto, S., Huber, F., Cordero, P. R. F., Meyer, M., Sato, S., Bongartz, P. & Lauterbach, L. Membrane-integrated gas fermentation for H_2-driven synthesis of 2-methylpyrrolidine by *Cupriavidus necator*. (Manuscript in preparation)

Author contributions

Halima Aliyu Alhafiz: Conceptualization, Experimental design, Methodology, Development of bioreactor system including mass flow controller, sensor and mass spectrometer integration, Autotrophic cultivations, Data analysis, Writing-original draft

Saya Kato: Autotrophic cultivations and Analytics

Florian Huber: Membrane design and fabrication, CFD analysis, SEM analysis,

Paul R. F. Cordero: Supervision, Writing-reviewing/editing

Moritz Meyer: Membrane design and fabrication, CFD analysis, SEM analysis

Shunsuke Sato: Supervision, Funding, Writing-reviewing/editing

Patrick Bongartz: Membrane design and fabrication, CFD analysis, SEM analysis

Lars Lauterbach: Conceptualization, Methodology, Funding, Supervision, Writing-review and editing

3.3.1 Chemolithoautotrophic growth performance in the membrane mini-fermenter

Two independent membrane-integrated gas fermentation experiments with recombinant *C. necator* were carried out under identical operating conditions to assess system performance and examine the corresponding dissolved gas profiles (Figure 3.9 A and B). Figure 3.9C shows the individual OD_{600} growth curves of two cultivations (cultivation A and B), illustrating biomass development over time. Both cultivations exhibited clear growth, with OD_{600} increasing from ~ 0.1 at the start of both cultivations to 5.1 and 7.9 in cultivations A and B, respectively. The corresponding final cell dry weights were 1.43 g/L for cultivation A and 2.21 g/L for cultivation B, confirming successful biomass formation in both experiments. The relationship between biomass formation and gas uptake is consistent with the known physiology of *C. necator*, which couples chemolithoautotrophic growth to energy generated from H_2 oxidation for CO_2 fixation (Lambauer and Kratzer, 2022; Weldon & Euler, 2025).

The dissolved gas profiles in Figure 3.9A and Figure 3.9B followed broadly comparable trends, but differences were observed in the dynamic behaviour of dissolved H_2. In cultivation A, dissolved H_2 decreased progressively from ~ 150% and approached very low values (0 to 5%) toward the end of the experiment. In cultivation B, however, dissolved H_2 remained elevated (50 to 100%) for a longer period and declined more slowly. Dissolved O_2 and CO_2 also fluctuated over time, but their overall trends were consistent with the same process configuration. Taken together, the data indicate that the two experiments were comparable in terms of experimental design and general gas behaviour, while still showing differences in detailed gas-transfer and uptake dynamics. This is consistent with the role of gas transfer limitations in membrane-based and other gas fermentation systems (Akkoyunlu et al., 2023; Lambauer and Kratzer, 2022).

The difference in dissolved H_2 behaviour can be interpreted in relation to biomass development. *C. necator* is a hydrogen-oxidizing chemolithoautotroph that uses H_2 as an

electron donor, O_2 as an electron acceptor, and CO_2 as the carbon source, thereby coupling biomass formation directly to gas uptake and intracellular redox balance (Weldon & Euler, 2025; Jahn et al., 2024). As cells grow, their gas demand increases under a constant gas supply (fixed inlet composition and flow rate), this leads to a decline in dissolved gas concentrations (Lambauer and Kratzer, 2022). The more pronounced decline in dissolved H_2 in cultivation A is consistent with tighter coupling between biomass accumulation and H_2 uptake, whereas the prolonged H_2 saturation in cultivation B suggests that H_2 delivery across the membrane remained higher than the rate of consumption. Since no changes were introduced between the two runs, these differences are most plausibly attributed to normal experimental variability, including differences in inoculum physiology, membrane transport behaviour, or sensor response (Wong et al., n.d., Deschamps et al., 2022).

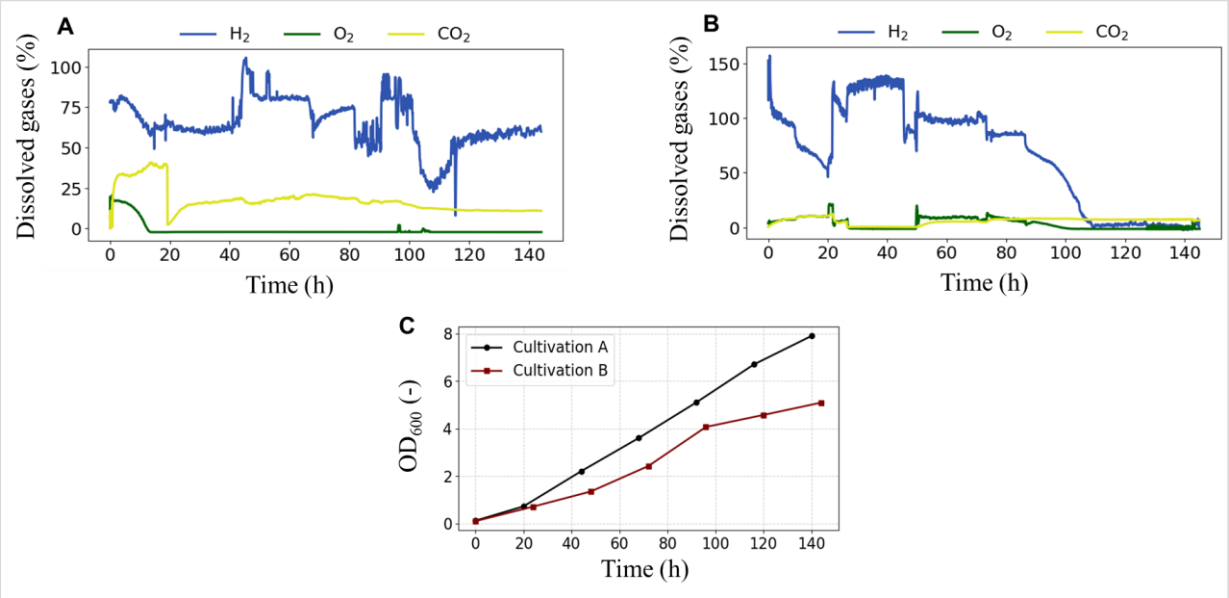

Figure 3.9: Dissolved gas profiles and growth curves from duplicate membrane-integrated *C. necator* cultivations: (A) cultivation A, (B) cultivation B, and (C) individual OD600 profiles for both runs.

Moreover, analysis of the off-gas composition provides further insight into gas transfer and substrate utilization within the reactor. Hydrogen remained the dominant component of the exhaust gas stream, accounting for approximately 90% of the off-gas composition, while

oxygen and carbon dioxide were detected only in minor fractions (Figure B2, supplementary information). Although such a high hydrogen fraction could initially suggest inefficient gas utilization, it is largely a consequence of the physicochemical properties of hydrogen. Hydrogen exhibits very low solubility in aqueous media compared with oxygen and carbon dioxide, which inherently limits the fraction of the supplied gas that can dissolve into the liquid phase at any given time. Furthermore, the geometry of the mini-fermenter may have contributed to this observation, as its short liquid path and minimal headspace likely provide limited gas holdup, such that poorly dissolved H_2 is rapidly carried out of the reactor rather than accumulating within the vessel. As a result, the high hydrogen concentration observed in the off-gas primarily reflects limited dissolution kinetics and continuous gas throughput rather than insufficient biological consumption.

Furthermore, to evaluate the potential for improving gas utilization efficiency, the off-gas from one cultivation was redirected to a second reactor inoculated with cells from an autotrophic preculture. As shown in Figure B3 (supplementary information), the culture exhibited a clear increase in OD_{600} over time, rising from approximately 0.08 to 0.25 within 15 h of cultivation. Because the preculture was grown autotrophically, no organic carbon sources were present at the time of inoculation, confirming that the observed growth was supported solely by the recycled gas stream. These results demonstrate that the off-gas still contained sufficient hydrogen, oxygen, and carbon dioxide to sustain chemolithoautotrophic metabolism of *C. necator*. This finding highlights the potential of off-gas recycling as a strategy to mitigate hydrogen losses and improve overall gas utilization efficiency in hydrogen-driven fermentation processes.

3.3.2 Hydrogen-driven biotransformation

Following confirmation that the membrane-aerated system supported autotrophic growth, the performance of the recombinant *C. necator* strain was evaluated through the reduction of the

imine substrate 2-methyl-1-pyrroline to the corresponding amine 2-methylpyrrolidine (Figure 3.10). This reaction was catalysed by a heterologously expressed imine reductase (IRED), which relies on NADPH as the reducing cofactor. In the present system, NADPH regeneration was coupled directly to the chemolithoautotrophic metabolism of *C. necator*, where hydrogen oxidation supplies reducing equivalents through the respiratory chain.

Product formation was initiated following induction of IRED expression and addition of the imine substrate to the culture medium. After induction, the concentration of 2-methylpyrrolidine increased progressively throughout the cultivation, indicating sustained catalytic activity of the whole-cell biocatalyst under autotrophic conditions. The product concentration reached a maximum value of 62.05 mM, corresponding to a conversion of approximately 77.6% based on the initial substrate concentration of 80 mM.

Analysis with gas chromatography showed that the substrate peak was no longer detectable at the end of the cultivation, indicating that the imine had largely disappeared from the liquid phase. However, the measured product concentration was lower than the theoretical maximum expected for complete conversion. This discrepancy could be attributed to losses associated with plastic or polymeric materials in the mini-fermenter set-up. Abiotic control experiments showed that in the membrane-only setup, 2-methyl-1-pyrroline concentrations remained relatively stable from 80 mM to 63–66 mM after 3 days, demonstrating limited loss to the PMP membrane itself. In contrast, the abiotic test performed with the silicone sampling loop alone revealed a strong decrease in 2-methyl-1-pyrroline concentration from 80 mM to 38, 29, 8, and 5 mM over 4 days, indicating substantial substrate retention or adsorption by the loop material. These findings confirm that the membrane was suitable for gas delivery, whereas the sampling loop was the main source of non-biological substrate loss. The imine substrate possesses moderate hydrophobicity and volatility, which can promote interactions with the plastic tubing used in the recirculation loop (Wang et al., 2022). Similar adsorption phenomena have been

reported for small hydrophobic metabolites in polymer-based microfluidic systems with recirculation loops, such as polydimethylsiloxane (PDMS) devices, where 20–80% losses occur due to surface partitioning, leading to apparent reductions in conversion when product formation is quantified solely from the liquid phase (Lenhart and Kennedy, 2023). Consistent with this interpretation, previous experiments by Schoenmakers et al., (2026) performed in serum bottle cultivations using glass vessels lacking polymeric surfaces achieved complete conversion of the same substrate under similar biochemical conditions, indicating that the lower apparent conversion observed here likely results from material interactions rather than limitations in enzymatic activity. Importantly, this limitation is specific to the mini-fermenter configuration (30 mL scale), where an external sampling loop was required for monitoring. At larger scales, inline sensors would be directly integrated into the reactor, eliminating the need for such recirculation loops and thereby preventing this source of apparent conversion loss.

Furthermore, scanning electron microscopy (SEM) of the membrane after fermentation (Figure B5, supplementary information) showed a roughened surface with irregular deposits, which may reflect fouling and possible biofilm formation by *C. necator*. This is possible because *C. necator* can attach to solid surfaces and form biofilms, and type IV pili, particularly the PilA pilin, are known to mediate early surface adhesion and the transition toward biofilm development. Therefore, using a ΔpilA strain provides a useful outlook for distinguishing whether the observed surface changes are driven by pili-dependent biofilm formation or by nonspecific membrane fouling (Lerch et al., 2017; Pohlschroder & Esquivel, 2015).

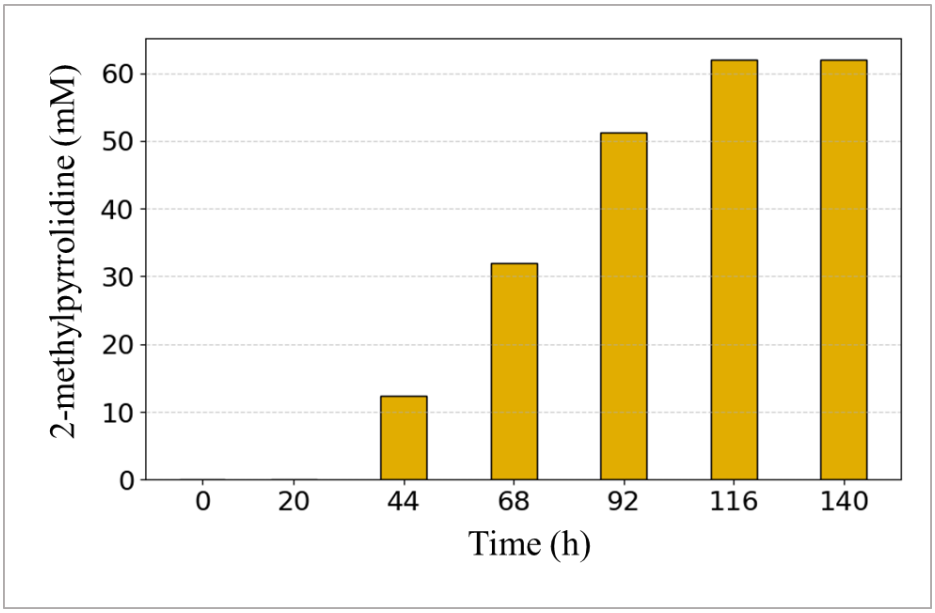

Figure 3.10: Time-course of 2-methylpyrrolidine production by *C. necator* for cultivation B

3.3.3 Hydrogen mass transfer performance

Hydrogen mass transfer is critical in autotrophic gas fermentation due to its extremely low aqueous solubility around 0.78 mM at 25 °C and 1 atm (Alhafiz et al., 2025a), making it the primary rate-limiting substrate for growth and redox-intensive reactions like hydrogenase-driven cofactor regeneration in *C. necator* (Zhang et al., 2022). To evaluate the performance of the membrane-based gas delivery system, the volumetric mass transfer coefficient for hydrogen ($k_La H_2$) was determined and compared with a bubble-based configuration under identical operating conditions. The membrane-aerated system achieved $k_La H_2$ of 25.7 h^{-1} compared to 9.4 h^{-1} for conventional bubble aeration resulting in a 2.7-fold improvement in the measurement (Figure B4, supplementary information) at 3 mL min^{-1} and 973 rpm (70% H_2; Table 3.1).

This enhancement stems from fundamentally different gas transfer mechanisms. Unlike bubble systems limited by short contact times, coalescence, and low interfacial area (Han & Al-Dahhan, 2007), membrane systems provide a stable, high-area gas-liquid interface for direct H_2 diffusion into bulk liquid. Consequently, the elevated $k_La H_2$enables sustained autotrophic

growth and efficient imine reduction within the same reactor. Beyond mass transfer performance, membrane aeration also improves operational safety by preventing the formation of explosive H_2/O_2 mixtures. The bubble-free configuration and absence of a reactor headspace ensure that undissolved gas exits the system immediately, while only dissolved hydrogen is present in the culture. (Deschamps et al., 2022).

Table 3.1: Volumetric mass transfer coefficient for hydrogen ($k_La H_2$) for mini-fermenter

	Membrane system	Bubble system
$k_La H_2$ (h^{-1})	25.7±2.9	9.4±0.6

3.3.4 Comparative analysis of membrane-based *C. necator* fermentation platforms

To contextualize the performance of the membrane-integrated mini-fermenter developed in this study, key performance indicators were compared with previously reported membrane-based gas fermentation systems for *C. necator* (Table 3.2). Li et al. (2025b) investigated a hollow fibre membrane bioreactor for autotrophic single-cell protein production, integrating a polymethylpentene membrane module with a large surface area (~190,000 mm²) into a 150 mL reactor. Although the membrane configuration improved gas dissolution compared with bubble-based systems, the process primarily targeted biomass production and achieved a maximum biomass concentration of approximately 0.44 g L^{-1}. In contrast, Di Bisceglie et al. (2025) employed a hollow fibre membrane contactor coupled to a gas bioreactor to deliver hydrogen in dissolved form while minimizing the formation of explosive gas mixtures. Using this approach, they reported 10 g L^{-1} biomass in a 7.5 L reactor and 2.85 g L^{-1} biomass in a 1 L configuration, and also demonstrated heterologous product formation in the form of 1.3 g L^{-1} isopropanol.

Compared with these systems, the membrane-integrated mini-fermenter used in the present study operates at a significantly smaller working volume of 30 mL, yet supported autotrophic growth of *C. necator* to approximately 2.2 g L^{-1} CDW. More importantly, the system enabled

hydrogen-driven whole-cell biocatalysis, producing 62.05 mM 2-methylpyrrolidine from an initial substrate concentration of 80 mM. While the reactor scale and membrane surface area are substantially smaller than those used in previous studies, the platform successfully combines safe gas delivery with controlled miniaturized fermentation and catalytic product formation. These results demonstrate that membrane-based gas fermentation can be effectively implemented in compact reactor systems for rapid process development while maintaining performance levels comparable to larger membrane reactor configurations.

Furthermore, Schoenmakers et al. (2025) utilized an identical chi.bio mini-fermenter platform (30 mL working volume) for autotrophic cultivation of engineered *C. necator* for isopropanol production achieving up to 1 g L^{-1} CDW via integrated electrolysis for in situ H_2 generation without membrane-mediated gas delivery. In direct comparison, the present membrane-integrated configuration yielded over 2-fold higher biomass, demonstrating that controlled, bubble-free H_2 delivery via hollow fiber membrane significantly enhances cellular performance within the same miniaturized platform. This advantage aligns with the work of Lai et al. (2021) where H_2-driven biogas upgrading with membrane biofilm reactors improved k_La up to 430 h^{-1} because biofilm formation encouraged counter diffusional substrate delivery. In addition, Ma et al. (2024) employed hollow fiber membrane bioreactor on mixed methanotrophic cultures for superior single-cell protein yields (1.36 g g^{-1} CH_4). Collectively, these works validate compact membrane systems' capacity to for efficient gas delivery in different cultivation systems.

Table 3.2: Key performance indicators for membrane-based gas fermentation with *C. necator*

Fermenter configuration and volume	Membrane position	Membrane area (mm^2)	Gas composition (H_2: O_2: CO_2)	Gas flowrate (mL/min)	$k_La H_2$ (h^{-1})	Product	Max. CDW (g/L)	Reference
HFMB, 150 mL	External	190 000	70:20:10	3.13	-	Single cell protein	0.44	Li et al., 2025b
Gas bioreactor with HFMC, 7.5 L	External	250 000	H_2 via membrane, CO_2 & O_2 sparged and automatically regulated	167 for H_2	-	Biomass	10	Di Bisceglie et al., 2025
Gas bioreactor with HFMC, 1 L	External	250 000	H_2 via membrane, CO_2&O_2 sparged and automatically regulated	15 for H_2	-	Isopropanol	2.85	
Chi.Bio mini-fermenter with HFM, 30 mL	Submerged	84 (per side)	70: 20: 10 (H_2 via a separate channel)	3.00	25.7	2-methyl pyrrolidine	2.2	This study

HFMB: hollow fibre membrane bioreactor; HFM: hollow fibre membrane; HFMC: hollow fibre membrane contactor; CDW: cell dry weight

3.3.5 Section summary

This section demonstrates the successful development of a membrane-integrated mini-fermenter for safe and efficient hydrogen-driven gas fermentation. The system enabled bubble-free gas delivery and physical separation of H_2 and O_2, ensuring non-explosive operation while supporting robust autotrophic growth of *C. necator* (2.2 g L^{-1} CDW).

Importantly, the system supported H_2-driven whole-cell biocatalysis, producing up to 62.05 mM 2-methylpyrrolidine with ~77.6% conversion. Observed discrepancies in conversion were attributed to external measurement loop substrate losses rather than biological limitations. Dissolved gas analysis revealed strong metabolic activity, with rapid oxygen consumption and high hydrogen availability governed by mass transfer limitations.

The membrane-based system significantly improved hydrogen mass transfer (2.7-fold higher than bubble aeration) while enhancing process safety. Off-gas recycling experiments further demonstrated potential for improved gas utilization. Overall, the platform combines safe gas handling, efficient mass transfer, and integrated biocatalysis, highlighting its suitability for intensified and scalable gas fermentation processes

3.4 Utilization of lignocellulosic biomass hydrolysates for growth and PHB production

This section investigates the suitability of different lignocellulosic feedstocks for PHB production by *C. necator* DSM 544. The biomasses were evaluated with respect to their composition, pretreatment performance, enzymatic hydrolysis efficiency, and fermentation potential to identify promising substrates for microbial bioconversion.

The work presented in this section forms the basis of a publication in Biotechnology reports.

© Authors, licensed under Creative Commons Attribution 4.0 International (CC BY 4.0).

Alhafiz, H. A., Longus, K., Verlinden, R. A. J., Lambauer, V., Kruschitz, A., & Kratzer, R.* (2025). Cultivation of *Cupriavidus necator strains* on hydrolyzed lignocellulosic feedstocks widely available in Europe. *Biotechnology reports (Amsterdam, Netherlands)*, *47*, e00899. https://doi.org/10.1016/j.btre.2025.e00899

Author contributions

Halima Aliyu Alhafiz: Writing – original draft, Visualization, Validation, Investigation, Formal analysis, Data curation.

Karin Longus: Validation, Methodology, Investigation, Data curation.

Rob A.J. Verlinden: Writing – review & editing, Resources, Project administration, Methodology, Investigation, Funding acquisition, Data curation, Conceptualization.

Vera Lambauer: Validation, Methodology, Investigation, Data curation.

Andreas Kruschitz: Writing – review & editing, Methodology, Investigation, Data curation.

Regina Kratzer: Writing – review & editing, Writing – original draft, Visualization, Supervision, Resources, Project administration, Funding acquisition, Conceptualization.

3.4.1 Biomass composition as basis for process evaluation

Widely available spruce, pine, beech, wheat straw and the emerging energy crop Miscanthus were selected as biomasses in the following experiments (Supplementary material, Figure C1). Biomass contents of cellulose, hemicellulose and lignin vary with growth environment and plant age. The main sugars obtained from the structural carbohydrates cellulose and hemicellulose were glucose, xylose, galactose, arabinose and mannose (Table 3.3). Wheat straw showed highest ash (4.3%), xylose (23.7%) and arabinose (3.8%) contents and lowest

lignin content (20.1%), galactose content was 2.2% and no mannose was found. Wheat straw together with beech and Miscanthus had glucose contents of ~39%. Beech biomass had the highest lignin content of 30.0% and a xylose concentration of 16.8% (galactose, arabinose and mannose were present in minor concentrations of 2.9, 1.3 and 1.7% respectively). Spruce and pine had glucose concentrations of 45-46%, ~6% xylose and ~14% mannose (arabinose 2%). Miscanthus had a relatively high ash content of 2.5%, a xylose content of 19.6% (minor contents of galactose, arabinose and mannose of 1.7, 2.3 and 1.2%). The reference pulp showed very high glucose content (75.9%) and only 1.6% lignin. The data were used to evaluate the efficiencies of the subsequent pretreatment and enzymatic hydrolysis steps.

3.4.2 Effects of steam explosion pretreatment on biomass composition

Biomass steam explosion uses high temperature steam and pressure differences to loosen the structure of lignocellulosic biomass, leading to increased accessibility of cellulose and hemicellulose for the subsequent enzymatic hydrolysis (Supplementary material, Figures C2a-e). We compared steam explosion pretreatment without acid at higher temperatures and at lower temperatures with 0.5% H_2SO_2. In general, a decrease in hemicellulose and lignin is expected as a result of the pretreatment. Table 3.3 shows the composition of the biomasses before (bold) and after pretreatment (only main types of monosaccharides are shown). The partial degradation of hemicellulose is generally seen as a decrease in the xylose fraction (xylose found in hemicellulose) and an increase in free xylose. This effect was particularly pronounced for wood samples B2 (beech chips steam exploded at elevated temperature of 180°C, with H_2SO_4), C1, C2, D1 and D2 (spruce and pine steam exploded with H_2SO_2). For most of the samples, the lignin content (% of total biomass) appeared to increase. However, comparisons of biomass composition before and after the pretreatment step are difficult to interpret due to washing losses of soluble components during steam explosion and a possible formation of pseudolignin by rearrangement and polymerization of furfural and HMF (Meng

and Ragauskas, 2017). The pretreated biomass samples were subjected to enzymatic hydrolysis.

Table 3.3: Composition of biomasses before (in bold) and after pretreatment (conditions see Table 2.5). (Note that sugar* concentrations refer to the sugars from the structural carbohydrates cellulose and hemicellulose and do not distinguish between cellulose and hemicellulose. Glucose, xylose and arabinose columns show free sugars obtained after pretreatment.)

Sample	Ash (%)	Lignin (%)	Glucose* (%)	Xylose* (%)	Galactose* (%)	Arabinose* (%)	Mannose* (%)	Glucose (%)	Xylose (%)	Arabinose (%)
A[1] Wheat straw	4.3±0.1	20.1±0.2	39.2±0.3	23.7±0.1	2.2±0.1	3.8±0.7	0	n.d	n.d	n.d.
A1	4.3±0.0	25.0±0.2	36.8±0.1	23.0±0.2	0	6.0±0.2	0	0.2	0.7	0.1
A2	5.9±0.0	28.9±1.2	40.7±1.0	19.2±0.35	0	0	0	0.1	0.3	0.3
A3	4.6±0.0	28.8±0.5	37.2±0.4	20.7±0.0	0	1.4±0.0	0	0.1	0.4	0.2
B[2] Beech	1.1±0.2	30.0±0.7	39.6±0.1	16.8±0.1	2.9±0.50	1.3±0.2	1.7±0.1	n.d	n.d	n.d.
B1	1.2±0.1	38.3±1.5	36.2±0.9	18.1±0.1	0	0	0	0.3	0.9	1.0
B2	1.4±0.2	34.4±0.0	37.8±0.7	7.4±0.4	0	0	0	1.3	11.35	2.8
B3	0.9±0.0	30.3±1.8	35.0±0.0	16.9±0.8	2.2±0.3	1.1±0.02	2.7±0.6	0.2	0.7	0.3
C[3] Spruce	0.2±0.0	26.2±1.6	46.1±1.6	5.7±0.1	2.6±0.1	1.8±0.1	13.5±0.0	n.d	n.d	n.d.
C1	0.3±0.0	30.2±0.2	42.6±1.2	2.1±0.1	2.1±0.1	1.0±0.3	13.1±0.7	0.8	4.5	0.7
C2	0.2±0.0	27.0±0.0	49.1±0.7	0.0±1.5	2.5±0.0	0.5±0.2	10.5±0.3	1.8	7.1	0.7
C3	0.3±0.0	27.8±1.2	42.8±1.1	5.2±0.1	2.6±0.1	1.7±0.1	14.9±0.3	0.1	0.4	0.6
D[4] Pine	0.2±0.1	26.5±1.2	44.8±0.9	5.6±0.2	3.0±0.0	2.3±0.0	14.4±0.3	n.d	n.d	n.d.
D1	0.3±0.0	35.5±0.3	35.2±0.1	3.6±0.1	2.4±0.2	0.8±0.1	10.5±0.1	1.3	6.5	1.1
D2	0.3±0.0	35.0±1.0	32.4±1.2	3.0±0.1	2.2±0.0	1.1±0.2	10.2±0.2	2.6	10.3	1.0
D3	0.2±0.0	35.8±1.2	39.1±1.0	3.8±0.2	2.1±0.3	1.2±0.0	12.2±0.0	0.1	0.9	0.7
E[5] Miscanthus	2.5±0.0	26.2±0.7	39.2±0.5	19.6±0.1	1.7±0.2	2.3±0.0	1.2±0.0	n.d	n.d	n.d.
E1	3.2±0.1	25.8±0.2	39.1±0.1	17.4±0.4	3.1±0.3	1.9±0.4	0	0.4	2.4	0.7
E2	3.0±0.0	26.0±0.3	39.2±0.1	16.1±0.1	2.9±0.0	1.2±0.1	0	1.1	3.8	0.9
E3	2.9±0.0	26.0±0.1	39.1±0.3	19.2±0.5	3.2±0.1	2.0±0.0	0	0.1	0.3	0.5
E4	3.1±0.2	26.8±0.2	38.3±0.2	19.9±0.0	2.2±0.3	1.4±0.0	0	0.1	0.9	0.5
pulp	0.2±0.0	1.6±0.2	75.9±0.2	7.5±0.2	0	4.1±0.0	8.5±0.0	0	0	0

[1]Deviation from e.g. (Geng et al., 2019) <1%. [2]Deviation from e.g. (Huang et al., 2016) <3%. [3]Deviation from e.g. (Azhar et al., 2011) <3%. [4]Deviation from e.g. (Zanão et al., 2019) <3%.[5]Relatively low glucose* in young plants (Gismatulina et al., 2022). n.d. not determined.

3.4.3 Enzymatic hydrolysis performance and inhibitor formation

Enzymatic hydrolysis of pretreated biomass samples using an enzyme cocktail (Cellic® CTec3 HS from Novozymes) was used to release soluble sugars. The slurry was subjected to filtration and the supernatant was analyzed for monosaccharides and inhibitory compounds (Table 3.4). The monosaccharides, the sugar degradation products HMF and furfural and the organic acids formic and acetic acid in the filtrates were analyzed. Wheat straw hydrolysates A2 and A3 had the highest glucose concentrations of 30.2 and 22.9 g/L, equal to hydrolysis yields of 57 and 39% (Table 3.4), respectively. This was followed by the Miscanthus hydrolysates E2 and E4 with glucose concentrations of 13.8 and 15.1 g/L (hydrolysis yields of 36 and 34%). The hydrolysed wood biomasses generally yielded lower glucose concentrations between 3.8 and 10.3 g/L, with the exception of the hydrolysates of beech biomass B3, which yielded 10.3 g/L glucose (hydrolysis yields below 41%). Incomplete hydrolysis was indicated by the low sugar concentrations, but was also evident in the filter cakes obtained (Figure C4 in the Supplementary material). The low enzymatic hydrolysis yields can be partly explained by the relative high loading of 15% dry biomass in the hydrolysis reaction slurry. Loadings of 15% of dry weight had previously led to maximum hydrolysis yields of 60 to 82% for different biomasses (Kristensen et al., 2009). Too large chip sizes (beech 20 × 10 × 5 mm, pine and spruce 25 × 7 × 3 mm) and stem sizes (wheat straw 25 × 3 mm and Miscanthus 40 × 5 mm) further contributed to incomplete hydrolysis. Measures to increase hydrolysis yields are lower solid loads and size reduction of the starting materials. In the present study, the enzyme loading was according to the supplier (Novozyme application sheet). In general, the hydrolysis yield can be improved by increasing the enzyme loading and the mixing quality.

Table 3.4: Sugar monomers, organic acids, furfural and HMF in the filtrates after enzymatic hydrolysis

Sample	Glucose (g/L)	Xylose (g/L)	Arabinose (g/L)	Mannose (g/L)	Formic acid (g/L)	Acetic acid (g/L)	Furfural (g/L)	HMF (g/L)	Hydrolysis yield (%)
Wheat straw A1	12.5±0.4	5.1±0.2	1.00±0.02	0.13±0.01	1.35±0.02	0.10±0.01	0.25±0.23	0.11±0.02	19
A2	30.2±1.8	19.8±1.0	0.47±0.01	1.45±0.15	1.68±0.07	0.20±0.01	1.07±0.09	0.36±0.02	57
A3	22.9±0.2	12.0±0.2	0.50±0.02	0.44±0.34	1.09±0.1	0.11±0.00	0.03±0.00	0.05±0.01	39
Beech B1	6.0±0.4	6.4±0.5	0.32±0.02	0.10±0.04	0.12±0.01	0.13±0.01	0.57±0.51	0.18±0.05	16
B2	6.6±0.2	14.1±0.1	0.34±0.01	0.11±0.01	0.31±0.00	0.22±0.00	1.19±0.25	1.04±0.80	29
B3	10.3±0.1	13.3±0.0	0.08±0.00	0.06±0.00	0.34±0.01	0.23±0.00	0.84±0.29	0.23±0.01	27
Spruce C1	4.1±0.0	9.3±0.1	1.28±0.02	5.82±0.11	0.03±0.00	0.09±0.00	0.34±0.04	0.41±0.02	23
C2	5.1±0.1	11.4±0.6	0.79±0.04	6.95±0.70	0.00±0.00	0.11±0.00	1.02±0.00	1.47±0.07	28
C3	5.4±0.1	3.4±0.2	1.09±0.15	1.38±0.12	0.39±0.24	0.04±0.03	0.49±0.27	1.04±0.88	12
Pine D1	3.8±0.1	8.8±0.2	1.40±0.03	3.75±1.84	0.02±0.00	0.09±0.00	0.21±0.01	0.30±0.01	23
D2	4.8±0.1	14.7±1.7	0.97±0.11	8.40±0.78	0.07±0.07	0.09±0.03	0.46±0.20	0.93±0.76	41
D3	4.7±0.6	3.4±0.3	0.73±0.06	3.44±1.89	0.15±0.01	0.43±0.03	0.43±0.03	0.26±0.01	15
Miscanthus E1	10.0±0.8	7.9±0.9	1.01±0.11	0.00±0.00	0.23±0.02	0.61±0.04	0.61±0.04	0.14±0.00	21
E2	13.8±0.1	12.6±0.1	0.77±0.01	3.60±0.86	0.35±0.00	2.17±0.52	2.17±0.52	0.57±0.00	36
E3	12.4±0.0	10.8±0.1	0.86±0.01	0.92±0.66	0.43±0.00	0.33±0.02	0.33±0.02	0.12±0.01	26
E4	15.1±0.5	14.2±0.2	0.35±0.01	1.30±0.39	0.52±0.00	1.43±0.30	1.43±0.30	0.25±0.01	34
Pulp	62.0±2.0	10.7±0.3	0.54±0.07	2.78±0.11	0.01±0.00	0.00±0.00	0.00±0.00	0.00±0.00	52

Novy et al. (2015) reported that increasing the enzyme concentration by 20% led to a 7% increase in the hydrolysis yield.

Low sugar concentrations in the wood hydrolysates are not only due to low enzyme yields, but also reflect the sugar degradation during steam explosion and the loss of soluble components in the aqueous fraction after steam explosion. The inhibitors formed during pretreatment by steam explosion were analyzed after enzymatic hydrolysis to quantify the amounts of potentially inhibitory compounds in the subsequent cultivation trials (Table 3.3). Wheat straw in particular showed relatively high formic acid concentrations of 1.1 to 1.7 g/L. As expected, the concentrations of furfural and HMF were highest in the heavily pretreated (acid and higher temperature) biomass samples. The highest concentrations of 2.17 g/L furfural and 1.47 g/L HMF were found in the samples of Miscanthus (E2) and spruce (C2), respectively. Overall, the hollow stems of the cereal grass wheat straw proved to be the most useful lignocellulosic raw material in terms of sugar yield. The highest glucose yields were obtained with wheat straw sample A2 (pretreated with acid at elevated temperatures) (Tables 3.2-3.3, Supplementary Figures A1-A4).

3.4.4 Growth of *C. necator* DSM 544 on lignocellulosic hydrolysates

Growth on hydrolysates with varying sugar and inhibitor loads was tested on *C. necator* DSM 544 (H1G+3), a glucose-utilizing mutant created from *C. necator* H16 by UV mutagenesis (Schlegel and Gottschalk, 1965), was tested on lignocellulose hydrolysates. Numerous by-products of lignocellulose pretreatment and hydrolysis are known inhibitors of microbial growth (Wang et al., 2014). We tested all hydrolysates diluted to 50% in deep-well plate cultivations with *C. necator* DSM 544 (Figure 3.11). In all deep-well plate cultivations the optical density increased at least 5-fold after one day. Growth correlated with the glucose concentration (Figure 3.12). The most obvious difference was higher OD_{600} values obtained for *C. necator* DSM 544 in cultivations with high glucose concentrations (pulp sample, reference

sample with 7.5 g/L glucose and 2.5 g/L xylose (G7.5/X2.5)). No major correlations to the concentrations of the inhibitors formic acid, acetic acid, furfural and HMF were found (tested as multivariate analysis of OD_{600} values versus glucose and different inhibitors, not shown). However, comparing the growth (Figure 3.11) in hydrolysates A2 and A3, it is seen that the cells grew to a higher OD in A3 compared to A2 despite the fact that the glucose concentration was higher in A2. Examining the different inhibitor concentrations of A2 it is seen that the sum of the analysed inhibitors is the highest of all samples in A2 (Figure 3.12) leading to approximately 50% reduction in the expected OD_{600} (in comparison to hydrolysate A3).

Furthermore, all hydrolysates were diluted to a glucose concentration of ~2 g/L in the culture medium. Very similar OD_{600} values were obtained with all hydrolysates and reference samples. Under the tested conditions no major inhibition was experienced. The highest furfural and HMF concentrations in the culture broths were of 1.1 g/L (Table 3.3, E2 diluted to 50%) and 0.74 g/L (Table 3.3, C2 diluted to 50%), respectively (Figure 3.11). These concentrations have previously shown to completely prevent growth of the alternative PHA producer *Paraburkholderia sacchari* IPT 101 (Dietrich et al., 2018).

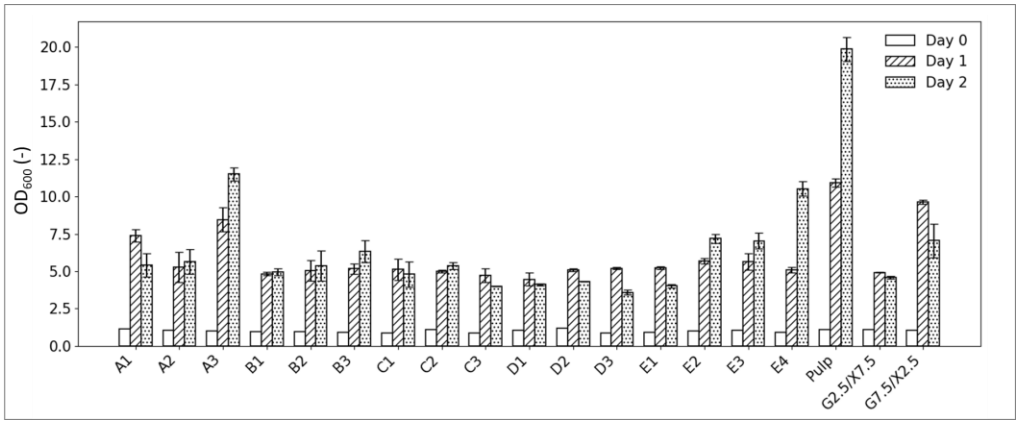

Figure 3.11: Growth of *C. necator* strain DSM 544 on different hydrolysates. Error bars indicate standard deviation from duplicate measurements.

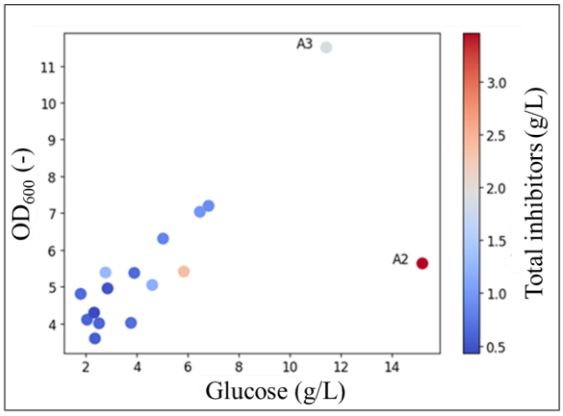

Figure 3.12: Effect of glucose and inhibitor concentration on the growth of *C. necator* DSM 544 on different hydrolysates. Each dot represents one deep-well plate cultivation (in biological duplicates).

3.4.5 PHB production from wheat straw hydrolysate A3

To evaluate the suitability of lignocellulosic hydrolysates for PHB production, wheat straw hydrolysate A3 was selected as the carbon source due to its lowest cumulative inhibitor concentration (Figure 3.13). Shake-flask cultivations (100 mL working volume) of *C. necator* DSM 544 were conducted in mineral medium MM1 supplemented with A3. The initial pH was adjusted to 6.8, and the cultures were inoculated to a starting OD_{600} of 0.4. The maximum CDW for the cultivation was 4.14 g/L with up to 24.2 ±0.3% PHB accumulation (Figure 3.13). The start and end concentrations of the components of the hydrolysate are shown in Figure 3.14. This yielded these results under glucose limitation, which depleted during cultivation and

halted further growth and PHB synthesis. The start and end NH_4-N concentrations were 2.5 g/L and 0.271±0.01 g/L respectively, indicating nitrogen limitation that promoted PHB accumulation. Compared to the initial composition, the concentrations of fermentable sugars decreased substantially during growth, confirming their utilization as primary carbon and energy source for both biomass formation and PHB accumulation, while organic acid concentrations changed only moderately. Optimization via fed-batch strategies could substantially enhance CDW and PHB titres (Soto et al., 2019). Together, these results demonstrate that wheat straw hydrolysate A3 generated by steam explosion pretreatment followed by enzymatic hydrolysis can support growth and significant PHB production by *C. necator* DSM 544.

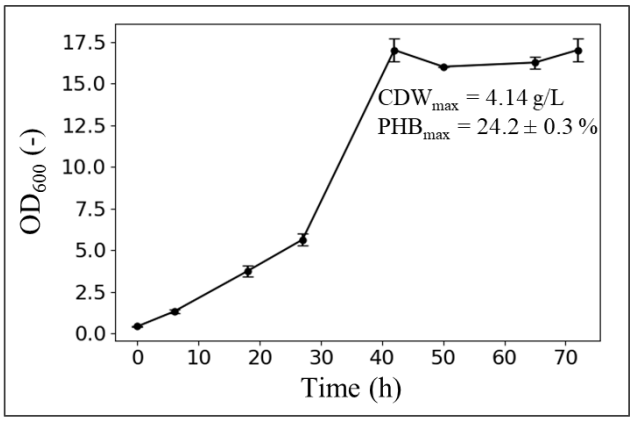

Figure 3.13: Growth and PHB production on wheat straw hydrolysate A3 by *C. necator* DSM 544. Error bars indicate standard deviation from duplicate measurements.

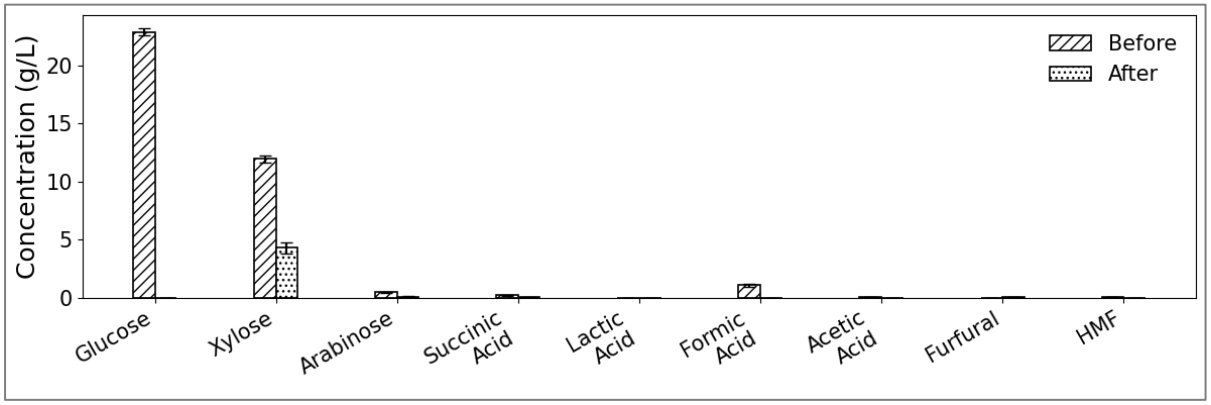

Figure 3.14: Sugar and organic acid concentrations before and after fermentation of wheat straw hydrolysate A3 by *C. necator* DSM 544. Error bars indicate standard deviation from duplicate measurements.

3.4.6 Section summary

This section evaluated different lignocellulosic feedstocks (spruce, pine, beech, wheat straw, Miscanthus and pulp) regarding their composition, pretreatment performance, enzymatic hydrolysis efficiency and suitability for PHB production with *C. necator* DSM 544. The biomasses showed distinct structural carbohydrate and lignin profiles, influencing sugar release during steam explosion and subsequent enzymatic hydrolysis. Wheat straw and Miscanthus generally provided higher glucose concentrations after hydrolysis, whereas wood-based biomasses yielded lower sugar concentrations, partly due to pretreatment severity, solids loading and particle size effects. Inhibitory compounds such as formic acid, acetic acid, furfural and HMF were formed during pretreatment, with higher concentrations observed under more severe conditions; however, growth experiments demonstrated that *C. necator* DSM 544 tolerated the diluted hydrolysates well, with biomass formation primarily correlating with glucose concentration rather than inhibitor levels. Based on its comparatively favourable sugar yield and lower cumulative inhibitor concentration, wheat straw hydrolysate A3 was selected for shake-flask cultivation, enabling PHB production (4.14 g/L CDW, 24.2% PHB) under nitrogen-limited conditions. Overall, the results identify wheat straw as the most promising feedstock under the tested conditions while highlighting the importance of optimizing pretreatment, hydrolysis and feeding strategies to enhance sugar yields and PHB titres.

3.5 Process modelling and simulation-guided evaluation of gas fermentation by *Cupriavidus necator*

This section presents the development, validation, and application of a kinetic model for autotrophic PHB production by *C. necator* DSM 544. The model, implemented in SuperPro Designer, integrates experimentally derived stoichiometric relationships with kinetic expressions describing biomass growth, PHB accumulation, and nutrient consumption. The model is first validated against experimental data through comparison of biomass concentration (CDW), PHB content, and ammonium depletion profiles. This is followed by a systematic sensitivity analysis to evaluate the robustness of the model to variations in key biological parameters and operating conditions, with particular emphasis on growth kinetics and gas supply limitations. Finally, the validated model is applied to assess process scalability by simulating the transition from laboratory scale (~1 L) to pilot scale (~10 L). The combined analysis provides insight into both the reliability of the model and the key factors governing process feasibility, highlighting the relative importance of biological kinetics and engineering constraints in autotrophic fermentation systems.

The work presented in this section forms the basis of a manuscript currently in preparation.

Alhafiz, H.A., Cordero, P. R. F., Kratzer, R. & Lauterbach, L. Process modelling and simulation-guided evaluation of gas fermentation by *Cupriavidus necator* using superpro designer. (Manuscript in preparation)

Author contributions

Halima Aliyu Alhafiz: Conceptualization, Model development and implementation in SuperPro Designer, Model validation, Sensitivity analysis, Scale-up simulations, Data analysis, and Visualization, Writing-original draft

Paul R. F. Cordero: Formal analysis, Writing-reviewing/editing

Regina Kratzer: Funding, Resources, Supervision, Writing-reviewing/editing

Lars Lauterbach: Funding, Resources, Supervision, Writing-reviewing/editing

3.5.1 Model validation against experimental data

The performance of the developed kinetic model was evaluated by comparing simulated and experimental profiles of biomass concentration (CDW), PHB accumulation, and ammonium consumption, as shown in Figures 3.15 A–C. Figure 3.15A demonstrates excellent agreement between simulated and experimental biomass (CDW) profiles across the full 142 h batch cycle, capturing the characteristic lag phase (0–30 h), exponential growth (30–70 h), and transition to stationary phase thereafter, culminating in 13–14 g L^{-1} final CDW. This accuracy validates the Monod-type kinetic structure (μ_{max} = 0.09 h^{-1}, ks = 0.3 mg O_2 L^{-1}), which aligns with literature values for *C. necator* H16 under $H_2/CO_2/O_2$ fermentation (0.09–0.33 h^{-1}) (Lambauer & Kratzer, 2022; Wong et al., n.d.). Figure 3.15B confirms PHB accumulation reaching 9–11 g L^{-1} (~72% CDW), while Figure 3.15C reproduces the ammonium sulphate ($(NH_4)_2SO_4$) depletion from ~2.7 g L^{-1} to zero by ~50 h, marking the onset of nutrient limitation. This NH_4^+ exhaustion directly triggers PHB accumulation in *C. necator* as nitrogen limitation diverts carbon flux from growth-associated metabolism to non-growth-associated polyhydroxyalkanoate (PHA) synthesis which is a well-documented metabolic switch in this organism where stationary phase PHB content reaches up to 80% CDW (Lambauer & Kratzer, 2022; Jahn et al., 2024).

3.5.2 Sensitivity analysis of model parameters and operating conditions

A sensitivity analysis was performed on the validated kinetic model for *C. necator* gas fermentation within SuperPro Designer, systematically varying the maximum specific growth rate (μ_{max}: 0.072–0.108 h^{-1}) and dimensionless empirical fitting coefficient (α: 0.8–1.2) across a full 3×3 interaction grid (±20% from baseline values of μ_{max} = 0.09 h^{-1} and α = 1.0). The analysis revealed strictly linear, additive parameter effects on final cell dry weight (CDW), with values spanning 12.57 g/L (μ_{max} = 0.072 h^{-1}, α = 0.8) to 14.32 g/L (μ_{max} = 0.108 h^{-1}, α = 1.2) which is a manageable ±5.1% deviation from the baseline 13.78 g/L. Contour plotting

of the parameter space confirmed smooth monotonic gradients without discontinuities or nonlinear interactions, characteristic of well-behaved Monod kinetics validated against experimental CDW profile (Figure 3.15D). The maintenance coefficient β (non-growth associated term, 0.002–0.005 h^{-1}) exhibited minimal influence (±1.6% CDW variation), underscoring that growth-associated metabolism dominates during the active batch phase typical of *C. necator* autotrophic cultivation (Grunwald et al., 2015; Amer & Kim, 2023). This robustness to ±20% parameter uncertainty is realistic given literature μ_max scatter of 0.09–0.4 h^{-1} for *C. necator* H16 confirms the model's suitability for process scale-up where kinetic parameter estimation from lab data carries inherent variability (Castro Gonzalez et al., 2025; Amer & Kim, 2023; Tanaka et al., 2025; Lambauer & Kratzer, 2022).

In addition, the influence of gas supply on process performance was evaluated through sensitivity analysis of the volumetric aeration rate (vvm). A range of 0.24–0.36 vvm was investigated for the 1 L reactor system. The results revealed a sharp threshold behaviour in biomass formation, with a critical transition occurring at approximately 0.25 vvm. At 0.24 vvm, final CDW drastically dropped to 0.047 g/L, representing less than 0.4% of the baseline biomass concentration. This indicates severe oxygen limitation, where the oxygen transfer rate is insufficient to meet the cellular oxygen demand. In contrast, at values above 0.27 vvm, biomass formation recovered fully, reaching approximately 13.78 g/L. This step-like transition highlights the strong dependence of autotrophic growth on oxygen availability and reflects the coupling between gas transfer and microbial kinetics in the model.

The observed threshold is consistent with OUR reported for *C. necator* lab-scale autotrophic cultivation, typically ranging from 0.13–1.25 mg O_2 L^{-1} h^{-1} during controlled growth (scaling to higher values at peak biomass) (Lambauer & Kratzer, 2022; Grunwald et al., 2015). At low aeration rates, O_2 delivery falls below cellular demand, leading to immediate growth inhibition via Monod-type limitation on dissolved O_2. This limitation was successfully avoided in 1 L

cultivations achieving a final CDW of 13.53 g/L, through LabVIEW control that dynamically ramped O_2 supply to maintain 2% DO saturation throughout the process. In the SuperPro Designer model, this behaviour is represented through a Monod limitation term with respect to dissolved oxygen (k_S = 0.3 mg/L), effectively capturing the experimentally validated threshold dynamics.

The baseline operating condition of 0.30 vvm lies safely above the identified threshold, providing a margin against oxygen limitation. However, the narrow transition region between oxygen-limited and kinetically controlled regimes underscores a key challenge in scaling autotrophic fermentation processes. Due to the low solubility of gaseous substrates, mass transfer limitations can quickly become the dominant constraint on process performance (Garcia-Ochoa & Gomez, 2005).

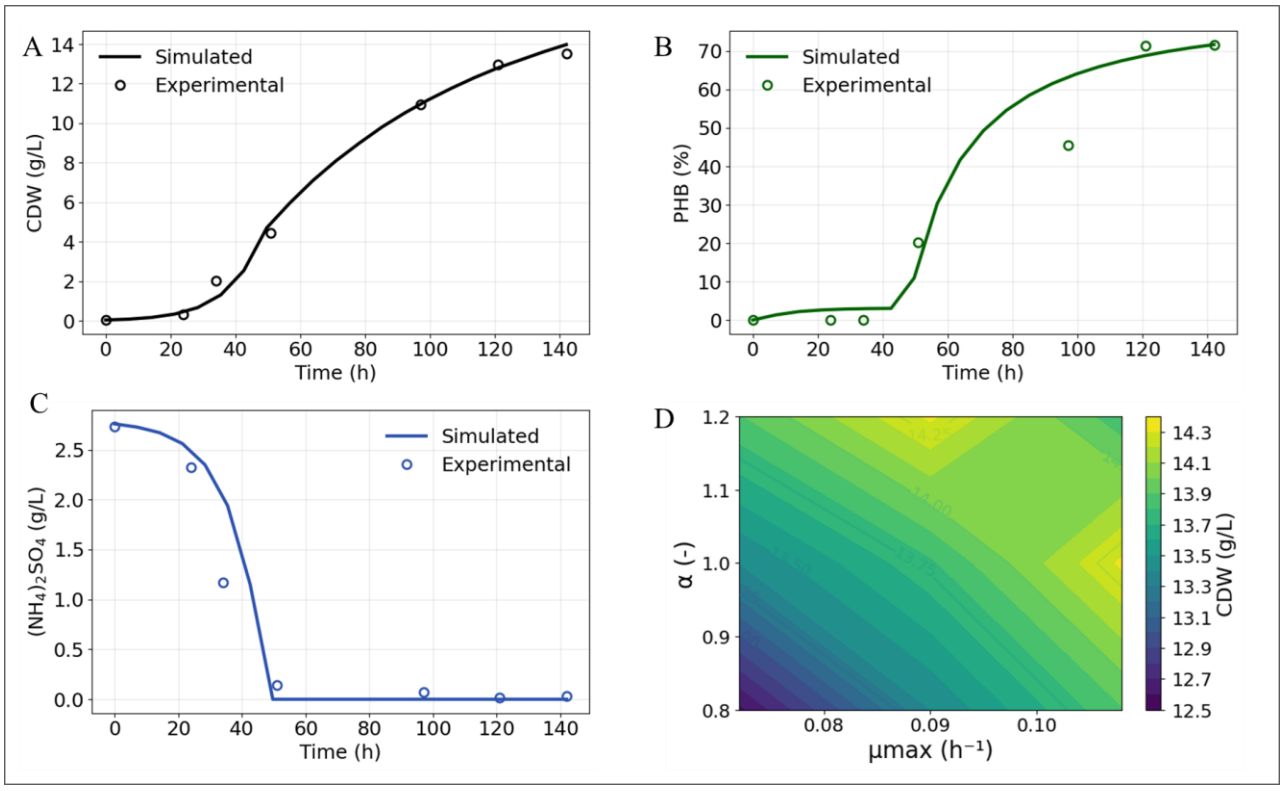

Figure 3.15: Validation and sensitivity analysis of *C. necator* gas fermentation model.
(A) CDW profiles: simulated vs. experimental); (B) PHB accumulation; (C) NH_4^+ depletion triggering PHB production; (D) μ_max–α sensitivity contour.

3.5.3 Scale-up assessment from laboratory to pilot scale

Scale-up from laboratory scale to a pilot-scale scenario was implemented in SuperPro Designer by proportionally increasing the inlet medium volume while maintaining identical medium composition, kinetic parameters, and operating conditions. The medium formulation was originally defined on a per-liter basis corresponding to a nominal 1 L system; however, due to additional volume contributions from dissolved gases and process streams, the resulting simulated working volume was approximately 1.27 L. This reflects the mass-balance-driven nature of SuperPro, where reactor volume is calculated from material inputs rather than strictly imposed. During scale-up, the same approach resulted in a working volume of approximately 12.8 L. All kinetic and stoichiometric parameters were kept constant, ensuring that the biological behaviour of the system remained unchanged. As shown in Figures 3.16A–C, the model preserved the temporal profiles of biomass growth, ammonium depletion, and PHB accumulation, with final biomass concentration of approximately 14.0 g/L and PHB concentration of approximately 10.9 g/L (~72% PHB content), indicating consistent metabolic behaviour across scales.

A comparison of key process performance indicators at both scales is presented in Table 3.5. Despite the increase in working volume, the final concentrations of biomass and PHB remained unchanged, confirming that the model predicts consistent concentration-based behaviour. In contrast, the total mass of PHB produced per batch increased proportionally with reactor volume, reaching approximately 0.139 kg per batch at the pilot scale. The batch duration remained approximately 140 h, resulting in a volumetric productivity of approximately 0.078 $g\ L^{-1}\ h^{-1}$ at both scales. This indicates that scale-up increased total production capacity without improving process intensity, as productivity remained unchanged. Overall, the results demonstrate that the process is scalable at the level of kinetic and stoichiometric modelling; however, the lack of improvement in volumetric productivity and the strong dependence on

gas supply indicate that engineering constraints, rather than intrinsic microbial kinetics, are likely to define the practical scale-up limits.

These scale-up results confirm the kinetic model's robustness and biological feasibility from lab to pilot scale, with linear capacity gains under preserved concentrations and productivity. This behaviour aligns with previous modelling studies of *C. necator* and PHA systems, where Monod-type kinetics and stoichiometric formulations transfer across scales provided environmental conditions remain constant. However, the lack of volumetric productivity improvement highlights gas-liquid mass transfer limitations as the primary engineering bottleneck for further scale-up, necessitating optimisation of aeration, mixing, and reactor geometry (Horvat et al., 2013; Mozumder et al., 2015; Lambauer & Kratzer, 2022).

Table 3.5: Comparison of process performance at laboratory and pilot Scale

Parameter	Lab scale	Pilot scale	Interpretation
Working volume (L)	1.27	12.80	~10× increase via feed scaling
Final CDW (g/L)	14.00	14.00	Consistent growth kinetics
Final PHB (g/L)	10.90	10.90	Consistent PHB accumulation
PHB content (%)	72	72	Metabolic behaviour preserved
Batch time (h)	142	142	Unchanged
Productivity (g/L/h)	0.078	0.078	No improvement with scale
Total PHB (kg/batch)	0.014	0.139	Scales with volume

3.5.4 Section summary

The results demonstrate that the developed kinetic model provides a robust and reliable framework for evaluating autotrophic PHB production by *C. necator* DSM 544. Validation against experimental data confirmed accurate prediction of biomass growth, ammonium depletion, and nitrogen-triggered PHB accumulation, while sensitivity analysis showed that model outputs are slightly sensitive to variations in biological parameters but highly sensitive to aeration rate, identifying oxygen transfer as a critical limiting factor. 10x scale-up from laboratory to pilot scale preserved concentration profiles and metabolic behaviour, with proportional increases in total PHB production but no improvement in volumetric productivity.

Overall, the results confirm that the process is scalable at the level of kinetic and stoichiometric modelling; however, they also highlight that engineering constraints, particularly gas–liquid mass transfer is likely to define the practical limits of scale-up.

4 General discussion

This thesis demonstrates that *C. necator* is a powerful and versatile platform for CO_2-based biotechnology because it combines autotrophic growth, redox flexibility, biopolymer synthesis, fine-chemical biocatalysis, and process scalability in a single organism. Unlike photosynthesis, which depends on light capture and is constrained by photonic losses, *C. necator* does not require land use, it uses H_2 oxidation as a direct source of ATP and reducing power for CO_2 fixation through the CBB cycle, making its carbon assimilation both controllable and independent of light. This positions *C. necator* as a particularly attractive "dark autotroph" for engineered biomanufacturing, while also making it a useful benchmark for comparing native and synthetic CO_2 fixation routes. However, the CBB cycle is not the most energy-efficient natural fixation pathway, fixation of 3 CO_2 requires 9 ATP and 6 NADH, whereas the reductive glycine pathway (rGlyP) fixes 2 CO_2 at the expense of only 1 ATP and 4 reducing equivalents. Compared with rGlyP and other C1 assimilation schemes, the CBB cycle is more ATP demanding, which has driven efforts to engineer more energy-efficient routes into *C. necator*. Recent studies demonstrate that replacing the CBB cycle with the rGlyP in *C. necator* increased biomass yield on formate by approximately 17% (Lu and Yu, 2017; Claassens et al., 2019; Claassens et al., 2020; Cotton et al., 2020; Leger et al., 2021; Orsi et al., 2023; Dronsella et al., 2025).

The energetic behaviour of *C. necator* is fundamentally shaped by the division of labour between soluble hydrogenase (SH) and membrane-bound hydrogenase (MBH). In earlier literature, SH and MBH were also referred to as Hos (soluble hydrogenase) and Hop (particulate/membrane-bound hydrogenase), respectively, particularly in the classical *Alcaligenes eutrophus* H16 studies. SH reduces NAD^+ to NADH in the cytosol and thereby supplies the reducing equivalents required for CBB-cycle CO_2 fixation, biosynthesis, and PHB formation, whereas MBH transfers electrons into the quinone pool and supports

respiratory energy conservation and ATP generation. In addition, MBH can indirectly support NADH formation through reverse electron transfer at respiratory complex I, where electrons from the reduced quinone pool are driven uphill to reduce NAD^+ when the proton motive force is sufficiently high. Notably, earlier physiological studies showed that SH-containing strains generally exhibited better growth than MBH-only strains under autotrophic conditions, consistent with the trend observed in this thesis. The calorimetric and physiological data further support this observation, indicating that SH-favoured metabolism promotes higher biomass formation and lower heat dissipation, whereas MBH-favoured metabolism appears energetically less efficient under the conditions tested. In a broader bioenergetic sense, this pattern fits with systems-level analyses showing that *C. necator* partitions energy and protein resources in ways that strongly affect growth efficiency and product formation (Jahn et al., 2021; Jahn et al., 2024; Lenz & Friedrich, 1998; Schink & Schlegel, 1978; Wright et al., 2022; Hogrefe et al., 1984; Schlegel & Bartha, 1961; Sporre et al., 2023).

Comparative hydrogenase studies provide important ecological and mechanistic insight, demonstrating that the classical *C. necator* model is not universal among Knallgas bacteria. Different species have evolved distinct hydrogenase complements, with some possessing both SH and MBH, while others rely on only one system. These variations reflect organism-specific strategies for coupling H_2 oxidation to ATP generation. For example, *Rhodococcus opacus* relies primarily on SH, whereas *Xanthobacter* SOF1 appears to depend on MBH alone, and organisms such as *C. necator* and *Hydrogenophaga pseudoflava* encode both systems. However, the phenotype observed in *H. pseudoflava*, where loss of SH has little effect but the MBH is essential, contrasts with *C. necator*, in which the SH typically dominates NADH generation and its loss has stronger physiological consequences. This suggests that in some organisms the MBH is indispensable for maintaining respiratory flux and proton motive force, while the SH may be redundant or replaceable under certain conditions. Overall, these

differences highlight that hydrogenase function is context dependent and that the energetic organization of Knallgas bacteria is not fixed, with species differing in their emphasis on reductant generation and respiratory energy conservation. In this context, *C. necator* can be regarded as a balanced and experimentally tractable for H_2-based metabolism. This diversity likely reflects evolutionary adaptation to substrate availability, oxygen exposure, and carbon fixation strategy, where organisms that depend more strongly on soluble reductant supply retain the SH, whereas those primarily challenged by maintaining energetic coupling under oxic conditions rely on MBH. These ideas are also consistent with broader discussions of C1-trophic and electrotrophic metabolism, which emphasize that no single energy architecture is universally optimal (Schink & Schlegel, 1978; Grzeszik et al., 1997; Porthun et al., 2002; Grenz et al., 2019; Siebert et al., 2025; Claassens et al., 2019; Cotton et al., 2020).

Moreover, the process performance results demonstrate that productive operation of *C. necator* depends on the coordinated control of gas composition, process safety, and mass transfer. In gas fermentation, safety is a critical consideration because H_2 and O_2 can form explosive mixtures, requiring operation below the lower explosive limits of hydrogen and oxygen (approximately 3.8 vol% H_2 in air and 4.8 vol% O_2 in mixtures with hydrogen) or the use of ATEX-certified knallgas fermenters. Consequently, H_2/O_2 mixtures must be carefully controlled to remain outside the explosive window while still supplying sufficient H_2, CO_2, and O_2 to sustain autotrophic growth and PHB formation. Achieving this balance is challenging, as system performance is often constrained by gas–liquid mass transfer. The inherently low solubility of H_2 can limit substrate availability and reduce productivity. Industrial and pilot-scale systems typically employ certified knallgas fermenters, and pressure-assisted reactor designs, such as jet-loop systems operated under elevated pressure, to enhance gas transfer and improve overall process performance. Within this context, the non-explosive setup used in this thesis demonstrates that safe autotrophic fermentation is feasible at small scale without

compromising product formation. The membrane-integrated system further improves this approach by enabling biologically favourable gas ratios without direct mixing of H_2 and O_2 in the gas phase. By separating both gases prior to diffusion into the liquid phase, the membrane enhances substrate delivery and alleviates a key limitation of hydrogen-based fermentation. Its robust performance at small scale suggests a potential for scale-up, especially when viewed alongside broader reactor-design literature emphasizing gas-handling and transfer intensification as key scale-up determinants (Pearcy et al., 2022; Miebach et al., 2023; Alhafiz et al., 2025a; Novak et al., 2025; Lambauer et al., 2023)

PHB production highlights the practical relevance of this system, as PHB is both the native storage polymer of *C. necator* and a biodegradable, CO_2-derived bioplastic of industrial interest. Under nitrogen limitation, carbon flux was successfully redirected from biomass formation toward PHB accumulation, demonstrating that the process can be tuned for product formation while maintaining safe operating conditions. In addition, the membrane platform enabled whole-cell synthesis of 2-methylpyrrolidine from 2-methyl-1-pyrroline, illustrating that *C. necator* can function not only as a gas-fermentation chassis for biomass and polymers, but also as a redox-driven catalyst for fine chemical synthesis. Efficient operation of this fine chemical synthesis relies on intracellular redox balancing, where transhydrogenases play a key role by mediating the interconversion of NADH and NADPH. This is particularly important in *C. necator*, as hydrogen oxidation initially generates reducing power in the form of NADH, it channels H_2-derived reducing equivalents into the appropriate cofactor pool, to support both growth and cofactor-dependent transformations. This cofactor-coupling logic is central to the broader concept of electromicrobial and gas-driven synthesis, where redox management determines whether energy input can be translated efficiently into product (Leung et al., 2015; Jahn et al., 2024; Jahn et al., 2021; Cotton et al., 2020; Sporre et al., 2023; Claassens et al., 2019; Westphal et al., 2018).

The lignocellulosic hydrolysate experiments extend the scope of this work by demonstrating that *C. necator* can also operate in indirect CO_2 conversion via biomass-derived feedstocks. The ability to sustain growth on steam-exploded hydrolysates, despite the presence of inhibitory compounds, indicates a level of physiological robustness that is relevant for integration into second-generation biorefinery concepts. This finding is significant because it connects plant-based carbon capture with microbial conversion within a single value chain, thereby complementing direct gas fermentation approaches. It also reinforces the broader idea that carbon conversion should not be viewed as a single-pathway problem, but as a portfolio of feedstock, metabolism, and process options that can be matched to local resource availability (Orsi et al., 2023; Shimizu et al., 2016)

Furthermore, the process-modelling results strengthens the link between experimentally observed gas fermentation behaviour with predictive process analysis. The SuperPro Designer model successfully reproduced biomass formation, ammonium depletion, and PHB accumulation, showing that the core dynamics of autotrophic cultivation can be captured in a structured kinetic-stoichiometric framework rather than described only empirically. This implies that the model can be used to analyze and anticipate process behaviour during the transition from growth to nitrogen-limited PHB synthesis. Sensitivity analysis identified aeration as the dominant operating parameter, with a clear oxygen-limitation threshold below which growth collapsed, consistent with the well-known dependence of hydrogen-oxidizing bacteria on gas–liquid mass transfer. The scale-up simulation further showed that moving from laboratory to pilot scale preserved the concentration trends and metabolic behaviour but did not improve volumetric productivity, indicating that larger reactors increase total output rather than process intensity unless gas transfer is intensified. Together, these results show that process performance in *C. necator* is governed not only by metabolism but also by reactor design, gas supply, and scale-dependent transfer limitations (Puiman et al., 2025; Lambauer

and Kratzer., 2022). As an outlook, future work could use a RAMOS-based respiration activity measurement setup to determine the heat transfer rate during autotrophic cultivation, enabling direct calculation of energy efficiency and a more rigorous comparison between SH- and MBH-dominated operating modes. This would add a thermodynamic layer to the current modelling framework and link heat dissipation, respiration, and product formation more quantitatively (Miebach et al., 2023).

Collectively, this thesis shows that *C. necator* is not simply a CO_2-fixing organism but a multi-purpose platform whose value lies in the integration of physiology, redox biology, process safety, and engineering design. Its native CBB-cycle autotrophy, its hydrogenase organization, its ability to support PHB and fine-chemical synthesis, and its compatibility with both direct gas fermentation and indirect biomass-derived feedstocks all make it an exceptionally tractable chassis for sustainable biomanufacturing.

References

Akkoyunlu, B., Daly, S., Cerrone, F., & Casey, E. (2023). Investigating Mass Transfer and Reaction Engineering Characteristics in a Membrane Biofilm Using *Cupriavidus necator* H16. Membranes (Basel), 13(12), 908. https://doi.org/10.3390/membranes13120908

Aleku, G. A. (2024). Imine reductases and reductive aminases in organic synthesis. ACS Catal., 14, 14308–14329. https://doi.org/10.1021/acscatal.4c04756

Alhafiz, H. A., Di Bisceglie, F., Meier, H. P. F., Weickardt, I., González, I. A. C., Navarro, J. G., Schoenmakers, P., Oyen, S. J., Lettau, E., Lombard, E., Cordero, P. R. F., Konarzycka-Bessler, M., Gorret, N., Schmidt, S., Schillberg, S., Mann, M., Guillouet, S. E., Kratzer, R., & Lauterbach, L. (2025a). *Cupriavidus necator* as a model organism for CO_2-based biotechnology. Methods Enzymol., 714, 163–194. https://doi.org/10.1016/bs.mie.2025.01.017

Alhafiz, H. A., Longus, K., Verlinden, R. A. J., Lambauer, V., Kruschitz, A., & Kratzer, R. (2025b). Cultivation of *Cupriavidus necator* strains on hydrolyzed lignocellulosic feedstocks widely available in Europe. Biotechnol Rep (Amst), 47, e00899. https://doi.org/10.1016/j.btre.2025.e00899

Alvira, P., Tomás-Pejó, E., Ballesteros, M., & Negro, M. J. (2010). Pretreatment technologies for an efficient bioethanol production process based on enzymatic hydrolysis: A review. Bioresour Technol., 101(13), 4851–4861. https://doi.org/10.1016/j.biortech.2009.11.093

Amabile, C., Abate, T., Chianese, S., Munoz, R., & Musmarra, D. (2024). Economic evaluation of a large-scale PHBV production facility: Impact of polymer content on the final selling price. Chem Eng Trans., 110, 259–264. https://doi.org/10.3303/CET24110044

Amer, M., & Kim, D. (2023). Minimizing the lag phase of *Cupriavidus necator* growth under autotrophic, heterotrophic, and mixotrophic conditions. Appl Environ Microbiol., 89(2), e0200722. https://doi.org/10.1128/aem.02007-22

Amin, F. R., Khalid, H., Zhang, H., Rahman, S., Zhang, R., Liu, G., & Chen, C. (2017). Pretreatment methods of lignocellulosic biomass for anaerobic digestion. AMB Express, 7, Article 72. https://doi.org/10.1186/s13568-017-0375-4

Aramvash, A., Shahabi, Z., Aghjeh, S. D., & Ghafari, M. D. (2015a). Utilization of a non-halogenated solvent for recovery of poly(3-hydroxybutyrate) from *Cupriavidus necator*. J Appl Polym Sci., 132(16), 41864. https://doi.org/10.1002/app.41864

Aramvash, A., Shahabi, Z., Aghjeh, S. D., & Ghafari, M. D. (2015b). Green extraction of poly(3-hydroxybutyrate) using 1,3-dioxolane: Effect on polymer properties and purity. Polym Degrad Stab., 119, 136–144. https://doi.org/10.1016/j.polymdegradstab.2015.05.009

Azhar, S., Wang, Y., Lawoko, M., Henriksson, G., & Lindström, M. (2011). Extraction of polymers from enzyme-treated softwood. BioResources, 6(4), 4606–4614. https://doi.org/10.15376/biores.6.4.4606-4614

Bansal, N., Jämsä, T., Yilmaz, S., Rocha, C., Saavedra, M. A., Donati, S., Orsi, E., & Claassens, N. J. (2026). The state of metabolic engineering in the versatile bacterial cell factory Cupriavidus necator H16. Metab Eng., 97, 102479. Advance online publication. https://doi.org/10.1016/j.ymben.2026.05.003

Baum, C., Zeldes, B., Poehlein, A., Daniel, R., Müller, V., & Basen, M. (2024). The energy-converting hydrogenase Ech_2 is important for the growth of the thermophilic acetogen *Thermoanaerobacter kivui* on ferredoxin-dependent substrates. Microbiol Spectr., 12(4), e0338023. https://doi.org/10.1128/spectrum.03380-23

Bongartz, P., Bator, I., Baitalow, K., Keller, R., Tiso, T., Blank, L. M., & Wessling, M. (2021). A scalable bubble-free membrane aerator for biosurfactant production. Biotechnol Bioeng., 118(9), 3545–3558. https://doi.org/10.1002/bit.27822

Borlinghaus, N., Weinmann, L., Krimpzer, F., Scheller, P. N., Al-Shameri, A., Lauterbach, L., Coquel, A.-S., Lattemann, C., Hauer, B., & Nestl, B. M. (2019). Cascade biotransformation to access 3-methylpiperidine in whole cells. ChemCatChem, 11(21), 5738–5742. https://doi.org/10.1002/cctc.201900702

Bugnicourt, E., Alméras, T., Bueno, M.-A., & Le Pluart, L. (2014). Polyhydroxyalkanoate (PHA): Review of synthesis, characteristics, applications and relative market. Int J Mol Sci., 15(12), 22689–22715. https://doi.org/10.3390/ijms151222689

Castro Gonzalez, I., Gorret, N., Lauterbach, L., & Guillouet, S. E. (2025). Glycerol-supplemented medium promotes transition of *Cupriavidus necator* from heterotrophic to lithoautotrophic growth. Biotechnol Lett., 48(1), 3. https://doi.org/10.1007/s10529-025-03671-8

Chen, G. Q. (2010). Plastics completely synthesized by bacteria: Polyhydroxyalkanoates. In G. Q. Chen (Ed.), *Plastics from bacteria: Natural functions and applications* (pp. 17–37). Springer. https://doi.org/10.1007/978-3-642-03287-5_2

Chisti, Y., & Moo-Young, M. (2003). Bioreactors. In R. A. Meyers (Ed.), *Encyclopedia of physical science and technology* (3rd ed., pp. 247–271). Academic Press. https://doi.org/10.1016/B0-12-227410-5/00067-3

Claassens, N. J., Bordanaba-Florit, G., Cotton, C. A. R., De Maria, A., Finger-Bou, M., Friedeheim, L., Giner-Laguarda, N., Munar-Palmer, M., Newell, W., Scarinci, G., Verbunt, J., de Vries, S. T., Yilmaz, S., & Bar-Even, A. (2020). Replacing the Calvin cycle with the reductive glycine pathway in *Cupriavidus necator*. Metab Eng., 62, 30–41. https://doi.org/10.1016/j.ymben.2020.08.004

Claassens, N. J., Cotton, C. A. R., Kopljar, D., & Bar-Even, A. (2019). Making quantitative sense of electromicrobial production. Nat Catal., 2, 437–447. https://doi.org/10.1038/s41929-019-0272-0

Cotton, C. A. R., Claassens, N. J., Benito-Vaquerizo, S., & Bar-Even, A. (2020). Renewable methanol and formate as microbial feedstocks. Curr Opin Biotechnol., 62, 168–180. https://doi.org/10.1016/j.copbio.2019.10.002

Cramm, R. (2009). Genomic view of energy metabolism in *Ralstonia eutropha* H16. J Mol Microbiol Biotechnol., 16(1–2), 38–52. https://doi.org/10.1159/000142893

Daniell, J., Köpke, M., & Simpson, S. D. (2012). Commercial biomass syngas fermentation. Energies, 5(12), 5372–5417. https://doi.org/10.3390/en5125372

De Oliveira Santos, W., David de Oliveira, R., Cabrera Gomez, J. G., & Antonio Carrillo Le Roux, G. (2025). Analysis of Poly-3-Hydroxybutyrate Production with Different Microorganisms Using the Dynamic Simulations for Evaluation of Economic Potential Approach. ACS Omega, 10(26), 27756–27774. https://doi.org/10.1021/acsomega.4c11178

Deschamps, L., Lemaire, J., Imatoukene, N., Lopez, M., & Theoleyre, M. A. (2022). Evaluation of Gas-to-Liquid Transfer with Ceramic Membrane Sparger for H_2 and CO_2 Fermentation. Membranes (Basel), 12(12), 1220. https://doi.org/10.3390/membranes12121220

Devi, A., Bajar, S., Kour, H., Kothari, R., Pant, D., & Singh, A. (2022). Lignocellulosic biomass valorization for bioethanol production: A circular bioeconomy approach. BioEnergy Res., 15, 1820–1841. https://doi.org/10.1007/s12155-022-10401-9

Di Bisceglie, F., Lombard, E., Kratzer, R., Gorret, N., Lorain, O., & Guillouet, S. E. (2025). Aerobic autotrophic isopropanol production under low H_2 atmosphere in Hollow Fiber Membrane Bioreactor. Bioresour Technol., 440, 133407. https://doi.org/10.1016/j.biortech.2025.133407

Dietrich, K., Dumont, M. J., Schwinghamer, T., Orsat, V., & Del Rio, L. F. (2018). Model study to assess softwood hemicellulose hydrolysates as the carbon source for PHB production in *Paraburkholderia sacchari* IPT 101. Biomacromolecules. https://doi.org/10.1021/acs.biomac.7b01446

Ding, L., Cui, L., Wang, Y., Dronsella, B., Liu, X., Luo, H., Huang, H., Su, X., Bai, Y., Zhang, J., Tu, T., Qin, X., Wang, Y., Wang, Y., Yao, B., Xue, X., Guo, G., & Wang, X. (2025). Fructose metabolism in Entner-Doudoroff pathway-deficient *Cupriavidus necator* H16 depends on the Calvin shunt. Microbiol Res., 298, 128222. https://doi.org/10.1016/j.micres.2025.128222

Down to Earth. (2025, January 17). Carbon dioxide emissions to hit 429.6 ppm in May 2025, highest in over 2 million years. https://www.downtoearth.org.in/climate-change/carbon-dioxide-emissions-to-hit-4296-ppm-in-may-2025-highest-in-over-2-million-yea

Dragelj, J., Hoffmann, S., & Knapp, E.-W. (2023). Stability and maturation of the large subunit of membrane-bound hydrogenase in *Cupriavidus necator*. Front Microbiol., 14, 1073315. https://doi.org/10.3389/fmicb.2022.1073315

Dronsella, B., Orsi, E., Schulz-Mirbach, H., Benito-Vaquerizo, S., Yilmaz, S., Glatter, T., Bar-Even, A., Erb, T. J., & Claassens, N. J. (2025). One-carbon fixation via the synthetic reductive glycine pathway exceeds yield of the Calvin cycle. Nat Microbiol., 10, 646–653. https://doi.org/10.1038/s41564-025-01941-9

Elisiário, M. P., De Wever, H., Van Hecke, W., Noorman, H., & Straathof, A. J. J. (2022). Membrane bioreactors for syngas permeation and fermentation. Crit Rev Biotechnol., 42(6), 856–872. https://doi.org/10.1080/07388551.2021.1965952

European Commission. (2019). The European Green Deal (COM/2019/640 final). https://commission.europa.eu/strategy-and-policy/priorities-2019-2024/european-green-deal_en

European Environment Agency. (2025). GHG emissions of all world countries - 2025 report. https://edgar.jrc.ec.europa.eu/report_2025

Fan, Q., Caserta, G., Lorent, C., Zebger, I., Neubauer, P., Lenz, O., & Gimpel, M. (2022). High-Yield Production of Catalytically Active Regulatory [NiFe]-Hydrogenase From *Cupriavidus necator* in *Escherichia coli*. Front Microbiol., 13, 894375. https://doi.org/10.3389/fmicb.2022.894375

Fang, C., Behr, M., Xie, F., Lu, S., Doret, M., Luo, H., Yang, W., Aldous, K., Ding, X., & Gu, J. (2008). Mechanism of chloroform-induced renal toxicity: non-involvement of hepatic cytochrome P450-dependent metabolism. Toxicol Appl Pharmacol., 227(1), 48–55. https://doi.org/10.1016/j.taap.2007.10.014

Friedrich, B., Buhrke, T., Burgdorf, T., & Lenz, O. (2005). A H_2-sensing multiprotein complex controls aerobic H_2 metabolism in *Ralstonia eutropha*. Biochem Soc Trans., 33(Pt 1), 97–101. https://doi.org/10.1042/BST0330097

Gand, M., Thöle, C., Müller, H., Brundiek, H., Bashiri, G., & Höhne, M. (2016). A NADH-accepting imine reductase variant: Immobilization and cofactor regeneration by oxidative deamination. J Biotechnol., 230, 11–18. https://doi.org/10.1016/j.jbiotec.2016.05.006

Garcia-Ochoa, F., & Gomez, E. (2005). Prediction of gas-liquid mass transfer coefficient in sparged stirred tank bioreactors. Biotechnol Bioeng., 92(6), 761–772. https://doi.org/10.1002/bit.20638

Garcia-Ochoa, F., & Gomez, E. (2009). Bioreactor scale-up and oxygen transfer rate in microbial processes: an overview. Biotechnol Adv., 27(2), 153–176. https://doi.org/10.1016/j.biotechadv.2008.10.006

Gemünde, A., Müller, F., & Harnisch, F. (2024). Unraveling the electron transfer in *Cupriavidus necator*. ChemElectroChem, 11(14), e202400273. https://doi.org/10.1002/celc.202400273

Geng, W., Narron, R., Jiang, X., Pawlak, J. J., Chang, H. M., Park, S., Jameel, H., & Venditti, R. A. (2019). The influence of lignin content and structure on hemicellulose alkaline extraction for non-wood and hardwood lignocellulosic biomass. Cellulose, 26, 3219–3230. https://doi.org/10.1007/s10570-019-02261-y

Gismatulina, Y. A., Budaeva, V. V., Kortusov, A. N., Kashcheyeva, E. I., Gladysheva, E. K., Mironova, G. F., Skiba, E. A., Shavyrkina, N. A., Korchagina, A. A., Zolotukhin, V. N., & Sakovich, G. V. (2022). Evaluation of chemical composition of *Miscanthus* × *giganteus* raised

in different climate regions in Russia. Plants (Basel), 11(20), 2791. https://doi.org/10.3390/plants11202791

Gotor-Fernández, V., & Gotor, V. (2020). Biocatalytic approaches for the reductive amination and reduction of imines. Biomolecules, 10(8), 1130. https://doi.org/10.3390/biom10081130

Grenz, S., Baumann, P. T., Rückert, C., Nebel, B. A., Siebert, D., Schwentner, A., Eikmanns, B. J., Hauer, B., Kalinowski, J., Takors, R., & Blombach, B. (2019). Exploiting *Hydrogenophaga pseudoflava* for aerobic syngas-based production of chemicals. Metab Eng., 55, 220–230. https://doi.org/10.1016/j.ymben.2019.07.006

Grunwald, S., Mottet, A., Grousseau, E., Plassmeier, J. K., Popović, M. K., Uribelarrea, J. L., Gorret, N., Guillouet, S. E., & Sinskey, A. (2015). Kinetic and stoichiometric characterization of organoautotrophic growth of *Ralstonia eutropha* on formic acid in fed-batch and continuous cultures. Microb Biotechnol., 8(1), 155–163. https://doi.org/10.1111/1751-7915.12149

Grzeszik, C., Ross, K., Schneider, K., Reh, M., & Schlegel, H. G. (1997). Location, catalytic activity, and subunit composition of NAD-reducing hydrogenases of some *Alcaligenes* strains and *Rhodococcus opacus* MR22. Arch Microbiol., 167(2-3), 172–176.

Gurría, P., González Hermoso, H., Cazzaniga, N., Jasinevicius, G., Mubareka, S., De Laurentiis, V., Caldeira, C., Sala, S., Ronchetti, G., Guillén, J., Ronzon, T., & M'barek, R. (2022). EU biomass flows: Update 2022. Publications Office of the European Union. https://doi.org/10.2760/082220

Han, L., & Al-Dahhan, M. H. (2007). Gas-liquid mass transfer in a high pressure bubble column reactor with different sparger designs. Chem Eng Sci., 62(1–2), 131–139. https://doi.org/10.1016/j.ces.2006.08.010

Hartmann, S., Kranz, C., & Sell, D. (2020). A membrane-bound [NiFe]-hydrogenase large subunit endopeptidase cleavage is dispensable for holoenzyme assembly but facilitates membrane targeting in *Ralstonia eutropha* (*Cupriavidus necator*). MicrobiologyOpen, 9(7), e1054. https://doi.org/10.1002/mbo3.1054

Hassan, S. S., Williams, G. A., & Jaiswal, A. K. (2019). Moving towards the second generation of lignocellulosic biorefineries in the EU: Drivers, challenges, and opportunities. Renew Sustain Energy Rev., 101, 590–599. https://doi.org/10.1016/j.rser.2018.11.041

Hendriks, A. T. W. M., & Zeeman, G. (2009). Pretreatments to enhance the digestibility of lignocellulosic biomass. Bioresour Technol., 100(1), 10–18. https://doi.org/10.1016/j.biortech.2008.05.027

Hogrefe, C., Römermann, D., & Friedrich, B. (1984). *Alcaligenes eutrophus* hydrogenase genes (Hox). J Bacteriol., 158(1), 43–48.

Horch, M., Lauterbach, L., Saggu, M., Hildebrandt, P., Lendzian, F., Bittl, R., Lenz, O., & Zebger, I. (2010). Probing the active site of an O_2-tolerant NAD^+-reducing [NiFe]-hydrogenase from *Ralstonia eutropha* H16 by in situ EPR and FTIR spectroscopy. Angew Chem Int Ed Engl., 49(44), 8026–8029. https://doi.org/10.1002/anie.201002197

Horvat, P., Vrana Špoljarić, I., Lopar, M., Atlić, A., Koller, M., & Braunegg, G. (2013). Mathematical modelling and process optimization of a continuous 5-stage bioreactor cascade for production of poly[-(R)-3-hydroxybutyrate] by *Cupriavidus necator*. Bioprocess Biosyst Eng., 36(9), 1235–1250. https://doi.org/10.1007/s00449-012-0852-8

Hoyt, K. O., Zhou, G., Gasparrini, W., Sliter, P. J., Hart, D. J., Khalil, A. S., & Woolston, B. M. (2025). Exploring C1 substrate cofeeding in *Eubacterium limosum* with AneVO, a low-cost anaerobic parallel bioreactor platform. bioRxiv. https://doi.org/10.1101/2025.05.02.651948

Hreggvidsson, G. O., Gustavsson, T., Holst, O., Kronsbein, K., Hjörleifsdottir, S., Skjenstad, T., & Kristjansson, J. K. (1995). Large scale cultivation of *Hydrogenobacter thermophilus* on H_2. Lett Appl Microbiol., 21(5), 277–281. https://doi.org/10.1111/j.1472-765X.1995.tb01059.x

Huang, Y., Wang, Z., Wang, L., Chao, Y., Akiyama, T., Yokoyama, T., & Matsumoto, Y. (2016). Hemicellulose composition in different cell wall fractions obtained using a DMSO/LiCl wood solvent system and enzyme hydrolysis. J Wood Chem Technol., 36(1), 56–62. https://doi.org/10.1080/02773813.2015.1074248

Inam, A., Taymaz, E. R., Uslu, M. E., Binay, B., & Deniz, I. (2022). Volumetric Mass Transfer Coefficient Measurement in a Stirred Tank Reactor. Methods Mol Biol., 2436, 17–25. https://doi.org/10.1007/7651_2021_415

International Agency for Research on Cancer. (1999). Chloroform (Group 2B). In *Overall evaluations of carcinogenicity: An updating of IARC monographs volumes 1 to 42*. World Health Organization. https://www.ncbi.nlm.nih.gov/books/NBK533635/

Jahn, M., Crang, N., Gynnå, A. H., Kabova, D., Frielingsdorf, S., Lenz, O., Charpentier, E., & Hudson, E. P. (2024). The energy metabolism of *Cupriavidus necator* in different trophic conditions. Appl Environ Microbiol., 90(10), e0074824. https://doi.org/10.1128/aem.00748-24

Jahn, M., Crang, N., Janasch, M., Hober, A., Forsström, B., Kimler, K., Mattausch, A., Chen, Q., Asplund-Samuelsson, J., & Hudson, E. P. (2021). Protein allocation and utilization in the versatile chemolithoautotroph *Cupriavidus necator*. eLife, 10, e69019. https://doi.org/10.7554/eLife.69019

Janasch, M., Crang, N., Asplund-Samuelsson, J., Sporre, E., Bruch, M., Gynnå, A., Jahn, M., & Hudson, E. P. (2022). Thermodynamic limitations of PHB production from formate and fructose in *Cupriavidus necator*. Metab Eng., 73, 256–269. https://doi.org/10.1016/j.ymben.2022.08.005

Jespersen, M. G., Vangsgaard, E. F., Saavedra, M. A., Donati, S., & Nielsen, L. K. (2025). Comparative Genomic Assessment of the *Cupriavidus necator* Species for One-Carbon Based Biomanufacturing. Microb Biotechnol., 18(7), e70201. https://doi.org/10.1111/1751-7915.70201

Jönsson, L. J., & Martín, C. (2016). Pretreatment of lignocellulose: Formation of inhibitory by-products and strategies for minimizing their effects. Bioresour Technol., 199, 103–112. https://doi.org/10.1016/j.biortech.2015.10.009

Judger, B.-E., Chen, Z., Tan, D. T. P., Lebhar, H., Welch, J., & Marquis, C. P. (2015). An analysis of the changes in soluble hydrogenase and global gene expression in *Cupriavidus necator* (*Ralstonia eutropha*) H16 grown in heterotrophic diauxic batch culture. Microb Cell Fact., 14, 42. https://doi.org/10.1186/s12934-015-0226-4

Juengert, J. R., Bresan, S., & Jendrossek, D. (2018). Determination of polyhydroxybutyrate (PHB) content in *Ralstonia eutropha* using gas chromatography and Nile red staining. Bio Protoc., 8(5), e2748. https://doi.org/10.21769/BioProtoc.2748

Jugder, B. E., Henke, B., Halder, P., Meier, C., & Friedrich, B. (2015). An analysis of the changes in soluble hydrogenase and membrane-bound hydrogenase in *Cupriavidus necator*. RSC Adv., 5, 8142-8159. https://doi.org/10.1039/c4ra15659h

Julinová, M., Šašinková, D., Minařík, A., Kaszonyiová, M., Kalendová, A., Kadlečková, M., Fayyazbakhsh, A., & Koutný, M. (2023). Comprehensive Biodegradation Analysis of Chemically Modified Poly(3-hydroxybutyrate) Materials with Different Crystal Structures. Biomacromolecules, 24(11), 4939–4957. https://doi.org/10.1021/acs.biomac.3c00623

Kähler, F., Carus, M., Porc, O., & vom Berg, C. (2021). Industry report: Turning off the tap for fossil carbon. Ind Biotechnol (New Rochelle N Y), 17(5), 245–258. https://doi.org/10.1089/ind.2021.29261.fka

Kataria, R., Mol, A., Schulten, E., Happel, A., & Mussatto, S. I. (2017). Bench scale steam explosion pretreatment of acid impregnated elephant grass biomass and its impacts on biomass composition, structure and hydrolysis. Ind Crops Prod., 106, 48–58. https://doi.org/10.1016/j.indcrop.2016.08.050

Katsyv, A., & Müller, V. (2022). A purified energy-converting hydrogenase from *Thermoanaerobacter kivui* demonstrates coupled H+-translocation and reduction in vitro. J Biol Chem., 298(8), 102216. https://doi.org/10.1016/j.jbc.2022.102216

Kawasumi, T., Igarashi, Y., Kodama, T., & Minoda, Y. (1984). Thermophilic, aerobic, H_2-oxidizing bacterium. Int J Syst Bacteriol. https://doi.org/10.1099/00207713-34-1-5

Kim, S., & Dale, B. E. (2005). Life cycle assessment of various pretreatment technologies. Biomass Bioenergy, 29(6), 426–439. https://doi.org/10.1016/j.biombioe.2005.06.002

Kircher, M. (2021). Bioeconomy – present status and future needs of industrial value chains. N Biotechnol., 60, 96–104. https://doi.org/10.1016/j.nbt.2020.09.005

Kitagawa, W., Okada, S., Toyama, H., & Tonomura, K. (2025). A promoter library for tuning gene expression in *Cupriavidus necator* under autotrophic conditions. Front Bioeng Biotechnol., 13, 1595440. https://doi.org/10.3389/fbioe.2025.1595440

Koh, S., Furutate, S., Imai, Y., Kanda, T., Tanaka, S., Tominaga, Y., Sato, S., & Taguchi, S. (2024). Microbial platform for tailor-made production of a biodegradable polylactide modifier: ultrahigh-molecular-weight lactate-based polyester LAHB. ACS Sustain Chem Eng., 12(16), 6145–6156. https://doi.org/10.1021/acssuschemeng.3c07662

Kohlmann, Y., Pohlmann, A., Otto, A., Becher, D., Cramm, R., Lütte, S., Schwartz, E., Hecker, M., & Friedrich, B. (2011). Analyses of soluble and membrane proteomes of *Ralstonia eutropha* H16 reveal major changes in the protein complement in adaptation to lithoautotrophy. J Proteome Res., 10(6), 2767–2776. https://doi.org/10.1021/pr101289v

Koller, M., Maršálek, L., de Sousa Dias, M. M., & Braunegg, G. (2017b). Producing microbial polyhydroxyalkanoate (PHA) biopolyesters in a sustainable manner. N Biotechnol., 37, 24–38. https://doi.org/10.1016/j.nbt.2016.05.001

Koller, M., Mukherjee, A., & Loos, J. (2017a). Polyhydroxyalkanoates (PHAs)—a biocatalyst for sustainable plastic production? In *Biodegradable Polyesters* (pp. 1–32). Walter de Gruyter GmbH. https://doi.org/10.1515/9783110640607-001

Kristensen, J. B., Felby, C., & Jørgensen, H. (2009). Yield-determining factors in high-solids enzymatic hydrolysis of lignocellulose. Biotechnol Biofuels, 2, 11. https://doi.org/10.1186/1754-6834-2-11

Lai, C.-Y., Zhou, L., Yuan, Z., & Guo, J. (2021). H_2-driven microbial biogas upgrading: Advances, challenges and solutions. Water Res., 197, 117120. https://doi.org/10.1016/j.watres.2021.117120

Lambauer, V., & Kratzer, R. (2022). Lab-Scale Cultivation of *Cupriavidus necator* on Explosive Gas Mixtures: Carbon Dioxide Fixation into Polyhydroxybutyrate. Bioengineering (Basel), 9(5), 204. https://doi.org/10.3390/bioengineering9050204

Lambauer, V., Hagenbuchner, C., Graber, M., Wiltsche, H., Subotić, V., Hochenauer, C., Reichhartinger, M., & Kratzer, R. (2025). Cost-efficient autotrophic high-cell-density cultivation of *Cupriavidus necator* enabled by model-based gas supply. Biotechnol Bioeng. https://doi.org/10.1002/bit.70079

Lambauer, V., Permann, A., Petrášek, Z., Subotić, V., Hochenauer, C., Kratzer, R., & Reichhartinger, M. (2023). Automatic control of chemolithotrophic cultivation of *Cupriavidus necator*: optimization of oxygen supply for enhanced bioplastic production. Fermentation, 9(7), 619. https://doi.org/10.3390/fermentation9070619

Lauterbach, L., & Lenz, O. (2013). Catalytic production of H_2O_2 and water by oxygen-tolerant [NiFe]-hydrogenase during H_2 cycling in the presence of O_2. J Am Chem Soc., 135(47), 17897–17905. https://doi.org/10.1021/ja408420d

Lauterbach, L., & Lenz, O. (2019). How to make the reducing power of H_2 available for in vivo biosyntheses and biotransformations. Curr Opin Chem Biol., 49, 91–96. https://doi.org/10.1016/j.cbpa.2018.11.020

Leger, D., Matassa, S., Noor, E., Shepon, A., Milo, R., & Bar-Even, A. (2021). Photovoltaic-driven microbial protein production can use land and sunlight more efficiently than conventional crops. Proc Natl Acad Sci U S A, 118(26), e2015025118. https://doi.org/10.1073/pnas.2015025118

Lenhart, A. E., & Kennedy, R. T. (2023). Evaluation of surface treatments of PDMS microfluidic devices for improving small-molecule recovery with application to monitoring

metabolites secreted from islets of Langerhans. ACS Meas Sci Au, 3(5), 380–389. https://doi.org/10.1021/acsmeasuresciau.3c00025

Lenz, O., & Friedrich, B. (1998). A novel multicomponent regulatory system mediates H_2 sensing in *Alcaligenes eutrophus*. Proc Natl Acad Sci U S A, 95(21), 12474–12479. https://doi.org/10.1073/pnas.95.21.12474

Lenz, O., & Friedrich, B. (1998). A novel multicomponent regulatory system mediates H_2 sensing in *Alcaligenes eutrophus*. Proc Natl Acad Sci U S A, 95(21), 12474–12479. https://doi.org/10.1073/pnas.95.21.12474

Lenz, O., Bernhard, M., Buhrke, T., Schwartz, E., & Friedrich, B. (2002). The H_2-sensing apparatus in *Ralstonia eutropha*. J Mol Microbiol Biotechnol., 4(3), 255–262.

Lerch, T. Z., Chenu, C., Dignac, M. F., Barriuso, E., & Mariotti, A. (2017). Biofilm vs. Planktonic Lifestyle: Consequences for Pesticide 2,4-D Metabolism by *Cupriavidus necator* JMP134. Front Microbiol., 8, 904. https://doi.org/10.3389/fmicb.2017.00904

Leung, J. H., Schurig-Briccio, L. A., Yamaguchi, M., Moeller, A., Speir, J. A., Gennis, R. B., & Stout, C. D. (2015). Structural biology. Division of labor in transhydrogenase by alternating proton translocation and hydride transfer. Science, 347(6218), 178–181. https://doi.org/10.1126/science.1260451

Levett, I., Birkett, G., Davies, N., Bell, A., Langford, A., Laycock, B., Lant, P., & Pratt, S. (2016). Techno-economic assessment of poly-3-hydroxybutyrate (PHB) production from methane—The case for thermophilic bioprocessing. J Environ Chem Eng., 4(4 Pt A), 3724–3733. https://doi.org/10.1016/j.jece.2016.07.033

Li, B., Veedu, A. P., Mekureyaw, M. F., & Zhang, Y. (2025b). Transforming greenhouse gases into protein powerhouses: Hollow fiber membrane bioreactors for efficient CO_2 bioconversion. Bioresour Technol., 433, 132715. https://doi.org/10.1016/j.biortech.2025.132715

Li, D., Yang, Y., Liu, R., Wu, Y., & Guo, F. (2025a). Review of Biopolymer Polyhydroxybutyrate (PHB) and Blends: Modification of Thermal and Mechanical Properties via Additive Manufacturing Processing. Polymers (Basel), 17(22), 3083. https://doi.org/10.3390/polym17223083

Li, F., Guo, Z., Wang, N., Xia, H., Liu, D., & Chen, S. (2019). Biodegradation of poly(3-hydroxybutyrate)-derived polymers with different 4-hydroxybutyrate fractions by a novel depolymerase from *Paecilomyces* sp. 1407. Polym Degrad Stab., 159, 107–115. https://doi.org/10.1016/j.polymdegradstab.2018.11.016

Liew, F. E., Nogle, R., Abdalla, T., Rasor, B. J., Canter, C., Jensen, R. O., Wang, L., Strutz, J., Chirania, P., De Tissera, S., Mueller, A. P., Ruan, Z., Gao, A., Tran, L., Engle, N. L., Bromley, J. C., Daniell, J., Conrado, R., Tschaplinski, T. J., Giannone, R. J., … Köpke, M. (2022). Carbon-negative production of acetone and isopropanol by gas fermentation at industrial pilot scale. Nat Biotechnol., 40(3), 335–344. https://doi.org/10.1038/s41587-021-01195-w

Liew, F., Martin, M. E., Tappel, R. C., Heijstra, B. D., Mihalcea, C., & Köpke, M. (2016). Gas fermentation—A flexible platform for commercial scale production of low-carbon fuels and

chemicals from waste and renewable feedstocks. Front Microbiol., 7, 694. https://doi.org/10.3389/fmicb.2016.00694

Lin, Y. C., & Ng, I. S. (2025). Rewiring *Cupriavidus necator* for enhanced polyhydroxybutyrate production via genetic toolkits and feeding strategy. Biotechnol Bioeng., 122(9), 2535–2544. https://doi.org/10.1002/bit.29043

Lopar, M., Špoljarić, I. V., Cepanec, N., Koller, M., Braunegg, G., & Horvat, P. (2014). Study of metabolic network of *Cupriavidus necator* DSM 545 growing on glycerol by applying elementary flux modes and yield space analysis. J Ind Microbiol Biotechnol., 41(6), 913–930. https://doi.org/10.1007/s10295-014-1439-y

Lu, Y., & Yu, J. (2017). Comparison analysis on the energy efficiencies and biomass yields in microbial CO_2 fixation. Process Biochem., 62, 151–160. https://doi.org/10.1016/j.procbio.2017.07.007

Ma, Y., Liu, T., Yuan, Z., & Guo, J. (2024). Single cell protein production from methane in a gas-delivery membrane bioreactor. Water Res., 259, 121820. https://doi.org/10.1016/j.watres.2024.12182

Martens, D. E., van den End, E. J., & Streefland, M. (2014). Configuration of bioreactors. Methods Mol Biol., 1104, 285–311. https://doi.org/10.1007/978-1-62703-733-4_19

Meng, X., & Ragauskas, A. J. (2017). Pseudo-lignin formation during dilute acid pretreatment for cellulosic ethanol. Recent Adv Petrochem Sci., 1–5. https://doi.org/10.19080/RAPSCI.2017.01.555551

Miebach, K., Finger, M., Scherer, A. M. K., Maaß, C. A., & Büchs, J. (2023). H_2 online monitoring based on thermal conductivity for anaerobic microorganisms. Biotechnol Bioeng. https://doi.org/10.1002/bit.28502

Miyahara, Y., Hiroe, A., Sato, S., Tsuge, T., & Taguchi, S. (2021). Microbial Polyhydroxyalkanoates (PHAs): from synthetic biology to industrialization. In *Biopolym Biomed Biotechnol Appl.* (pp. 231–264). Wiley. https://doi.org/10.1002/9783527818310.ch8

Morlino, M. S., García, R. S., Savio, F., Zampieri, G., Morosinotto, T., Treu, L., & Campanaro, S. (2023). *Cupriavidus necator* as a platform for polyhydroxyalkanoate production: an overview of strains, metabolism, and modeling approaches. Biotechnol Adv., 69, 108264. https://doi.org/10.1016/j.biotechadv.2023.108264

Mosier, N., Wyman, C., Dale, B., Elander, R., Lee, Y. Y., Holtzapple, M., & Ladisch, M. (2005). Features of promising technologies for pretreatment of lignocellulosic biomass. Bioresour Technol., 96(6), 673–686. https://doi.org/10.1016/j.biortech.2004.06.025

Mozumder, M. S. I., Garcia-Gonzalez, L., De Wever, H., & Volcke, E. I. P. (2015). Poly(3-hydroxybutyrate) (PHB) production from CO_2: Model development and process optimization. Biochem Eng J., 98, 107–116. https://doi.org/10.1016/j.bej.2015.02.031

Mozumder, M. S. I., Goormachtigh, L., Garcia-Gonzalez, L., De Wever, H., & Volcke, E. I. P. (2014). Modeling pure culture heterotrophic production of polyhydroxybutyrate (PHB). Bioresour Technol., 155, 272–280. https://doi.org/10.1016/j.biortech.2013.12.103

Nguyen, T. H., Ishizuna, F., Sato, Y., Arai, H., & Ishii, M. (2019). Physiological characterization of poly-β-hydroxybutyrate accumulation in the moderately thermophilic H_2-oxidizing bacterium *Hydrogenophilus thermoluteolus* TH-1. J Biosci Bioeng., 127(6), 686–689. https://doi.org/10.1016/j.jbiosc.2018.11.011

Nishihara, H., Igarashi, Y., & Kodama, T. (1991). Growth characteristics and high cell-density cultivation of a marine obligately chemolithoautotrophic hydrogen-oxidizing bacterium *Hydrogenovibrio marinus* strain MH-110 under a continuous gas-flow system. J Ferment Bioeng., 72(5). https://doi.org/10.1016/0922-338X(91)90087-W

Novak, K. D., Heidinger, P., Schwendenwein, D., Haneder, F., Martinjak, D., Hochenauer, C., Schwab, H., & Reisinger, C. (2025). Performance of a pilot scale pressurized deep-jet gas bioreactor for SCP production with *Cupriavidus necator* H16. J Biotechnol., 408, 1–14. https://doi.org/10.1016/j.jbiotec.2025.08.013

Novy, V., Longus, K., & Nidetzky, B. (2015). From wheat straw to bioethanol: Integrative analysis of a separate hydrolysis and co-fermentation process with implemented enzyme production. Biotechnol Biofuels, 8, 46. https://doi.org/10.1186/s13068-015-0232-0

Orsi, E., Nikel, P. I., Nielsen, L. K., & Donati, S. (2023). Synergistic investigation of natural and synthetic C1-trophic microorganisms to foster a circular carbon economy. Nat Commun., 14, 6673. https://doi.org/10.1038/s41467-023-42166-w

Paloyan, A., Tadevosyan, M., Ghevondyan, D., Khoyetsyan, L., Karapetyan, M., Margaryan, A., Antranikian, G., & Panosyan, H. (2025). Biodegradation of polyhydroxyalkanoates: current state and future prospects. Front Microbiol., 16, 1542468. https://doi.org/10.3389/fmicb.2025.1542468

Pearcy, N., Garavaglia, M., Millat, T., Gilbert, J. P., Song, Y., Hartman, H., Woods, C., Tomi-Andrino, C., Reddy Dommaraju, R., Choe, B.-K., Fell, D. A., Poolman, M., King, J. R., Winzer, K., Cross, J. T., & Minton, N. P. (2022). A genome-scale metabolic model of *Cupriavidus necator* H16 integrated with TraDIS and transcriptomic data reveals metabolic insights for biotechnological applications. PLoS Comput Biol., 18(5), e1010106. https://doi.org/10.1371/journal.pcbi.1010106

Pohlschroder, M., & Esquivel, R. N. (2015). Archaeal type IV pili and their involvement in biofilm formation. Front Microbiol., 6, 190. https://doi.org/10.3389/fmicb.2015.00190

Porthun, A., Bernhard, M., & Friedrich, B. (2002). Expression of a functional NAD-reducing [NiFe] hydrogenase from the gram-positive *Rhodococcus opacus* in the gram-negative *Ralstonia eutropha*. Arch Microbiol., 177(2), 159–166. https://doi.org/10.1007/s00203-001-0371-5

Public Health England. (2024, August 5). Chloroform: Toxicological overview. GOV.UK. https://www.gov.uk/government/publications/chloroform-properties-incident-management-and-toxicology/chloroform-toxicological-overview

Puiman, L., Bokelmann, C., Simpson, S. D., Spormann, A. M., & Takors, R. (2025). Dos and don'ts for scaling up gas fermentations. Curr Opin Biotechnol., 93, 103294. https://doi.org/10.1016/j.copbio.2025.103294

Reij, M. W., Keurentjes, J. T. F., & Hartmans, S. (1998). Membrane bioreactors for waste gas treatment. J Biotechnol., 59(3), 155–167. https://doi.org/10.1016/S0168-1656(97)00169-7

Schiffels, J., Baumann, M. E. M., & Selmer, T. (2013). An innovative cloning platform enables large-scale production and maturation of an oxygen-tolerant [NiFe]-hydrogenase from *Cupriavidus necator* in *Escherichia coli*. PLoS One, 8(7), e68812. https://doi.org/10.1371/journal.pone.0068812

Schink, B., & Schlegel, H. G. (1978). Mutants of *Alcaligenes eutrophus* defective in autotrophic metabolism. Arch Microbiol., 117(2), 123–129. https://doi.org/10.1007/BF00402299

Schlegel, H. G., & Gottschalk, G. (1965). Verwertung von Glucose durch eine Mutante von *Hydrogenomonas* H16. Biochem Z., 341, 249–259. PMID: 14267686

Schlegel, H. G., & von Bartha, R. (1961). „Leerlauf"-H_2-Oxydation und „Rückkoppelung" bei Knallgasbakterien. Naturwissenschaften, 48, 414–415.

Schoelmerich, M. C., & Müller, V. (2019). Energy conservation by a hydrogenase-dependent chemiosmotic mechanism in an ancient metabolic pathway. Proc Natl Acad Sci U S A, 116(13), 6329–6334. https://doi.org/10.1073/pnas.1818580116

Schoenmakers, P., Calabrese, D., Hattemer, J.-L., de la Asunción Vest, D., Tatar, A., Cordero, P. R. F., & Lauterbach, L. (2026). H_2-driven whole-cell conversion of diamines to N-heterocycles by recombinant *Cupriavidus necator*. ChemCatChem, 18(7), e70716. https://doi.org/10.1002/cctc.70716

Schoenmakers, P., Rad, R., Ihl, A., Weickardt, I., Guillouet, S., Apfel, U. P., & Lauterbach, L. (2025). Isopropanol production from carbon dioxide by *Cupriavidus necator* using a zero-gap cell with culture broth as catholyte. iScience, 28(8), 113018. https://doi.org/10.1016/j.isci.2025.113018

Schröder, V., & Holtappels, K. (2005). Explosion characteristics of H_2-air and H_2-O_2 mixtures at elevated pressures. IGEM conference paper of the International Conference on H_2 Safety 2005. https://www.H2knowledgecentre.com/content/conference216

Shimizu, R., Dempo, Y., Nakayama, Y., Nakamura, S., Bamba, T., Fukusaki, E., & Fukui, T. (2016). Corrigendum: New insight into the role of the Calvin cycle: Reutilization of CO_2 emitted through sugar degradation. Sci Rep., 5, 11617. https://doi.org/10.1038/srep11617

Shuler, M. L., & Kargi, F. (2017). *Bioprocess engineering: Basic concepts* (3rd ed.). Prentice Hall.

Siebert, D. L., Grieshaber, S., Blombach, B., Sieber, V., & Al-Shameri, A. (2025). Biochemical and Mechanistic Insights into O_2 Scavenging and Stability of the Soluble Hydrogenase from

Hydrogenophaga pseudoflava. ACS Omega, 11(1), 1769–1777. https://doi.org/10.1021/acsomega.5c09877

Singh, J., Suhag, M., & Dhaka, A. (2015). Augmented digestion of lignocellulose by steam explosion, acid and alkaline pretreatment methods: A review. Carbohydr Polym., 117, 624–631. https://doi.org/10.1016/j.carbpol.2014.10.012

Sohn, Y. J., Son, J., Jo, S. Y., Park, S. Y., Yoo, J. I., Baritugo, K. A., Na, J. G., Choi, J. I., Kim, H. T., Joo, J. C., & Park, S. J. (2021). Chemoautotroph *Cupriavidus necator* as a potential game-changer for global warming and plastic waste problem: A review. Bioresour Technol., 340, 125693. https://doi.org/10.1016/j.biortech.2021.125693

Soto, L. R., Byrne, E., van Niel, E. W. J., & Janssen, A. J. H. (2019). H_2 and polyhydroxybutyrate production from wheat straw hydrolysate using *Caldicellulosiruptor* species and *Cupriavidus necator*. Int J Hydrogen Energy, 44(6), 3344–3353. https://doi.org/10.1016/j.ijhydene.2018.10.119

Sporre, E., Karlsen, J., Schriever, K., Asplund-Samuelsson, J., Janasch, M., Strandberg, L., Karlsson, A., Kotol, D., Zeckey, L., Piazza, I., Syrén, P.-O., Edfors, F., & Hudson, E. P. (2023). Metabolite interactions in the bacterial Calvin cycle and implications for flux regulation. Commun Biol., 6, 947. https://doi.org/10.1038/s42003-023-05318-8

Sun, C. (2017). *Dynamic metabolic studies of Cupriavidus necator producing polyhydroxybutyrate from glycerol* (Doctoral dissertation, The University of Manchester). https://research.manchester.ac.uk/en/studentTheses/dynamic-metabolic-studies-of-c-necator-producing-phb-from-glycero

Sun, X., Tyran, M., & Angelidaki, I. (2019). Syngas fermentation process development for production of biofuels and chemicals: A review. Bioresour Technol Rep., 7, 100263. https://doi.org/10.1016/j.biteb.2019.100263

Tanaka, K., Ishizaki, A., Kanamaru, T., & Kawano, T. (1995). Production of poly(D-3-hydroxybutyrate) from CO_2, H_2, and O_2 by high cell density autotrophic cultivation of *Alcaligenes eutrophus*. Biotechnol Bioeng., 45(3), 268–275. https://doi.org/10.1002/bit.260450312

Teramoto, H., Shimizu, T., Suda, M., & Inui, M. (2022). H_2 production based on the heterologous expression of NAD^+-reducing [NiFe]-hydrogenase from *Cupriavidus necator* in different genetic backgrounds of *Escherichia coli* strains. Int J Hydrogen Energy, 47(52), 22010–22021. https://doi.org/10.1016/j.ijhydene.2022.05.018

Towler, G., & Sinnott, R. (2012). *Chemical engineering design: Principles, practice and economics of plant and process design* (2nd ed.). Butterworth-Heinemann.

Turco, R., Santagata, G., Corrado, I., Pezzella, C., & Di Serio, M. (2021). In vivo and Post-synthesis Strategies to Enhance the Properties of PHB-Based Materials: A Review. Front Bioeng Biotechnol., 8, 619266. https://doi.org/10.3389/fbioe.2020.619266

Vijayendran, B. R. (Ed.). (2023). *Green materials for an emerging circular and sustainable economy*. Bio prods. ISBN 978-3-11-079121-1

Vitaku, E., Smith, D. T., & Njardarson, J. T. (2014). Analysis of the structural diversity, substitution patterns, and frequency of nitrogen heterocycles among U.S. FDA approved pharmaceuticals. J Med Chem., 57(24), 10257–10274. https://doi.org/10.1021/jm501100b

Vlaeminck, E., Acuña Lopez, P., Uitterhaegen, E., Quataert, K., Delmulle, T., De Winter, K., & Soetaert, W. (2024). Pressure fermentation to boost CO_2-based poly(3-hydroxybutyrate) production using *Cupriavidus necator*. Bioresour Technol., 408, 131162. https://doi.org/10.1016/j.biortech.2024.131162

Wang, W., Yang, S., Hunsinger, G. B., Pienkos, P. T., & Johnson, D. K. (2014). Connecting lignin-degradation pathway with pre-treatment inhibitor sensitivity of *Cupriavidus necator*. Front Microbiol., 5, 247. https://doi.org/10.3389/fmicb.2014.00247

Wang, Y., Liu, Y., Han, Q., Lin, H., & Liu, F. (2022). A novel poly(4-methyl-1-pentene)/polypropylene (PMP/PP) thin film composite (TFC) artificial lung membrane for enhanced gas transport and excellent hemo-compatibility. J Membr Sci., 649, 120359. https://doi.org/10.1016/j.memsci.2022.120359

Weldon, M., & Euler, C. (2025). Physiology-informed use of *Cupriavidus necator* in biomanufacturing: a review of advances and challenges. Microb Cell Fact., 24(1), 30. https://doi.org/10.1186/s12934-025-02643-x

Westphal, L., Wiechmann, A., Baker, J., Minton, N. P., & Müller, V. (2018). The Rnf Complex Is an Energy-Coupled Transhydrogenase Essential To Reversibly Link Cellular NADH and Ferredoxin Pools in the Acetogen *Acetobacterium woodii*. J Bacteriol., 200(21), e00357-18. https://doi.org/10.1128/JB.00357-18

Wilde, E., & Schlegel, H. G. (1982). Oxygen tolerance of strictly aerobic H_2-oxidizing bacteria. Antonie Van Leeuwenhoek, 48(2), 131–143. https://doi.org/10.1007/BF00405198

Wong, T. S., Tee, K., Singh, J., & Appleton, M. (n.d.). Gas fermentation of *Cupriavidus necator* H16 at elevated pressure. H.E.L Group. https://helgroup.com/application-notes/appnote3-gas-fermentation-of-cupravidus-necator-170220/

Wongmoon, C., & Napathorn, S. C. (2022). Optimization for the efficient recovery of poly(3-hydroxybutyrate) using the green solvent 1,3-dioxolane. Front Bioeng Biotechnol., 10, 1086636. https://doi.org/10.3389/fbioe.2022.1086636

Wright, J. J., Biner, O., Chung, I., Burger, N., Bridges, H. R., & Hirst, J. (2022). Reverse Electron Transfer by Respiratory Complex I Catalyzed in a Modular Proteoliposome System. J Am Chem Soc., 144(15), 6791–6801. https://doi.org/10.1021/jacs.2c00274

Yang, B., & Tucker, M. P. (2013). Laboratory pretreatment systems to understand biomass deconstruction. In C. E. Wyman (Ed.), *Aqueous pretreatment of plant biomass for biological and chemical conversion to fuels and chemicals* (pp. 489–521). John Wiley & Sons. https://doi.org/10.1002/9780470975831.cH23

Yang, B., & Wyman, C. E. (2008). Pretreatment: The key to unlocking low-cost cellulosic ethanol. Biofuels Bioprod Biorefin., 2(1), 26–40. https://doi.org/10.1002/bbb.49

Yu, J., & Lu, Y. (2019). Carbon dioxide fixation by a H_2-oxidizing bacterium: Biomass yield, reversal respiratory quotient, stoichiometric equations and bioenergetics. Biochem Eng J., 152, 107369. https://doi.org/10.1016/j.bej.2019.107369

Zanão, M., Colodette, J. L., Oliveira, R. C., Almeida, D. P., Gomes, F. J., & Carvalho, D. M. D. (2019). Evaluation of kraft-PS cooking for eucalypt and pine wood chip mixtures. J Wood Chem Technol., 39(2), 149–165. https://doi.org/10.1080/02773813.2018.1533979

Zhang, L., Jiang, Z., Tsui, T. H., Loh, K. C., Dai, Y., & Tong, Y. W. (2022). A Review on Enhancing *Cupriavidus necator* Fermentation for Poly(3-hydroxybutyrate) (PHB) Production From Low-Cost Carbon Sources. Front Bioeng Biotechnol., 10, 946085. https://doi.org/10.3389/fbioe.2022.946085

Zhu, L., Xu, B., Wu, X., Lei, J., Hacker, D. L., Liang, X., & Wurm, F. M. (2020). Analysis of volumetric mass transfer coefficient (kLa) in small- (250 mL) to large-scale (2500 L) orbitally shaken bioreactors. 3 Biotech, 10(9), 397. https://doi.org/10.1007/s13205-020-02352-9

Supplementary information

Appendix A: establishment of stable non-explosive gas fermentation of *C. necator*

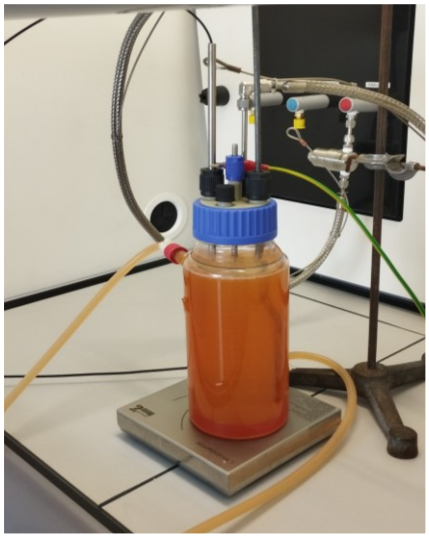

Figure A1: Set-up for DURAN flask cultivation



Figure A2: Set-up for 1.2 L stirred tank bioreactor

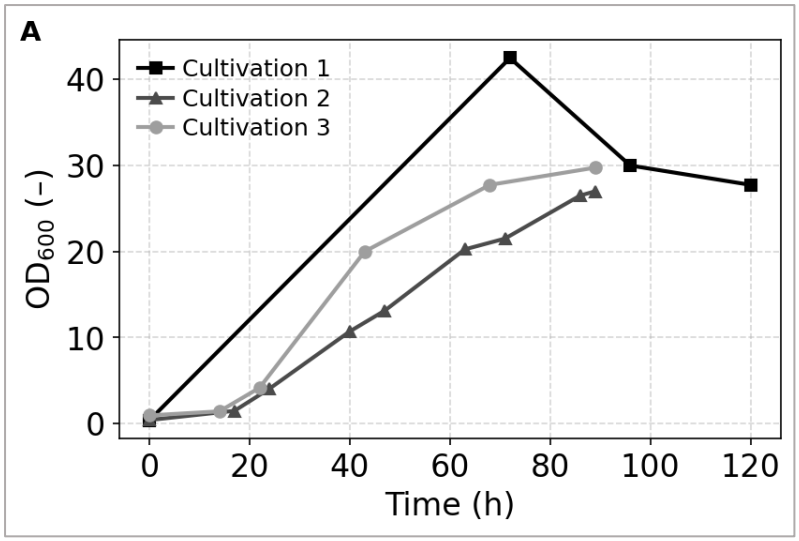

Figure A3: Growth performance of cultivations 1-3 under different buffering strategies

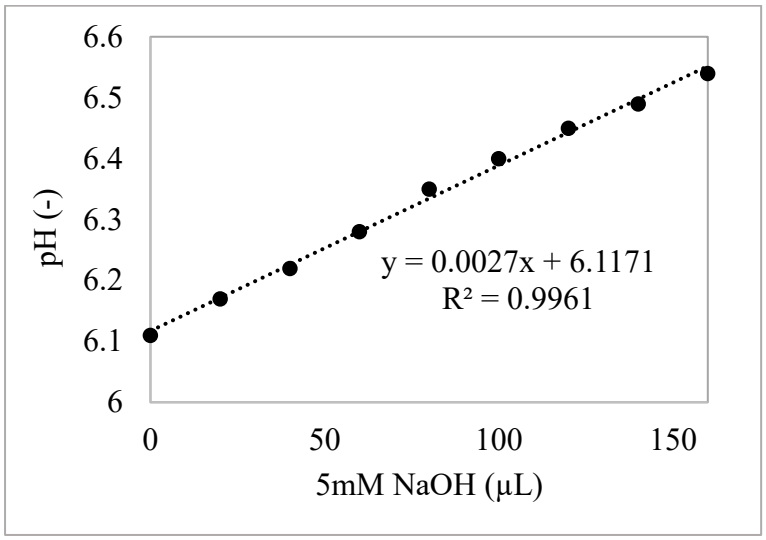

Figure A4: Calibration for manual pH control.

Appendix B: membrane-integrated gas fermentation for 2-methylpyrrolidine biosynthesis

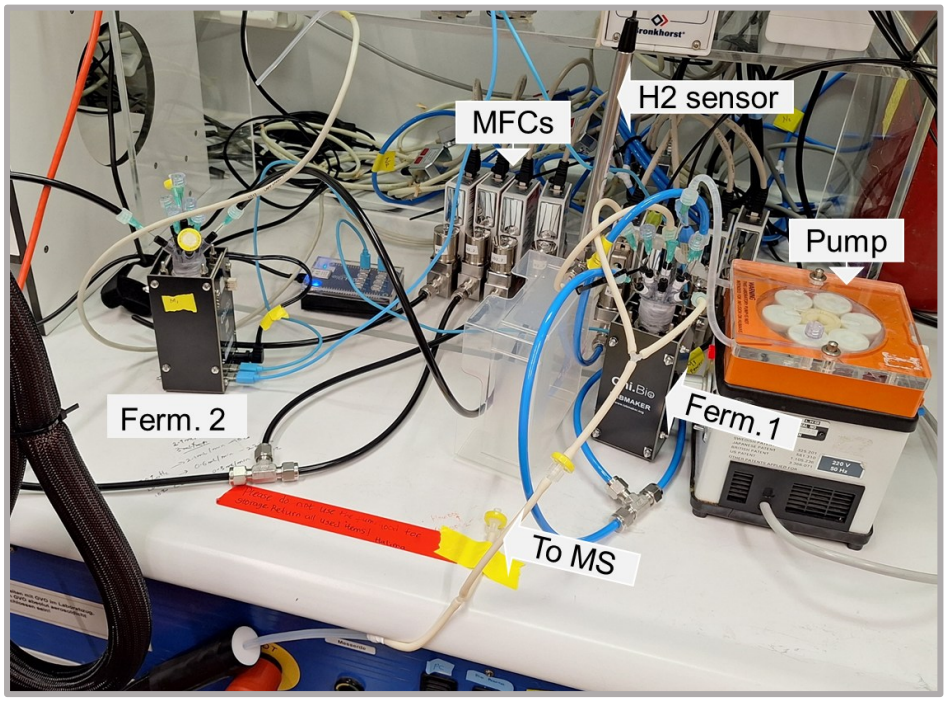

Figure B1: Set-up for membrane-integrated mini-fermenter cultivation

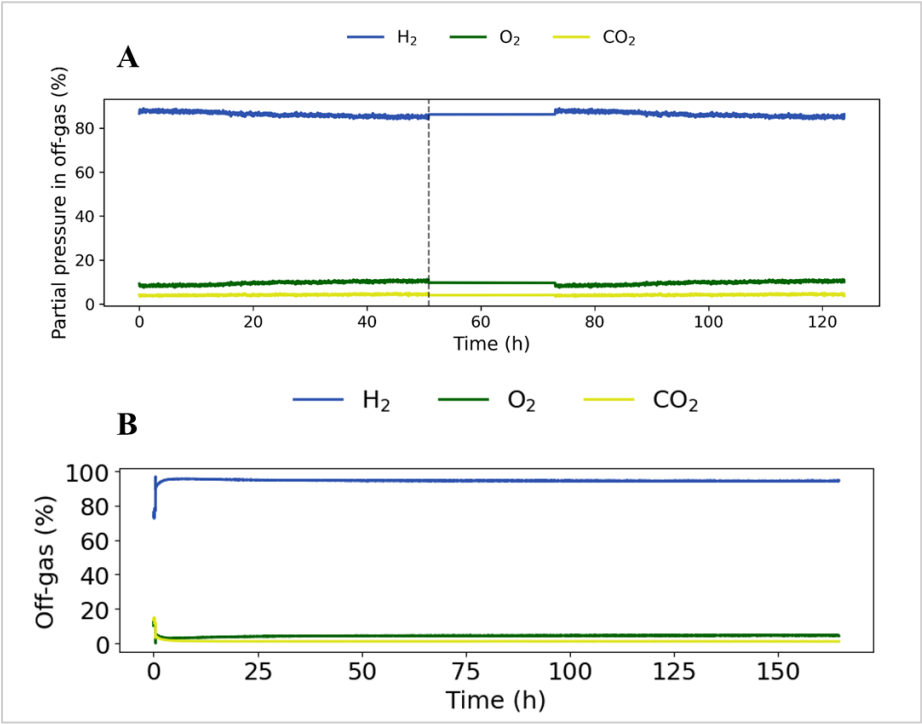

Figure B2: Off-gas composition during membrane-integrated H_2-powered imine reduction by *C. necator*. A and B represent Cultivation A and B.

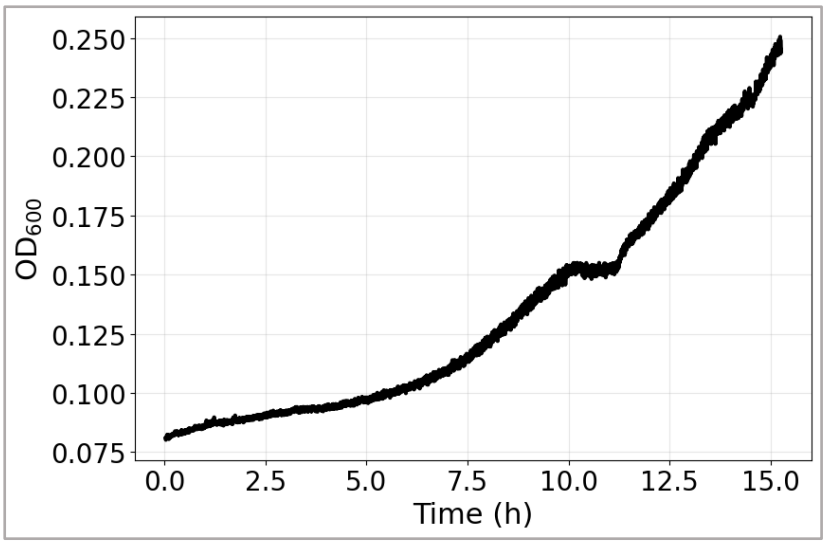

Figure B3: Cultivation from recycled off-gas. Preculture used was grown autotrophically in serum bottles, so there were no sugars present at the point of inoculation.

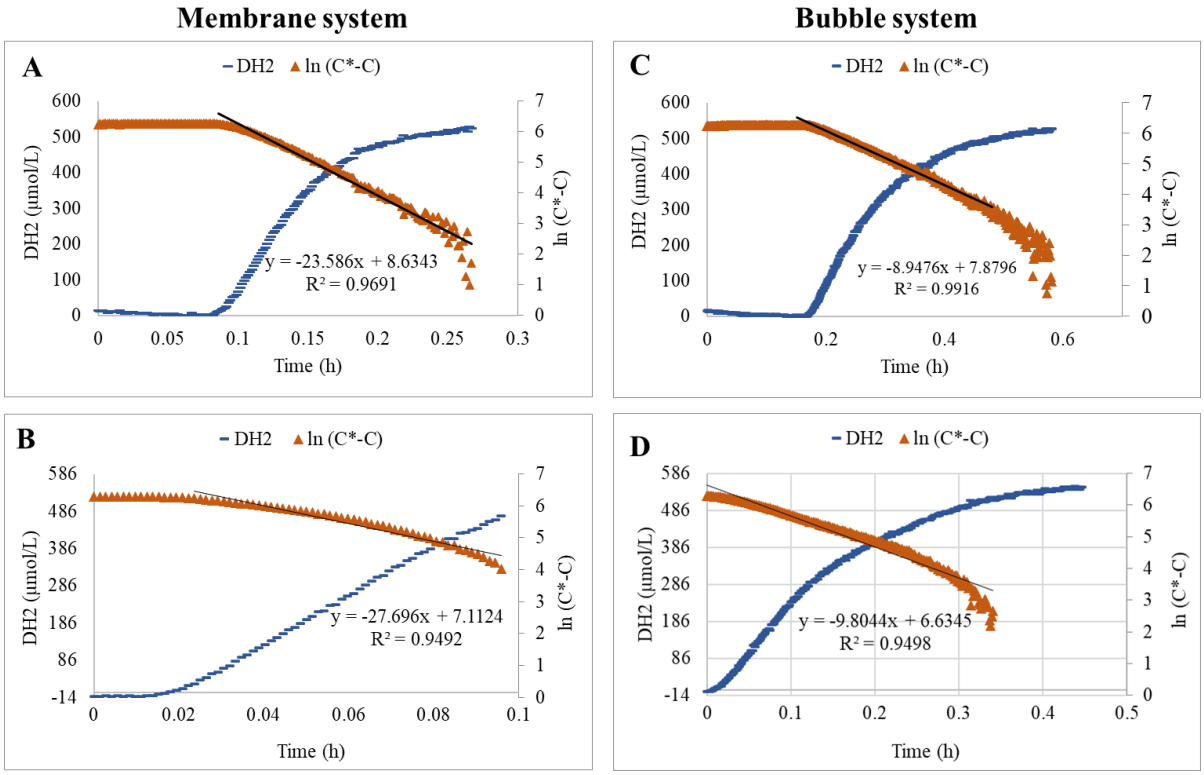

Figure B4: Illustration of k_La determination for set-up with membrane and without membrane. Duplicates for membrane system (A&B); Duplicate for bubble system (C&D)

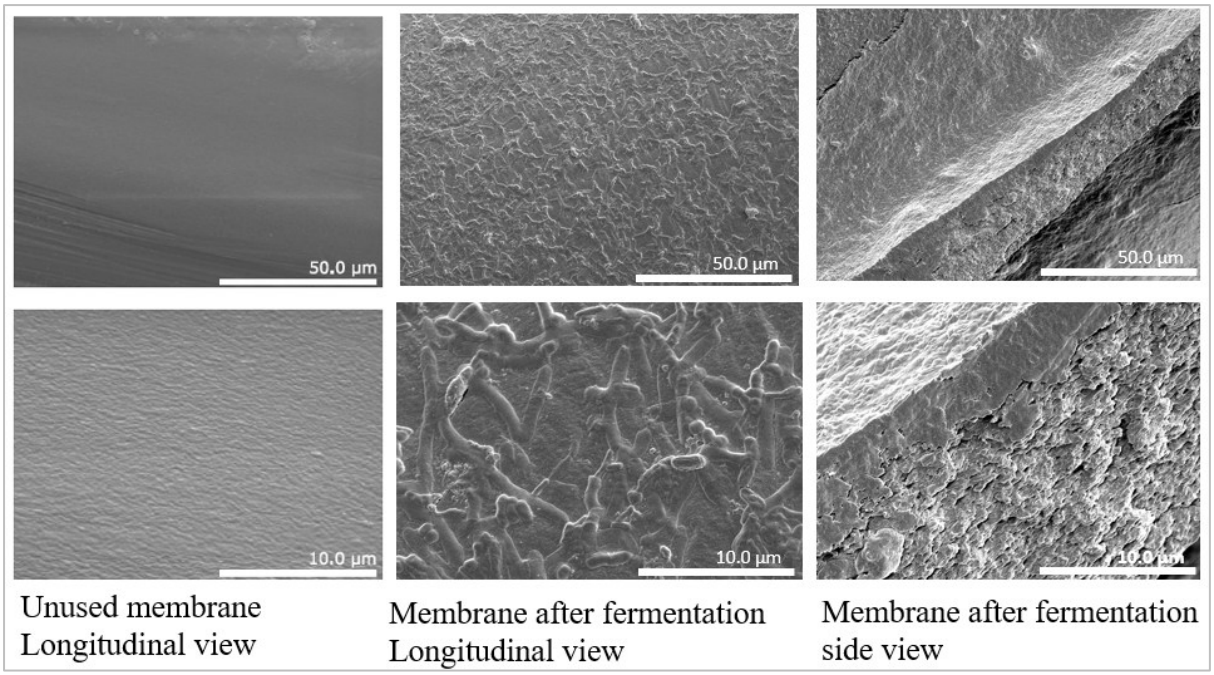

Figure B5: SEM analysis of membrane before and after fermentation

Appendix C: utilization of lignocellulosic biomass hydrolysates for heterotrophic growth



Figure C1: Photos of chopped raw wheat straw, beech, spruce, pine, miscanthus biomasses with scale.

Table C1: Moisture content (%) of the raw biomass samples.

Sample	Biomass	Moisture content (%)
A	Wheat straw	6.6
B	Beech	30.4
C	Spruce	29.1
D	Pine	38.4
E	Miscanthus	11.2
	NBKS pulp	3.0

Table C2: Steam explosion conditions and moisture content after pretreatment.

Biomass	Pretreatment Conditions	Sample #	Moisture content (%)
A Wheat straw	No additive, 160°C	A1	58.0
	0.5% H_2SO_4, 160°C	A2	41.3
	No additive, 180°C	A3	46.4
B Beech	0.5% H_2SO_4, 160°C	B1	45.9
	0.5% H_2SO_4, 180°C	B2	51.9
	No additive, 190°C	B3	48.4
C Spruce	0.5% H_2SO_4, 160°C	C1	44.5
	0.5% H_2SO_4, 180°C	C2	44.2
	No additive, 190°C	C3	41.3
D Pine	0.5% H_2SO_4, 160°C	D1	49.9
	0.5% H_2SO_4, 180°C	D2	51.0
	No additive, 190°C	D3	51.7
E Miscanthus	0.5% H_2SO_4, 160°C	E1	38.1
	0.5% H_2SO_4, 180°C	E2	45.2
	No additive, 180°C	E3	43.5
	No additive, 190°C	E4	48.3



Figure C2a: Photos of pretreated wheat straw with scale. 612/A1 steam explosion (180°C/10 minutes); 620/A2 0.5% H_2SO_4 + steam explosion (160°C/10 minutes); 617/A3 steam explosion (160°C/10 minutes).

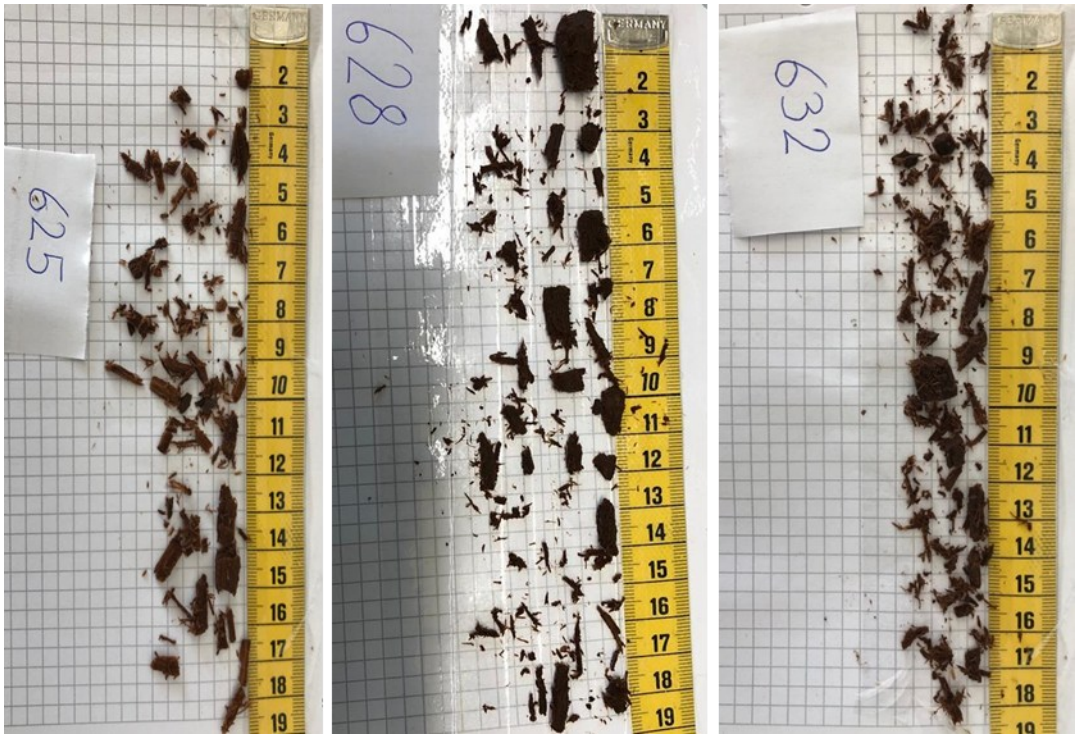

Figure C2b: Photos of pretreated beech with scale. 625/B1 0.5% H_2SO_4 + steam explosion (160°C/10 minutes); 628/B2 0.5% H_2SO_4 + steam explosion (180°C/10 minutes); 632/B3 steam explosion (190°C/10 minutes).

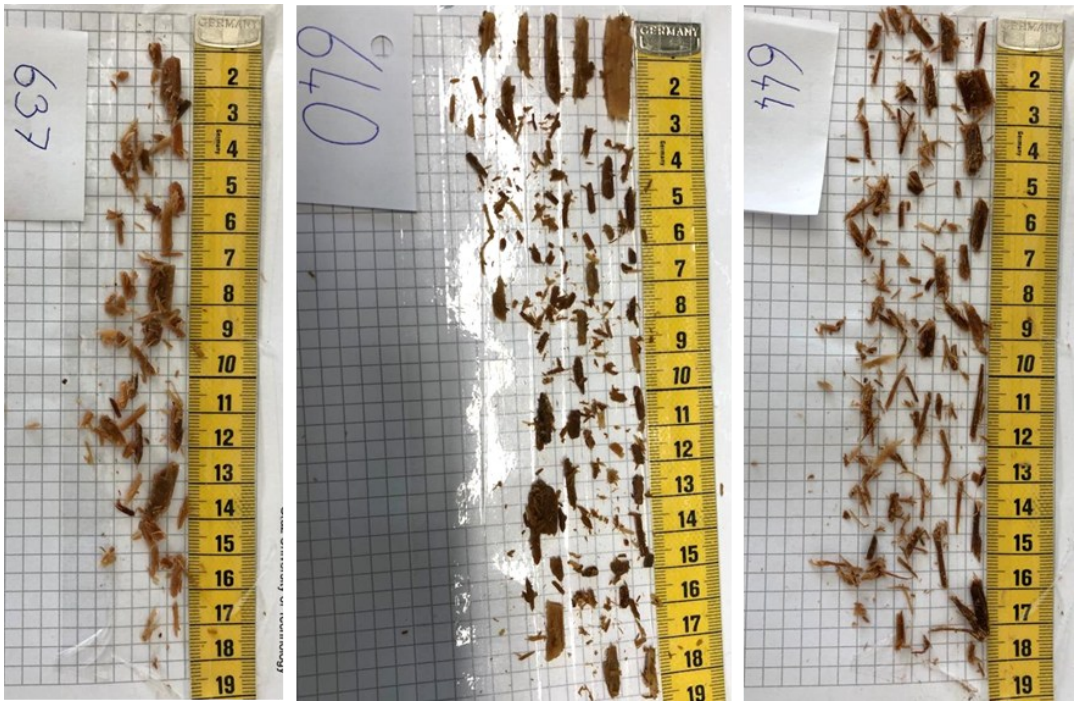

Figure C2c: Photos of pretreated spruce with scale. 637/C1 0.5% H_2SO_4 + steam explosion (160°C/10 minutes); 640/C2 steam explosion (190°C/10 minutes); 644/C3 0.5% H_2SO_4 + steam explosion (180°C/10 minutes).

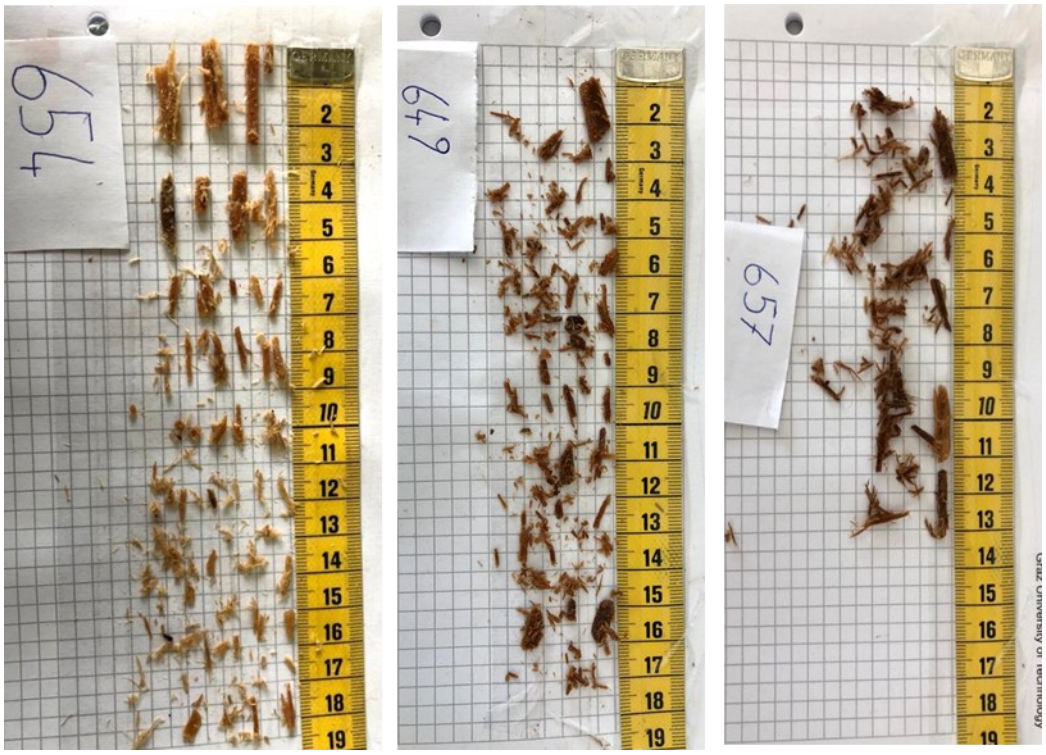

Figure C2d: Photos of pretreated pine with scale. 654/D1 steam explosion (190°C/10 minutes); 649/D2 0.5% H_2SO_4 + steam explosion (180°C/10 minutes); 657/D3 0.5% H_2SO_4 + steam explosion (160°C/10 minutes).

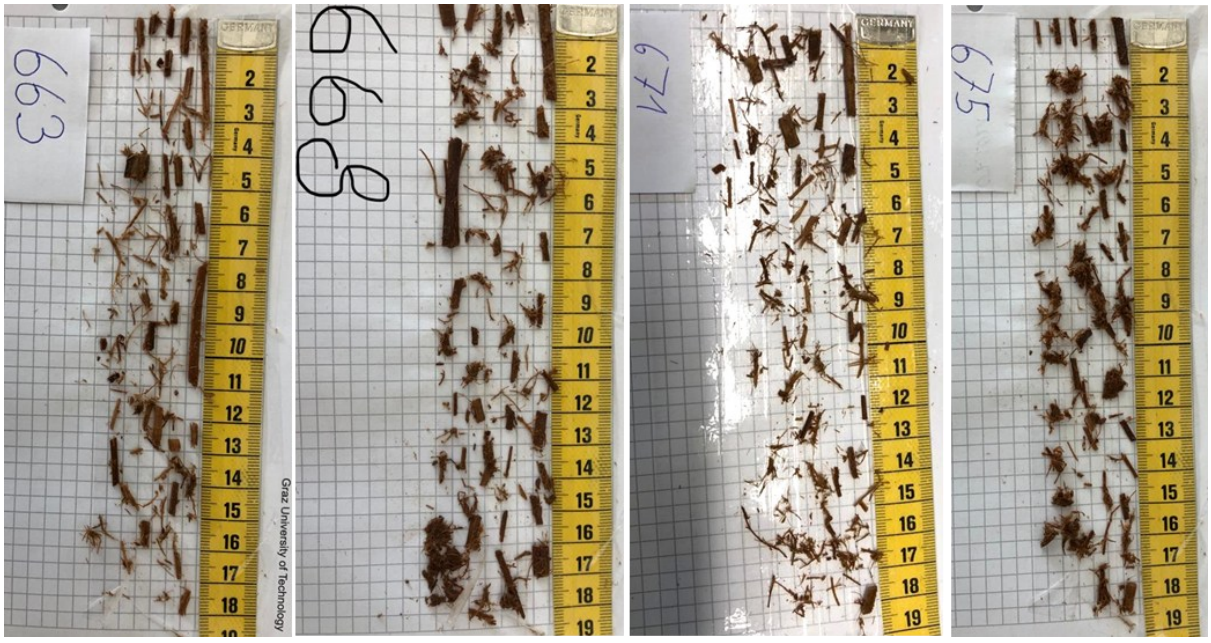

Figure C2e. Photos of pretreated miscanthus with scale; 663/E1 0.5% H2SO4 + steam explosion (160°C/10 minutes); 668/E2 0.5% H2SO4 + steam explosion (180°C/10 minutes); 671/E3 steam explosion (180°C/10 minutes); 675/E4 steam explosion (190°C/10 minutes); E: 1% NaOH + steam explosion (180°C/10 minutes).



Figure C3: Vacuum filtration set-up. Büchner funnel (PP, 390mL) with two glass fiber filter circles (MN 85/70 BF, 0.6µm from Macherey-Nagel). Vacuum adjusted to 100mbar with vacuum gauge).

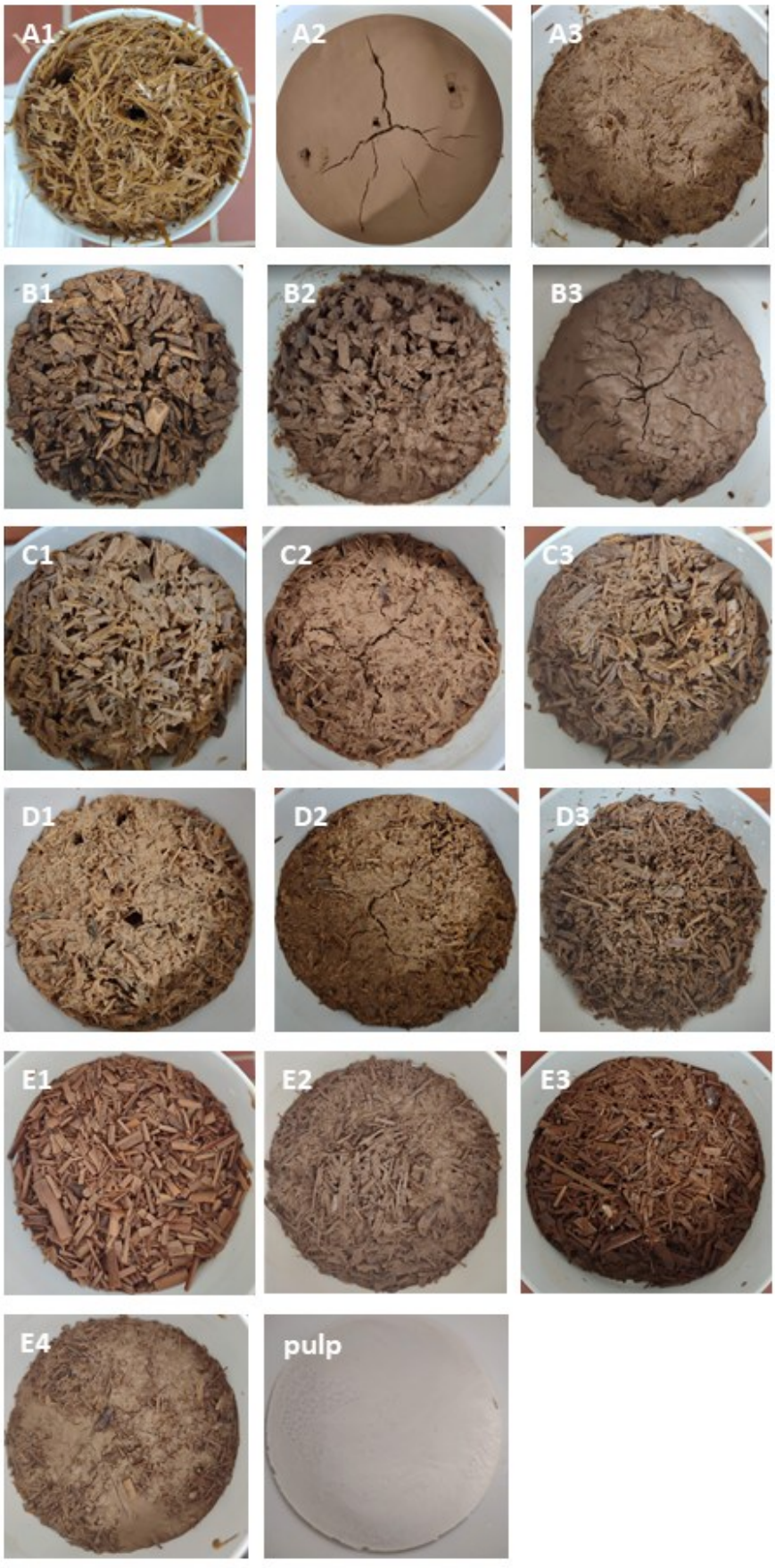

Figure C4: Photos of filter cakes obtained by lab-scale vacuum filtration

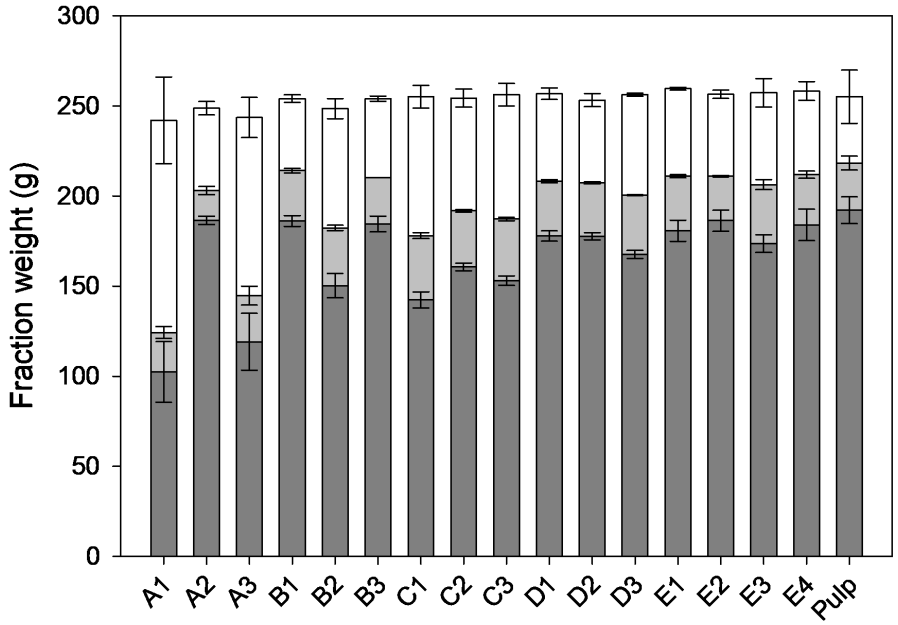

Figure C5: Filtration mass balances including filtrate (dark gray), dried filter cake (gray) and residual filtrate in the wet filter cake (white).

Appendix D: stoichiometry derivation for process modelling of chemolithoautotrophic growth of *C. necator* DSM 544

Growth Equation

The stoichiometry for growth and PHB accumulation can be defined based on the reactant and product species. Equation 1 shows the stoichiometry for growth of *C.necator* on CO_2, H_2 and CO_2 to produce biomass (with empirical formula $CH_{1.68}O_{0.46}N_{0.24}$), water as well as sulfuric acid generated from ammonium sulphate dissociation. The coefficients a, b, c, d, e and f can be calculated based on elemental balances.

$$aCO_2 + bH_2 + cO_2 + d(NH_4)_2SO_4 \rightarrow CH_{1.68}O_{0.46}N_{0.24} + eH_2O + fH_2SO_4 \quad 1$$

Considering a 1 C-mol for the biomass, a can be set to 1 (a = 1) and the number of moles of nitrogen on the left-hand side of the equation should be equal to that on the right-hand side as shown in equation 2, making d to be equals to 0.12. Considering that H_2SO_4 is the product (NH4)2SO4 dissociation, their coefficients have to be the same to have a balanced equation, making f = d = 0.12.

$$2d = 0.24 \quad 2$$

Elemental balances for H and O are shown in Equation 3 and 4 respectively.

$$2b + 8d = 1.68 + 2e + 2f \quad 3$$

$$2a + 2c + 4d = 0.46 + e + 4f \quad 4$$

The coefficient of O_2 (c) can be calibrated from the oxygen uptake rate (OUR) data of the non-PHB biomass of our cultivation which happens to lie between 0 to 34 hours as shown in Equation 5.

$$c = \frac{\Delta nO_2}{\Delta X} = \frac{\int_0^{34} OURdt}{\Delta X} \quad 5$$

Where:

$\int_0^{34} OUR\, dt$ is the area under the curve of the OUR graph which means the total amount of oxygen utilized by *C. necator* from 0 to 34 hours and can be calculated from the summation of the uptake rates (Equation 6).

ΔX is the change in the number of moles of PHB-free biomass from 0 to 34 hours (Equation 7).

$$\int_0^{34} OUR\, dt = \sum(OUR, 0-12h), (OUR, 12-22h), (OUR, 22-24h), (OUR, 24-34h) \quad 6$$

$$\Delta X = \frac{\text{non-PHB biomass from 0-34h (2.03-0.06)}}{\text{molecular weight of biomass per C-mol (24.4)}} \quad 7$$

Plugging in the OUR values in Equation 6 and converting to mole units by dividing by the molecular weight of O_2 (32 g/mol) gives a value of 0.231 mol O_2 L^{-1}. Solving for ΔX in Equation 7 gives a value 0.0807 mol L^{-1}. Putting these values into equation 5 gives a value of 2.87 mol O_2 per C-mol biomass for coefficient c, translating to the O_2 demand be *C. necator* DSM 545 under the fermentation conditions. Additionally, solving for b and e in Equation 3 and 4, and inputting the values of all the coefficients into Equation 1 gives the complete

stoichiometric equation for the growth of *C. necator* DSM 545 on CO2, shown in Equation 8. This is in line with the findings of Yu and Lu (2019)

$$CO_2 + 7.76H_2 + 2.87O_2 + 0.12(NH_4)_2SO_4 \rightarrow$$

$$CH_{1.68}O_{0.46}N_{0.24} + 7.28H_2O + 0.12H_2SO_4 \quad 8$$

Neutralization Equation

The H_2SO_4 generated from $(NH_4)_2SO_4$ makes the medium acidic for *C. necator* which prefers an almost neutral pH (6.2 to 6.9), making it necessary to neutralize it with a base like NaOH. Equation 9 shows the neutralization reaction using NaOH.

$$H_2SO_4 + 2NaOH \rightarrow Na_2SO_4 + 2H_2O \quad 9$$

PHB Equation

The stoichiometric equation for PHB production is derived using $C_4H_6O_2$ as the repeating unit as shown in Equation 10. Balancing carbon atoms with a one-monomer PHB unit requires that x equals 4 in Equation 10, ensuring carbon conservation on both sides of the reaction. Applying oxygen and hydrogen atom balance to both sides of the reaction results in Equation 11 and 12 respectively. Substituting y and w in Equation 10 with Equation 11 and 12, as well as x as 4 leads to Equation 13. From Equation 13, an assimilation only assumption is made by setting z = o, showing the formation of PHB from CO_2 without the energy flow from O_2 (14). Dividing through Equation 14 by 4 convers the it to a per C-mol basis (Equation 15).

$$xCO_2 + yH_2 + zO_2 \rightarrow C_4H_6O_2 + wH_2O \quad 10$$

$$w = 6 + 2z \quad 11$$

$$y = 9 + 2z \quad 12$$

$$4CO_2 + (9 + 2z)H_2 + zO_2 \rightarrow C_4H_6O_2 + (6 + 2z)H_2O \quad 13$$

$$4CO_2 + 9H_2 \rightarrow C_4H_6O_2 + 6H_2O \quad 14$$

$$CO_2 + 2.25H_2 \rightarrow CH_{1.5}O_{0.5} + 1.5H_2O \quad 15$$

Introducing O2 considers the energy flow term (respiration). Making reference to Equation 16, a mole of O2 burns 2 moles of H2 to form 2 moles of H2O. Assuming r mol O2 per C-mol PHB is required for the energy generation, 2r moles has to be added to the H2 term and H2O term (Equation 17). Equation 18 can be used to calculate the O2 required to produce a one C-mol PHB without biomass.

$$2H_2 + O_2 \rightarrow 2H_2O \quad 16$$

$$CO_2 + (2.25 + 2r)H_2 + rO_2 \rightarrow CH_{1.5}O_{0.5} + (1.5 + 2r)H_2O \quad 17$$

$$r = \frac{\int_{51}^{142} OUR\ dt - a\Delta X}{\Delta PHB} \quad 18$$

Where:

$\int_{51}^{142} OUR\, dt$ is the area under the curve of the OUR graph which means the total amount of oxygen utilized by *C. necator* from 51 to 142 hours and can be calculated from the summation of the uptake rates (Equation 19).

a is the mole of O_2 used for PHB-free biomass formation.

ΔX and ΔPHB is the change in the number of moles of biomass and PHB from 51 to 142 hours respectively (Table 1).

$$\int_{51}^{142} OUR\, dt = \sum(OUR, 51 - 97h), (OUR, 97 - 121h), (OUR, 121 - 142h) \quad 19$$

Solving Equation 18 by inputting the respective OURs, ΔX and ΔPHB for the different time intervals indicated in Table 1 results in r equals 2.3 mol O_2. Plugging in the value of r to Equation 17 and multiplying through by 4 to have the normal PHB formula ($C_4H_6O_2$) gives the stoichiometric Equation for the production of PHB by *C.necator* DSM 545 (Equation 20). This stoichiometric equation is close to that reported by Tanaka et al. (1991) and Mozumder et al. (2015).

$$4CO_2 + 27.4H_2 + 9.2O_2 \rightarrow C_4H_6O_2 + 24.H_2O \quad 20$$

Appendix E: contribution of different hydrogenase strains to energy efficiency

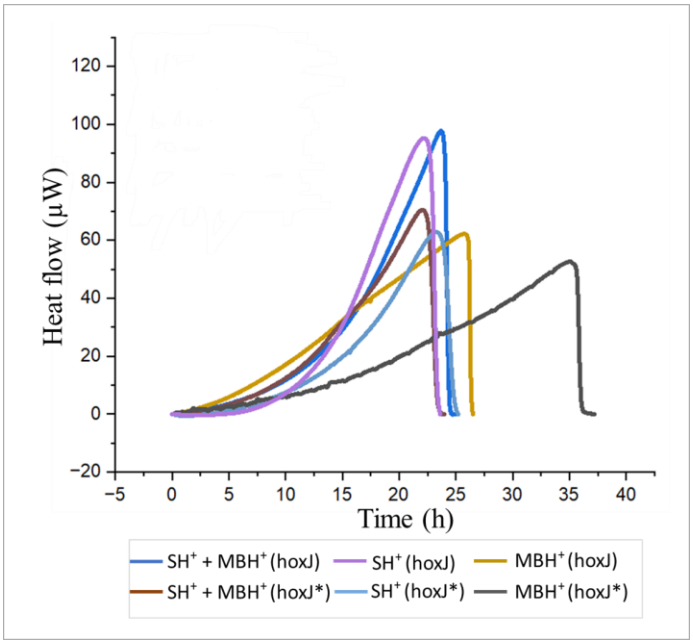

Figure E1: Heat flow profiles of *C. necator* hydrogenase knockout strains cultivated with 3.8%, H_2, 7.3% O_2, 13% CO_2, 75.9% N_2 in a TAM IV isothermal microcalorimeter. Data represents triple experiments.